

EVALUATION OF USEFULNESS AND REPEATABILITY FOR PEDESTRIAN PROTECTION FLEX-PLI

Yong-Won YOON

Gyu-Hyun KIM

Korea Automobile Testing and Research Institute
Korea

Jae-Moon LIM

Department of CAD & Graphics, Daeduk University
Korea

Gyung-Jin PARK

Department of Mechanical Engineering, Hanyang University
Korea

Paper Number 11-0425

ABSTRACT

Pedestrian-vehicle traffic accidents are a globally recognized safety concern. UN/ECE/WP29 established the Global Technical Regulation (GTR) for pedestrian safety on 12 November 2008. GTR is expected to significantly reduce the injuries of pedestrians in the event of frontal impacts. Recently, a new pedestrian lower legform named Flex-PLi has been developed for the body model of the human lower leg. Flex-PLi is introduced, and the characteristics of the model are identified through a comparison study with an existing lower legform. Usability, durability and repeatability are evaluated by using real vehicle impact tests. Moreover, the model is examined by considering the possibility of its application to pedestrian safety GTR phase 2.

INTRODUCTION

Of the various types of traffic accidents, the pedestrian-vehicle accident shows a very high death rate, 36% (as of 2008).¹⁾ Accordingly, studies to protect pedestrians have actively been conducted around the world.²⁻³⁾ These studies led to the establishment of a global standard for the protection of pedestrians, GTR (Global Technical Regulation), which was established and declared in November 2008.⁴⁾ Member countries that signed the agreement, including Korea, are planning to introduce GTR to protect their own pedestrians. In Korea, a new safety standard for automobiles based on GTR was adopted in December 2008. ⁵⁾ The standard for protecting pedestrians will be applied to new vehicles from 2013, and to existing vehicles from 2018.

The assessment of the degree of pedestrian protection offered by an automobile is performed by calculating the body injury rate, which is obtained from the impact of headform or legform hitting a real

vehicle. Unfortunately, the lower legform currently used (European Enhanced Vehicle Committee Working Group 17 Lower legform) has been criticized for its lack of duplicability of body. ⁶⁾

A newer legform, Flex-PLi (Flexible-Pedestrian Legform impactor), which is an improved model of the existing lower legform, was first developed in Japan in 2000. In 2005, the European Union (EU) organized the Flex-Technical Evaluation Group. The major focus for the group was evaluating the technical aspects of Flex-PLi for legal application.

European countries, the USA, and Japan have been leading the Round Robin Test of Flex-PLi. Korea also has participated in the test, and played a key role in the global society. In this paper, Flex-PLi was first introduced and used for the evaluation test for protecting pedestrians in Korea. Its differences from the existing legforms were confirmed, and procedures and methods of evaluation in the real car test were then established using Flex-PLi. Finally, with the car test, the validity of legal application was examined by analyzing characteristics of usefulness, durability and repeatability of Flex-PLi.

Flex-PLi

As seen in Fig. 1, Flex-PLi offers an improvement compared to the existing lower legforms by having structure and characteristics similar to that of a human body. It is an advanced legform model having full flexibility over the whole legform. ⁸⁾



Fig. 1 Flex-PLi

2.1 Trend in Flex-PLi development

Fig. 2 provides a stepwise illustration of the development trend of Flex-PLi. Flex-PLi has been developed in Japan since 2000. Its design was established in 2002, and has been evolved with the change of its name from Flex-G in 2005 to Flex-GT in 2006.⁹⁾

However, the development led by Japan Automobile Manufacturers Association and Japan Automobile Research Institute faced realistic problems, such as difficulties in full-scale production and verification of durability. FTSS, a well known American dummy manufacturer, eventually acquired the development department of Flex-PLi in 2007, and the final version of the Flex PLi GTR model is about to be released.¹⁰⁾

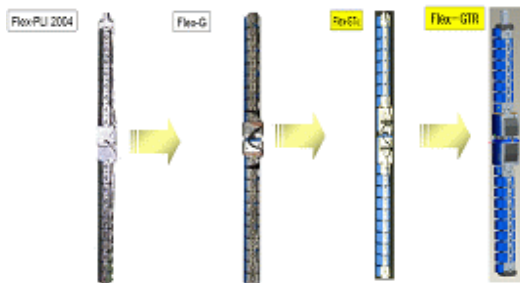


Fig. 2 Trend in development of Flex-PLi

2.1 Movement of Flex-TEG

The EU is now conducting active research in cooperation with Flex-TEG, a technical assessment group carrying out the second stage of GTR research for pedestrian protection. Flex-TEG was established in 2005 and has held 10 conferences as of December 2009. Since the first conference was opened by the World Automobile Manufacturers Association in France, BAST in Germany has held the following

conferences thus far.

3. Vehicle test for Flex-PLi

3.1 Preparation of Flex-PLi for the test

The procedure of the car test for Flex-PLi is shown in Fig. 3.¹¹⁾ In brief, the procedure was as follows: basic preparation for Flex-PLi was conducted; a correction test using pendulum was conducted before the car test was executed; the condition of Flex-PLi was checked; rubber parts and skins were assembled on it; and finally, the car impact test was conducted. After the test was completed, the same procedure was repeated.

General Flow of the Flex-GTR Car testing

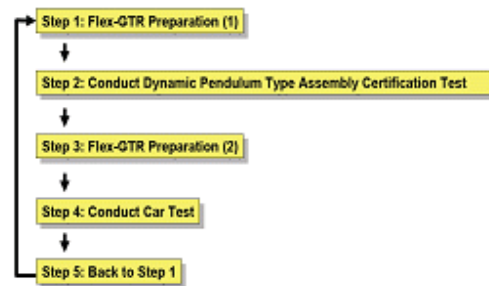


Fig. 3 The procedure diagram of the car test for Flex-PLi

The check points for fastening conditions during test preparation of Flex-PLi are shown in Fig. 4.¹²⁾ Joint bolts were tightened with pre-determined torque (8 Nm), and clearance existence was checked. It was checked to determine whether the bolts were connected inside the central knee part, and whether any nuts and washers were protruded out of the surface level.

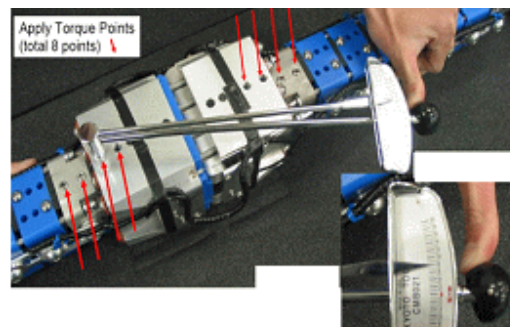


Fig. 4 Preparation and check for fastening condition of Flex-PLi

Fig. 5 illustrates a clearance check in the test preparation of Flex-PLi. 12) A thickness measuring gauge that is specially manufactured was used. Thickness of internal wires in the parts of femur and tibia were measured for their clearance. For femur, the clearance was maintained at 8 mm of thickness, and 9 mm for tibia.

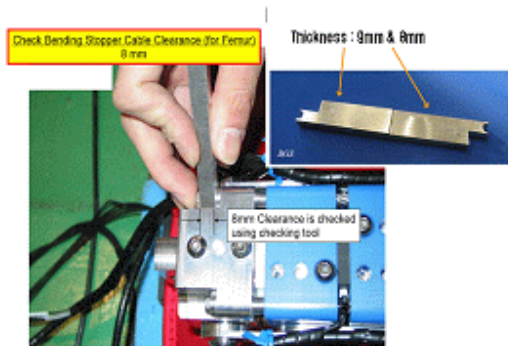


Fig. 5 Preparation of Flex-PLi - check for clearance

3.2 Correction test for Flex-PLi

The correction test for Flex-PLi can be roughly divided into the static correction test and the dynamic correction test. The dynamic correction test is further broken down into pendulum type and impact type. A pendulum type dynamic correction test for Flex-PLi was carried out by fixating the tibia part of Flex-PLi on the correction device, lifting it up to 15° above the horizontal (15° hanging angle), and releasing it to freely swing down. Data obtained from this activity were checked for correction if they were located between the maximum and minimum level. Fig. 6 below shows the dynamic correction test.¹²⁾

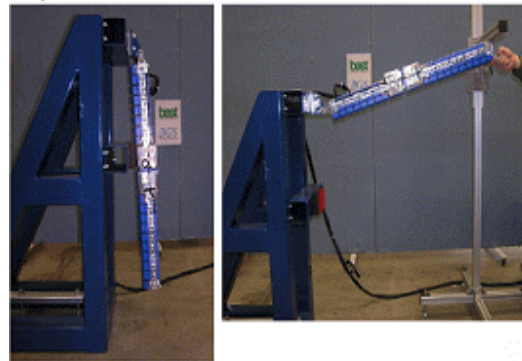


Fig. 6 Dynamic correction of Flex-PLi

Fig. 7 shows how to assemble Flex-PLi.¹²⁾ On completion of the correction test, rubber parts and outer skin were put on Flex-PLi. The femur and tibia parts were covered with absorption material made from rubber, and the outer skin was mounted to complete the assembly. All preparation for the test was completed by assembling Flex-PLi. When disassembly was required after the test, the procedure above was carried out in reverse order.

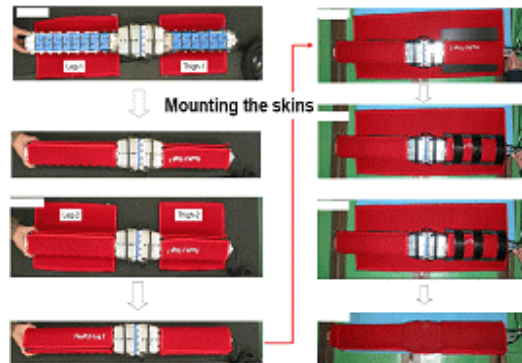


Fig. 7 How to mount skins on Flex-PLi

3.3 Test method for Flex-PLi

The test for Flex-PLi was conducted by creating impact to the impact zone on the vehicle with Flex-PLi. The impact velocity is 11.1 ± 0.2 m/s. Fig. 8 shows the system configuration for the car test. The configuration consists of a stationary back plate for Flex-PLi, a power supply, a PC for downloading data after the impact test, and its specific application for analyzing data. The system configuration is relatively simple, because the system for data measurement is installed inside Flex-PLi. The car test started by installing Flex-PLi on the projectile. Power was

provided from a cable linked to the power supply until discharging started, and the cable was set to be automatically separated. From that moment, Flex-PLi freely fell down to the test car without having any external cable linked to it. The difference between Flex-PLi and the existing lower legform was that Flex-PLi could eliminate the concern of data loss resulting from disconnection of measuring cable.



Fig. 8 Test method for Flex-PLi – System configuration

3.4 Car Test for Flex-PLi

The car test was done using Flex-PLi. The test car was chosen from among Korean cars that satisfy GTR requirements to protect pedestrians when tested with the existing lower legform.

The purpose of the assessment test was as follows: checking the fulfillment of GTR by Flex-PLi when an existing model meets the criteria; evaluating the repeatability of Flex-PLi when the test repeats on the same impact zone; and finally, identifying the durability and user-friendly characteristics of Flex-PLi during the test.

In Fig. 9, the purpose and method of the test are summarized with pictures. The main goals of the test were to evaluate repeatability and to check fulfillment of the regulation. The explanation includes impactor type, impact velocity, impact zone, impact point, impact times, and impact height.



Purpose of assessment test

- (1) Check the fulfillment of GTR by Flex-PLi when existing model meets the criteria
- (2) Evaluate repeatability of Flex-PLi when the test repeats on the same impact zone

Test Method

impactor type	Flex-PLi
impact velocity	11.1 ± 0.2 m/s
impact zone	EEVC WQ17 Lower legform (Green zone)
impact point	2 Same cars (Same point)
impact times	3 impact per 1 Car
impact height	75mm (From ground level)

Fig. 9 Car test for Flex-PLi – purposes and method

The zones on which the existing lower legform satisfied the impact test were selected as impact zones. The repetitive test was conducted by testing 2 identical cars without exchanging test material, such as a bumper, and alternating the turn to test. 3 impacts were provided to a car, and 2 cars were tested, which means the test was conducted 6 times in total. Fig. 10 shows pictures before and after the car test using Flex-PLi.



Fig. 10 Pictures before and after the car test for Flex-PLi

Data measurement for Flex-PLi basically consists of 7 bending moments, 3 of which are in the femur and 4 in the tibia, and 4 knee elongations and 1 knee acceleration, which totals 12 channels. Fig. 11 illustrates the data from the test by dividing it into bending moments in the femur and tibia, elongation in the knee, and knee acceleration.

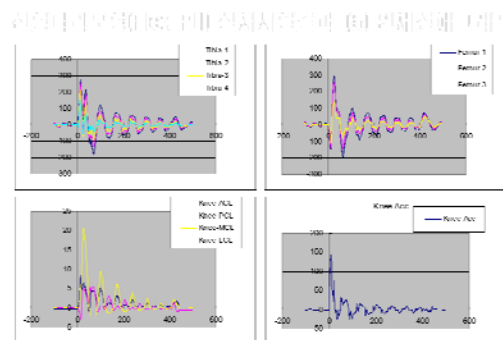


Fig. 11 Car test for Flex-PLi - Test data

In the basic data channel measured from Flex-PLi, tibia bending moment (criteria for Tibia: 340 Nm) and knee elongation (Knee-MCL: 22 mm) are regulated by the second amendment of GTR. Table 1 highlights the two weakest points for protection of pedestrians from the impact test of the 6 total tests.

Flex-PLi test results were proven to meet criteria value for body injury on the whole. The maximum value of bending moment for tibia 1 was 285.4 Nm, and for knee elongation was 20.7 mm, both of which can be analyzed to satisfy body injury criteria for Flex-PLi.

	unit	Max.	Min.		unit	Max.	Min.
Femur-3	(Nm)	154.0	-106.8	Femur-3	(Nm)	143.1	-103.5
Femur-2	(Nm)	270.1	-145.3	Femur-2	(Nm)	260.1	-141.9
Femur-1	(Nm)	307.4	-195.2	Femur-1	(Nm)	299.0	-194.5
Tibia-1	(Nm)	285.4	-173.7	Tibia-1	(Nm)	282.6	-177.9
Tibia-2	(Nm)	251.1	-133.5	Tibia-2	(Nm)	256.4	-138.7
Tibia-3	(Nm)	214.3	-87.4	Tibia-3	(Nm)	219.4	-80.3
Tibia-4	(Nm)	153.4	-50.8	Tibia-4	(Nm)	159.7	-55.9
Knee-ACL	(mm)	8.1	-1.4	Knee-ACL	(mm)	8.4	-0.8
Knee-PCL	(mm)	8.3	-2.3	Knee-PCL	(mm)	5.7	-2.8
Knee-MCL	(mm)	20.2	-2.1	Knee-MCL	(mm)	20.7	-2.1

Table 1. Body injury assessments from car test for Flex-PLi.

The test result of Flex-PLi was also compared with that of the existing lower legform. The purpose of this comparison is to judge the legal validity of Flex-PLi and lower legform for the same impact zones. Fig. 12 shows the number calculated from the result of Flex-PLi and existing lower legform tests.

Body injury level for the existing lower legform was measured for knee bending angle, shear displacement, and tibia acceleration. The criteria base is converted to 100% for each measurement. The test result is assumed to meet the criteria when it does not exceed this value. The car used for this test showed around 78%, 38%, and 74% for bending angle, shear displacement and acceleration, respectively. This proves that not only does the existing lower legform meets the criteria, but also that significant room can be secured when compared to the criteria.

Meanwhile, body injury level for Flex-PLi test was calculated with criteria base of 100 for knee elongation and tibia bending moment. Knee elongation was about 78% and tibia bending moment about 89%, both of which meet the criteria. However, the differences from the criteria base shown by the lower legforms were likely to reduce.

The comparative result between Flex-PLi and the existing lower legform should not be uniformly applied to unspecified cars. It may well be limited to the unique characteristics of the car used in this test.

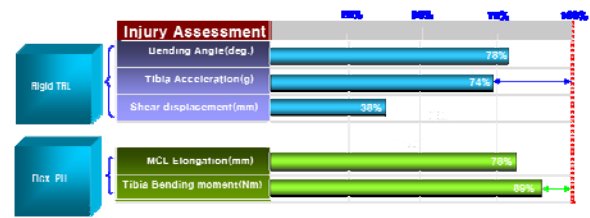


Fig. 12 Comparison between EEV WG17 Lower Legform and Flex-PLi

Repeatability of Flex-PLi was confirmed. On the whole, it was proven to be excellent. Fig. 13 shows the test result of repetitive impact for tibia 1 bending moment and knee elongation at the L1 zone out of 3 impact zones. The result from repetitive tests showed almost identical characteristics in the graphs.

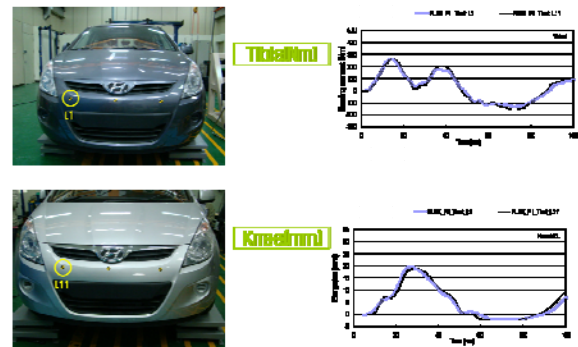


Fig. 13 Car test for Flex-PLi – Repeatability

Excellent repeatability appeared on tibia bending and MCL (Medial Collateral Ligament), injury assessment items for Flex-PLi. However, ACL (Anterior Cruciate Ligament) and PCL (Posterior Cruciate Ligament), which are now being discussed globally for monitoring, showed relatively low-toned repeatability.

The results of the Flex-PLi test with mean value and standard deviation are shown in Table 2.

		TIBIA 1	TIBIA 2	TIBIA 3	TIBIA 4	MCL	ACL	PCL
L1	TEST-1	261.4	234.9	194.1	150.5	19.7	8.5	10.1
	TEST-2	266.7	237	204.7	156.9	18.9	8.9	7.6
	MEAN	264.1	236	199.4	153.7	19.3	8.7	8.65
	ST.DEV	3.748	1.485	7.495	4.525	0.566	0.283	1.768
	C.V	0.014	0.006	0.038	0.029	0.029	0.033	0.2
	C.V(%)	1.42	0.63	3.76	2.94	2.93	3.25	19.97
L2		TIBIA 1	TIBIA 2	TIBIA 3	TIBIA 4	MCL	ACL	PCL
	TEST-1	253.6	242.7	188.1	175.9	18.4	7.8	6.4
	TEST-2	239	228.8	187.9	170.2	19.4	7.5	8
	MEAN	246.3	235.8	188	173.1	18.9	7.65	7.2
	ST.DEV	10.32	9.829	0.141	4.031	0.707	0.212	1.131
	C.V	0.042	0.042	8E-04	0.023	0.037	0.028	0.157
C.V(%)	4.19	4.17	0.06	2.33	3.74	2.77	15.71	
L3		TIBIA 1	TIBIA 2	TIBIA 3	TIBIA 4	MCL	ACL	PCL
	TEST-1	282.6	256.4	219.4	159.7	20.7	8.4	5.7
	TEST-2	285.4	251.1	214.3	153.4	20.2	8.1	6.3
	MEAN	284	253.8	216.9	156.6	20.45	8.25	6
	ST.DEV	1.98	3.746	3.606	4.455	0.354	0.212	0.424
	C.V	0.007	0.015	0.017	0.028	0.017	0.026	0.071
C.V(%)	0.70	1.48	1.66	2.85	1.73	2.57	7.07	

Table.2 Car test for Flex-PLi – Reliability

62% of all results were given as “Good,” which means a Coefficient of Variation of less than 3%, and 24% belong to “Acceptable,” which means a Coefficient of Variation in the range of 3~7%.

MCL, a criteria for injury assessment of Flex-PLi, was generally located in the range of 3~7% of Coefficient of Variation, “Acceptable.” However, in the case of PCL, it was assessed as “Marginal,” which falls in the range of 7~10%, and “Not Acceptable,” which has a higher coefficient than 10%.

PCL has not been selected as a base criteria for injury level assessment of Flex-PLi. However, all PCL values were classed as “Marginal” and “Not Acceptable” in the test for analysis. Thus, improvement of the vulnerable repeatability of PCL is demanded.

4. Conclusion

In this paper, a car test using Flex-PLi was conducted to assess the protection of pedestrians by automobiles, and the following conclusions were obtained:

- 1) Consumable parts required by EEVC WG17 lower legforms, such as bending ligament and flash form, are not needed for usability of Flex-PLi. Without the concern of data loss and damage to the cable after impact test, convenience and efficiency for users are confirmed to be improved.
- 2) Around 62% of all results were “Good,” meaning a Coefficient of Variation of less

than 3%, and 24% were “Acceptable,” meaning a Coefficient of Variation in the range of 3~7%. Generally, repeatability appeared to be excellent, but in the case of PCL, further investigation and supplementation is required for its vulnerable repeatability.

- 3) In terms of the durability of Flex-PLi, problems like destruction of device and failure did not occur during the test. Nevertheless, evaluation for durability is reserved because of the relatively short assessment period.
- 4) Automobiles that meet the criteria for EEVC WG17 lower legform also seemed to satisfy the criteria for Flex-PLi. However, Flex-PLi showed a decreased margin (in case of tibia bending moment), while EEVC WG17 lower legform secured a significant margin to the criteria level. It is believed that this comparative result between Flex-PLi and the existing lower legform should not be uniformly interpreted and applied to unspecified cars, because it may well be limited to the unique characteristics of the car used in this test.
- 5) More countries and automobile-related organizations are required to take part in the limitative round robin tests that are performed by the EU, the USA, Japan, and Korea. This will promote benefits to those participating countries based on exchange of opinions and the identification of global trends.
- 6) Ongoing supplementation should be explored to develop a user-friendly control program and provide measures for unpredictable rebound situations due to the use of a flexible device.

Acknowledgements

This research was undertaken as part of the “Coordination Project for Global Safety Standard” of Ministry of Land, Transport and Marine Affairs (MLTM), and the “Technology Innovation Project” of the Ministry of Knowledge and Economy in Korea.

References

- 1) Korea National Police Agency "2009 Traffic Accident Statistics," Issue No 11-1320000-000011-10, 2009. 07
- 2) J. W. Lee, "Introduction of Pedestrian Head Protection Test Method in Korea-NCAP," Spring Conference of KSAE, 2006.
- 3) Peter J. Schuster, "Current Trends in Bumper Design for Pedestrian Impacts," SAE, 2006-01-0464.
- 4) "Global Technical Regulation No.9 Pedestrian Safety" online at <http://unece.org/trans/wp29/180a92>.
- 5) Order. 75 from MLTM "Standard for Automobile Safety. Sec. 102-2 Protection of Pedestrians", issued in 2008. 12. 08
- 6) "EEVC Working Group 17 Report" online at http://uncec.org/trans/wp29grsp/pedestrian_10.
- 7) "Agenda for the first meeting of Flex-PLi Technical Evaluation Group" online at <http://unece.org/trans/doc/2006/wp29grsp/teg-001e>.
- 8) Atsuhiko Konosu, "Evaluation Tests for Pedestrian Legform Impactors," 19th International Technical Conference on the Enhanced Safety of Vehicles, 2005
- 9) "Flex-G and Flex-GT: a Comparison of Test Results" online at <http://unece.org/trans/doc/2007/wp29grsp/teg-036e>.
- 10) "Flex-PLi GTR Development Prototypes" online at <http://unece.org/trans/doc/2009/wp29grsp/teg-071e>.
- 11) "Phase 2 of the Global Technical Regulation-Flex PLi" ECE/TRANS/WP29/GRSP/2009/21, 24 September 2009.
- 12) "Flex-GT Handling and Usage" online at <http://unece.org/trans/doc/2007/wp29grsp/teg-037e>.

A NEW ADVANCEMENT IN PEDESTRIAN SAFETY: FINITE ELEMENT (FE) MODELING OF THE FLEX-PLI GTR

Chirag, Shah
Wen-Ren, Harn
Hong, Zhou
Christian, Kleessen
Fuchun, Zhu
Robert, Kant

Humanetics Innovative Solutions, Inc.
USA
Paper Number 11-0237

ABSTRACT

The lower limb is one of the most frequently injured body regions in crashes involving pedestrians. A biofidelic FLEXible-Pedestrian Legform Impactor Global Technical Regulations (FLEX-PLI GTR) device has been developed with aim to advance global pedestrian safety regulations. It has been achieved under directions of the Flex-PLI Technical Evaluation Group (FLEX-PLI TEG). The FLEX-PLI GTR device is the latest development and successor of the earlier GT version.

The FLEX-PLI GTR device has major three regions: femur, knee and tibia. Central to the device are solid bone cores made of fiberglass representing tibia and femur bones. These bone cores have bending moment measuring capabilities at several locations along their axes. They are encased with segmental structures to achieve flexible human like bending behavior during pedestrian crashes. The outermost skin and flesh of the device consists of several rubber and neoprene foam layers. The knee region contains two knee blocks representing human like knee and has ligament elongations measuring capabilities to be used as injury criteria in regulations.

This paper documents the development and dynamic validations of the FLEX-PLI GTR FE models from its hardware counterpart. The models have been developed in four widely used FE codes that is LS-Dyna, Pam-Crash, Abaqus, and Radioss. The geometry and inertia properties of models are obtained from available drawings and hardware. The connectivity and structural integrity of models are established by experiments and verified against hardware. The material properties of models are implemented from material test data. These models are then validated against a variety of dynamic loading cases at component, assembly, and full

legform levels. The femur and tibia bone bending moments and knee ligament elongations from the model output are compared to test data to evaluate model performance and injury predictability. A description of the model development is restricted to LS-Dyna FE code. However, model validation results are extended to include all four FE codes.

The FLEX-PLI GTR models revealed very promising performance in all validation cases and can be potentially used in future pedestrian safety regulations. The models were found to be very cost effective (in terms of CPU times) and reliable for pedestrian safety simulations.

INTRODUCTION

Pedestrian safety has posed new challenges and serious concerns in traffic accidents involving pedestrians and vehicles in recent years. The lower limb was found to be the most frequently injured body region with AIS 2 to 6 level injuries in 32.6% of cases worldwide.

In 1998, the European Enhanced Vehicle-Safety Committee proposed a test procedure to assess protection to the lower extremity of a pedestrian during a collision [1]. A legform Impactor composed of rigid long bones was utilized in this procedure. The Japan Automobile Research Institute (JARI) and the Japan Automobile Manufacturer Association, Inc. (JAMA) have been developing a biofidelic flexible pedestrian legform Impactor (FLEX-PLI) since 2002 [2]. As opposed to a legform impactor with rigid bone parts, the FLEX-PLI is more biofidelic especially for its long bone parts, which have human-like bending characteristics [3]. The FLEX-PLI also provides extended injury assessment capabilities, including long bone bending moment at multiple

locations and knee ligament elongations in comparison to other pedestrian legforms [3].

In 2005, the FLEX-PLI Technical Evaluation Group (FLEX-TEG) was settled under the ECE/WP29/GRSP/Informal Group on Pedestrian Safety in order to evaluate FLEX-PLI hardware performance. Another objective of the FLEX-TEG is to assess the impactor as a regulatory purpose test tool for a Global Technical Regulation on Pedestrian Safety (PS-GTR). The ministry of Land, Infrastructure, Transport, and Tourism of Japan (JMLIT) has been supporting FLEX-TEG activities by conducting technical evaluation tests on the FLEX-PLI. The JAMA and JARI have continued to improve and upgrade FLEX-PLI, and in 2007 the 5th version, called Type GT (FLEX-GT) was produced. After the settlement of the FLEX-TEG, the FLEX-PLI GT was evaluated and improved its performance, and the final 6th version, type GTR (FLEX-GTR), was agreed by the FLEX-TEG members in April 2008 [4].

The objective of this paper is to present the development of the FLEX-PLI GTR LS-Dyna model. Remaining three models are developed in similar ways with some code specific differences. All the four models are then evaluated against full legform dynamic calibration and full legform rigid plate loading cases. Development of these models is supported by a consortium comprised of auto makers.

FLEX-PLI GTR Model

The FLEX-PLI GTR LS-Dyna model v1.1 is shown in Figure 1 and its hardware counterpart is shown in Figure 2. The FLEX-PLI GTR device has three major regions: femur, knee and tibia (Figure 1). These regions are covered with rubber and neoprene foam layers representing the skin and flesh of the device. Fundamental structures for the femur and tibia regions are constructed segmental with bone cores at the center to achieve bending flexibility representing human like responses during pedestrian crashes. The knee region is comprised of two knee blocks representing condyles like a human knee. Springs and cables are used to replicate the ligaments of the knee.

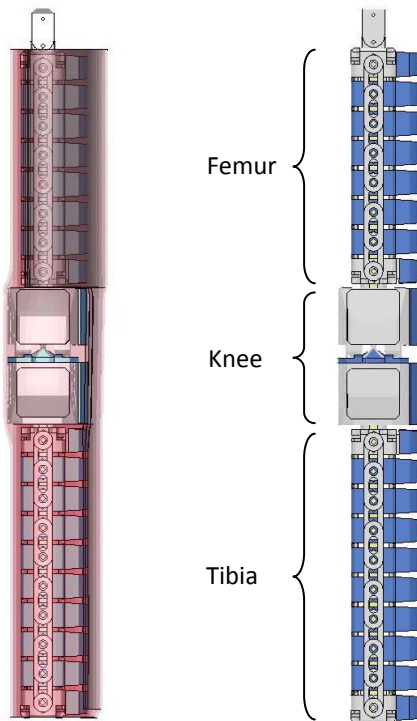


Figure 1: FLEX-PLI GTR LS-DYNA model

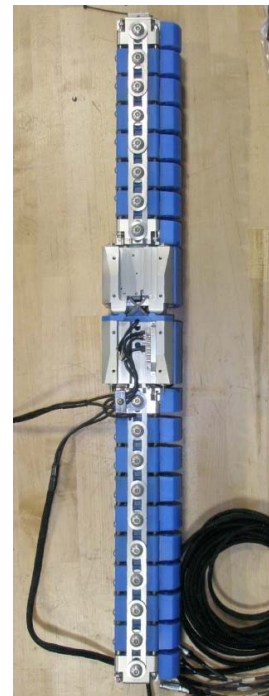


Figure 2: FLEX-PLI GTR hardware without skin

Table 1: Model statistics

	LS-Dyna	Radioss	Pam-Crash	Abaqus
Number of Nodes	126,534	117,067	120,362	113,122
Number of Elements (including rigid)	214,553	81,585	88,256	79,301
Initial Time-step Size (micro second)	0.85	0.91	0.95	0.91
Development Solver Version	971 R5.0	v10.0	Pam-Crash 2009	6.7pr3f

The model geometry and inertia properties are obtained from available drawings and detailed inspection of the physical impactor. The model connectivity and structural integrity are inspected by experiments and verified against hardware. The mesh size in the model was developed to achieve sufficient accuracy at minimal CPU cost. Table 1 describes model statistics for all four FLEX-PLI GTR models.

Bone Core:

The femur and tibia bone cores are made of fiberglass reinforced plastic (FRP) material in the physical device. An appropriate material model is developed to be used for the bone core model. Strain gauges are used at top and bottom surface of the bone core to measure bending moments in the bones at several locations in the femur and tibia regions (Figure 3). Local section force outputs were used to model the strain gauges.

Femur and tibia:

Figures 4a and 4b show femur and tibia assemblies and a partial section cut through them. These regions are structurally similar with the only differences being the length and number of segments. The bone core lies in the middle of square housings (known as inner segments) which are chained together by links down their flanks. Additional deformable nylon pieces known as impact segments are attached to inner segments and function as a load path during impact. The stopper cables which limit the maximum bending of the bone cores are modeled explicitly to behave in the same way as the physical device. Rubber buffers are glued to the inner segments to avoid direct contact between the inner segments. Appropriate material models are used for all the deformable components in the femur and tibia regions.

Knee:

The FLEX-PLI GTR knee model is shown in Figure 5. The knee has two blocks or condyles, one attaching to femur and the other attaching to the tibia. The condyle surface on the tibia block has nylon material to reduce friction and to avoid metal to metal contact.

Four kinds of ligament cables, ACL (Anterior Cruciate Ligament), MCL (Medial Collateral Ligament), PCL (Posterior Cruciate Ligament) and LCL (Lateral Collateral Ligament) are modeled as weak spring elements to represent potentiometers to measure knee ligament elongations at ACL, MCL, LCL and PCL locations. Deformable springs and cables in the knee area are modeled to achieve appropriate knee behavior similar to the physical impactor. Appropriate material models are used for all the deformable components in the knee region.

Flesh:

The flesh of the FLEX-PLI GTR model is comprised of several layers of neoprene and rubber sheets as shown in Figure 6. Appropriate material models are developed from quasi-static and dynamic material tests to model layers of the neoprene and rubber sheets.

Instrumentation:

Table 2 depicts the instrumentation modeling for the FLEX-PLI GTR CAE models. Total of 30 channels are modeled and can be used as injury prediction capabilities of the CAE models. Femur and tibia bending moments are output from local sections defined at strain gauge locations (Figure 3). Knee ligament elongations are output of discrete elements in the knee area (Figure 5). All linear accelerations and angular rate outputs are from nodes modeled at exactly the same locations as in the physical legform.

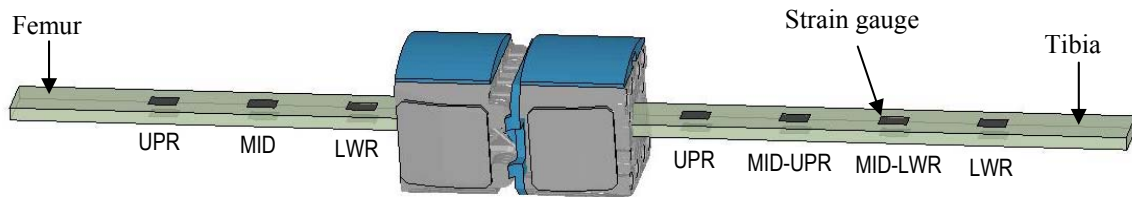


Figure 3: FLEX-PLI GTR bone cores

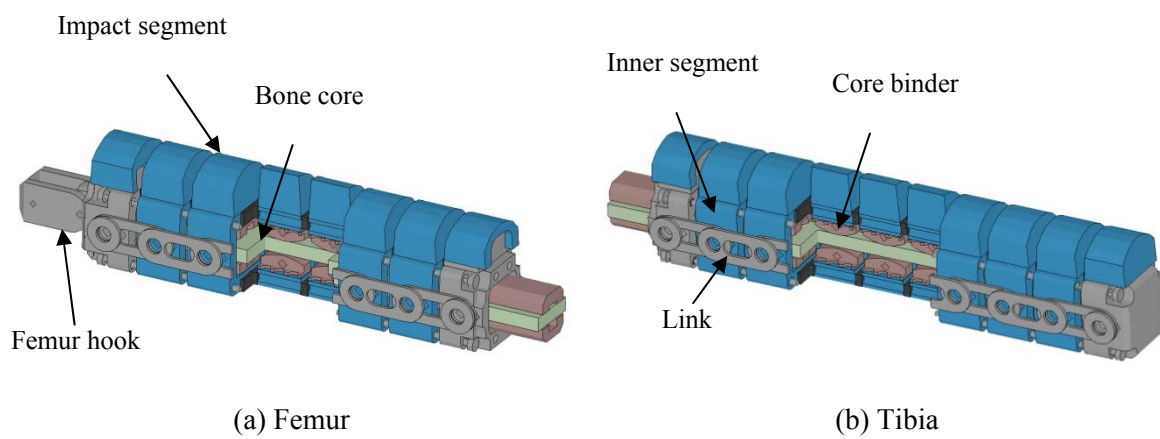


Figure 4: FLEX-PLI GTR femur and tibia models

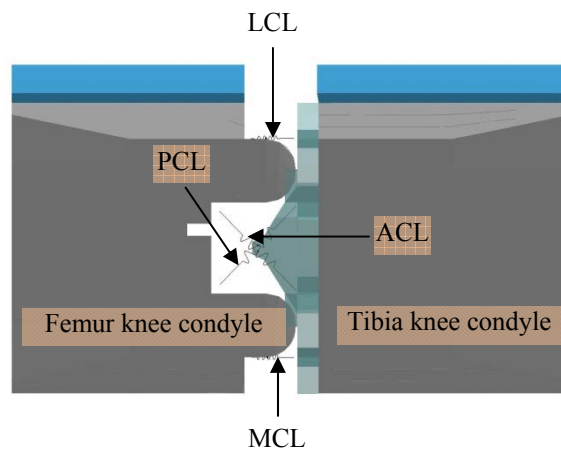


Figure 5: FLEX-PLI GTR knee model

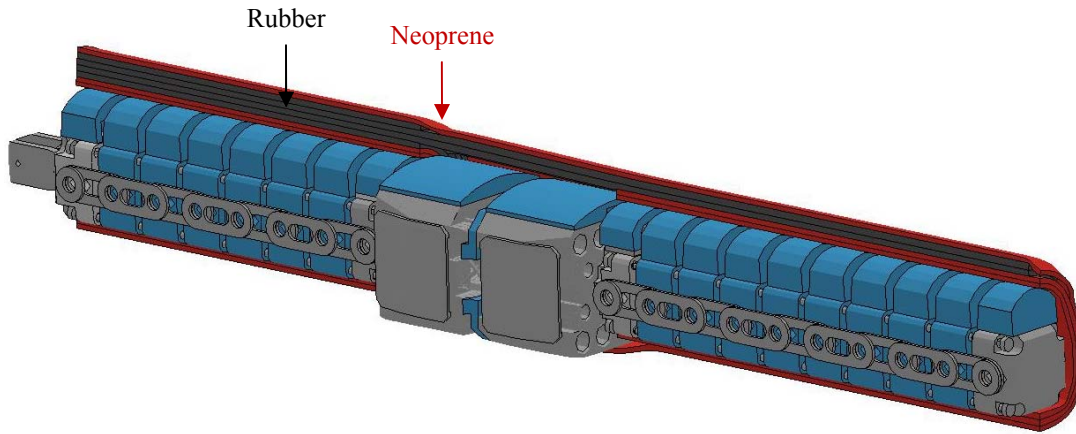


Figure 6: FLEX-PLI GTR flesh model

Table 2: Instrumentation and injury channels

Physical legform instrumentation modeled in the FLEX-PLI GTR CAE Models	Number of Channels
Knee ligament elongation: ACL, MCL, LCL, PCL	4
Femur Bending Moments: 1 (lower), 2 (mid), and 3 (upper)	3
Tibia Bending Moments: 1 (upper), 2 (mid-upper), 3(mid-lower) and 4(lower)	4
Tibia angular rate: ω_x , ω_y , ω_z	3
Femur angular rate: ω_x , ω_y , ω_z	3
Tibia top and bottom accelerations: a_x , a_y , a_z	6
Femur top and bottom accelerations: a_x , a_y , a_z	6
Knee acceleration: a_y	1
Total Channels	30

MODEL VALIDATIONS

Model assembly dynamic calibration validation:

The whole internal structure of the FLEX-PLI GTR was assembled from the calibrated femur, tibia and knee models and a model of the test jig was created according to the dynamic calibration test specification. As shown in Figure 7, the lower end of the tibia is connected to the jig via a pin joint and the leg is released to freely swing down from a position 15 degrees above horizontal. Additional ballast mass was attached to the femur end to reach injury threshold levels.

Calibration requirements are defined by peak value of knee MCL, PCL, ACL, and LCL elongations, three

femur bending moments and four tibia bending moments. The graphs in Figures 8 through 10 show that the FLEX-PLI GTR models satisfy all calibration requirements and also predicts the shape of output over time with great accuracy.

Full legform validation:

The FLEX-PLI GTR models were also evaluated for the performance at full legform level. A rigid flat impactor was used to impact the leg at different locations at an initial speed of 8 m/s. The physical legform was hung at the femur attachment hook with a quick release mechanism. The release provided quick detachment of the leg after initial impact contact. Three such cases (LC1, LC2, and LC6) are presented here as shown in Figure 11.

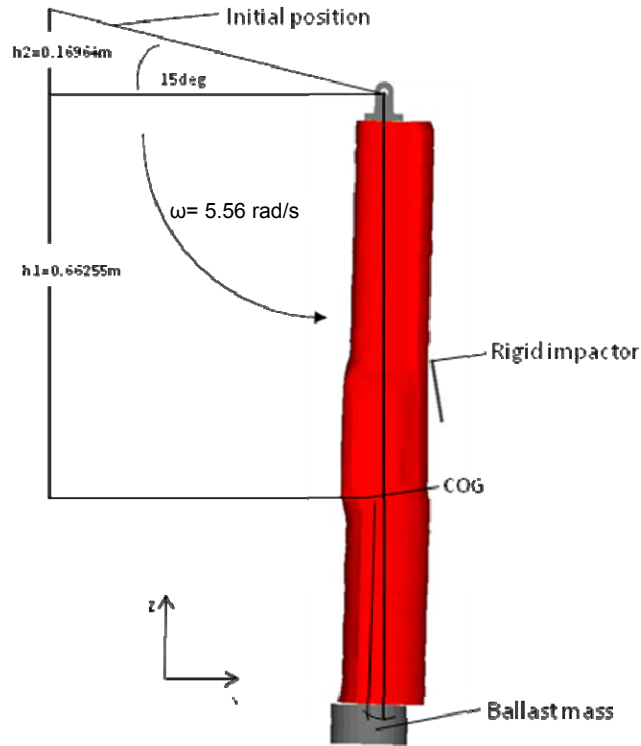


Figure 7: Assembly dynamic calibration setup

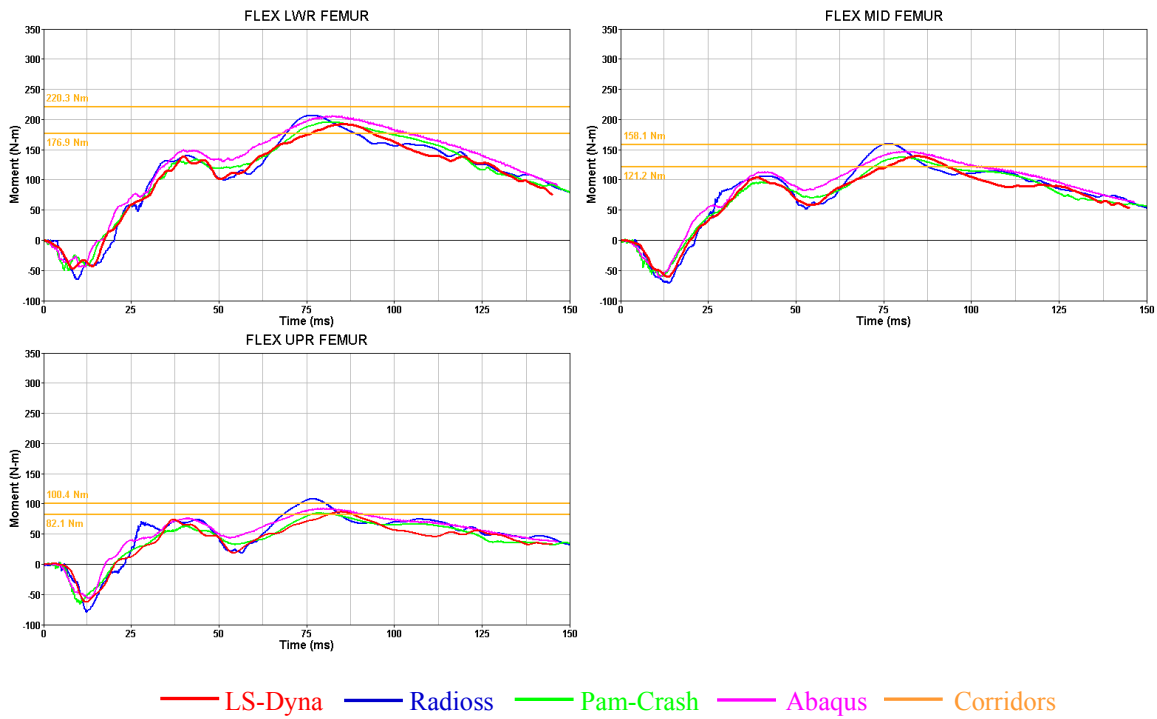


Figure 8: Assembly dynamic calibration femur moment results

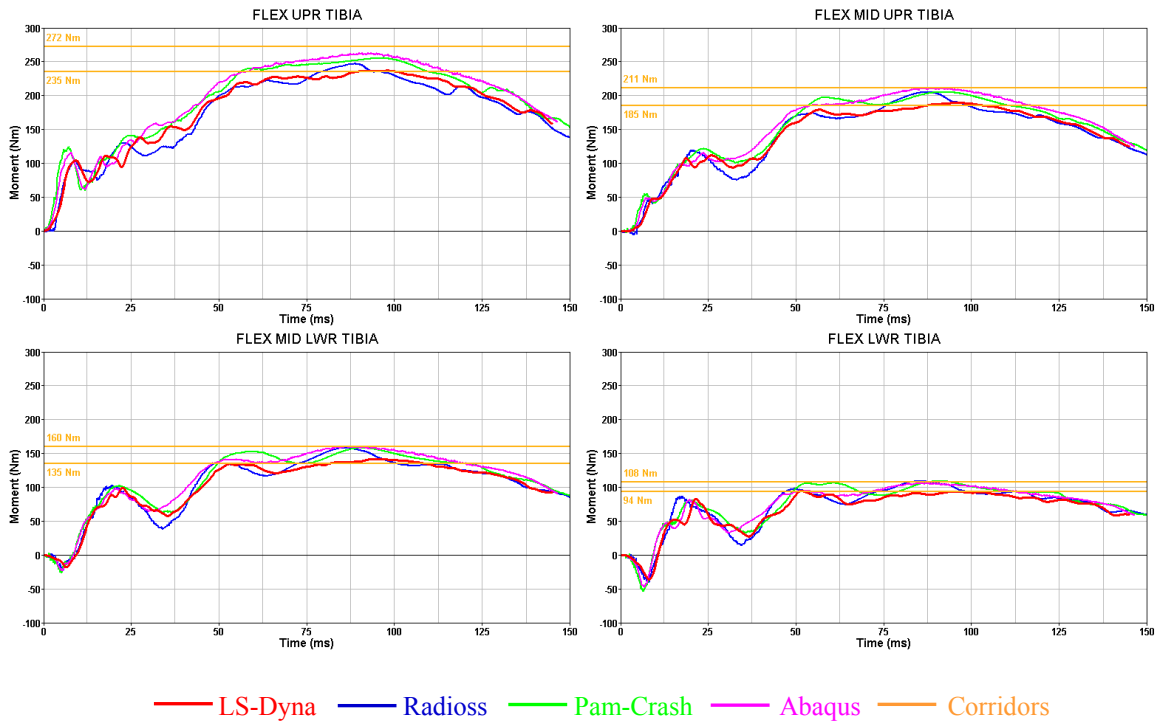


Figure 9: Assembly dynamic calibration tibia moment results

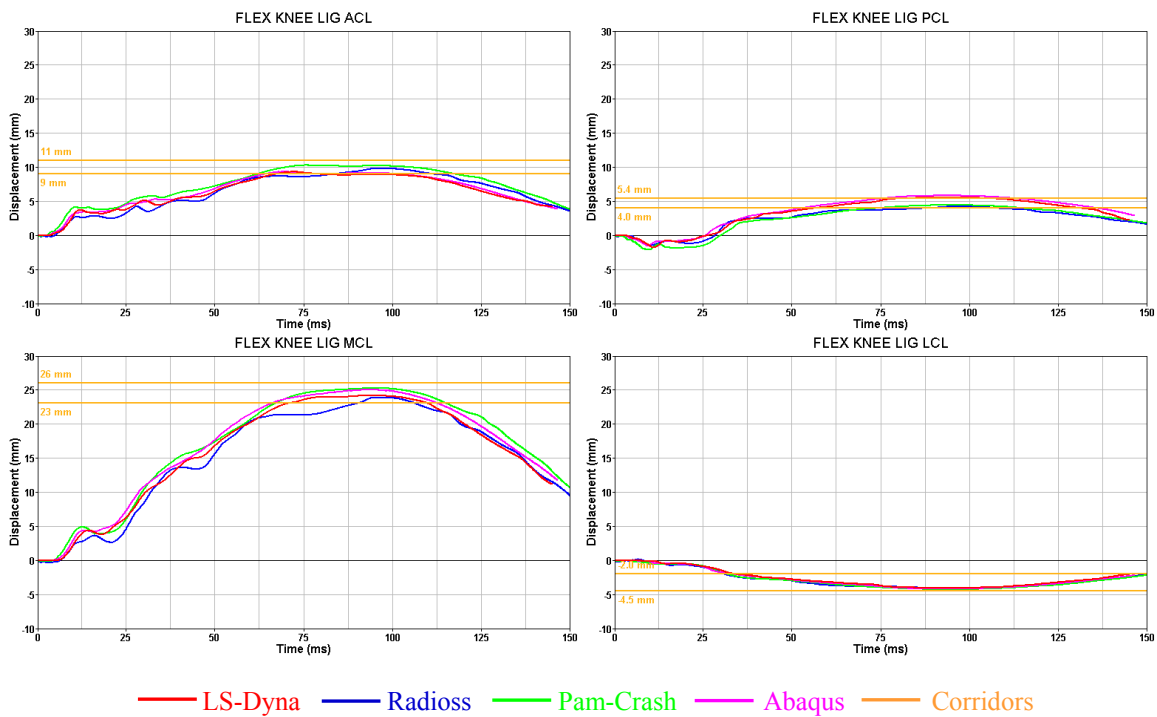


Figure 10: Assembly dynamic calibration knee ligament elongation results

The models were set up to mimic these tests and ligament elongations and bending moments are compared with test data. Results of the simulation output for the bending moments and knee ligament

elongations compared to test data for case LC1 is presented in Figures 12 through 14. Similar level of correlation was achieved for the other two load cases, LC2 and LC6.

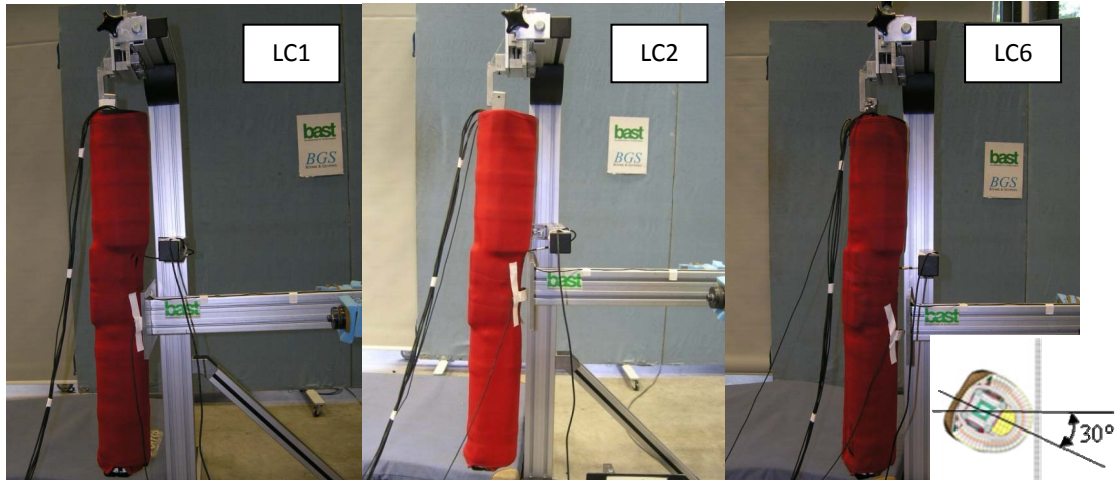


Figure 11: Full legform validation test setups

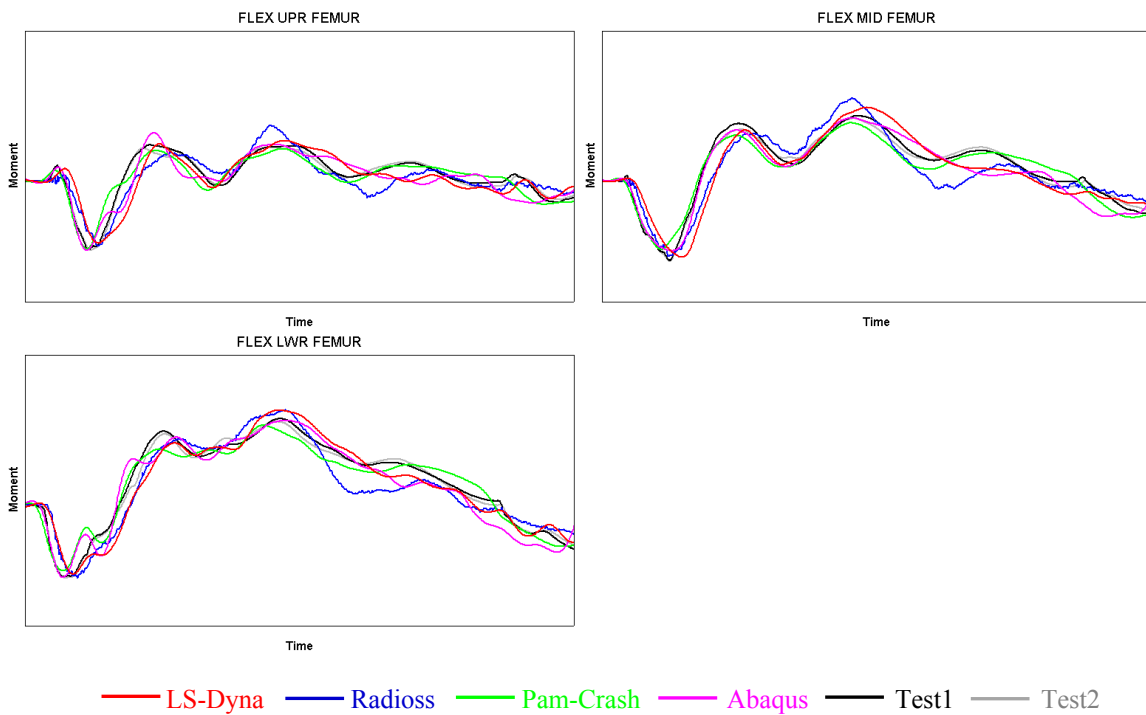


Figure 12: Full legform femur moment results for case LC1

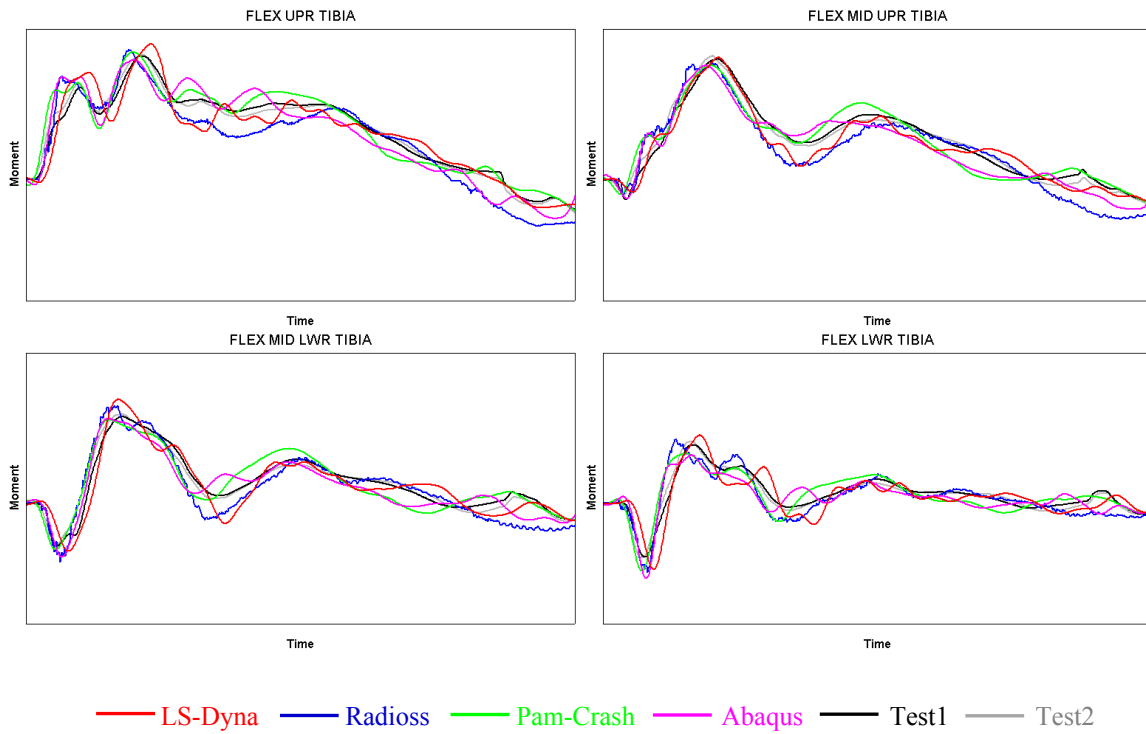


Figure 13: Full legform tibia moment results for case LC1

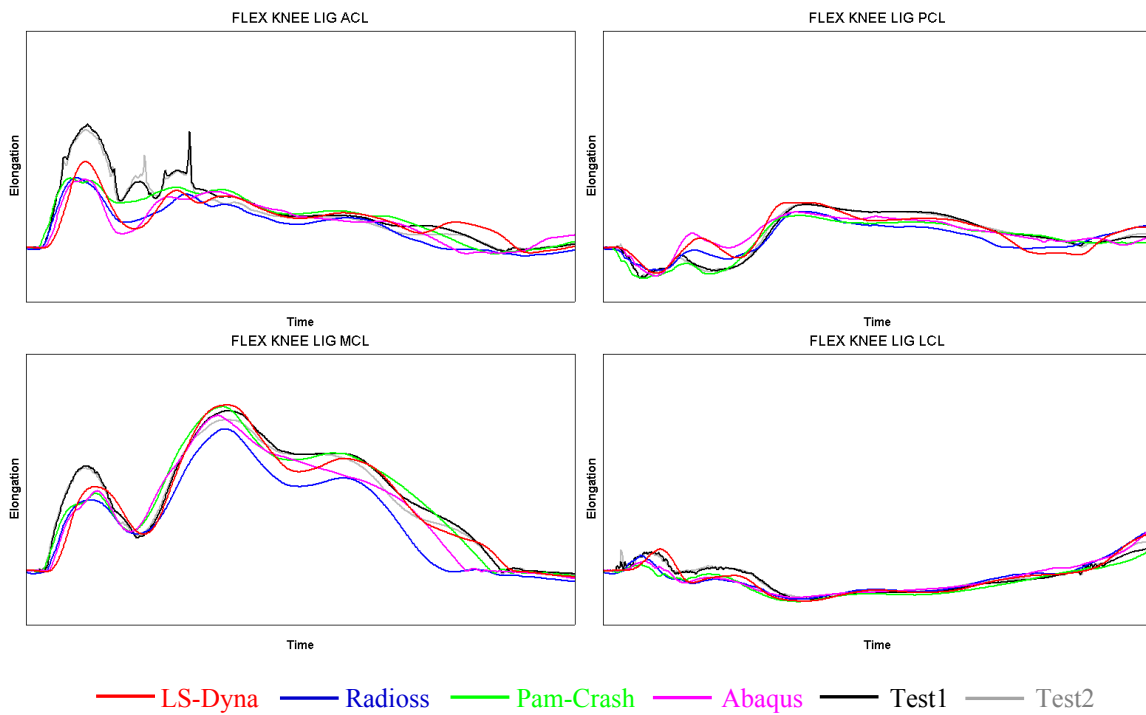


Figure 14: Full legform knee elongation results for case LC1

CONCLUSIONS

The following conclusions can be drawn from the current study:

- FLEX-PLI GTR CAE models in four widely used FE codes (LS-Dyna, Pam-Crash, Abaqus, and Radioss) are being successfully developed within an industry consortium.
- Excellent correlation of injury values were achieved for all validation cases.
- Majority of the peak value errors fell within 15% for all the validation cases.
- The models have an efficient CPU time.

ACKNOWLEDGMENT

The authors would like to acknowledge the FLEX-PLI GTR industry modeling consortium for supporting development of the models.

REFERENCES

- [1] European Enhanced Vehicle-safety Committee: EEVC Working Group 17 report (1998). "Improved test methods to evaluate pedestrian protection afforded by passenger cars".
- [2] Konosu A. and Tanahashi M. (2003) "Development of a biofidelic pedestrian legform impactor: Introduction of JAMA-JARI legform impactor ver. 2002", Proc. 18th ESV, Paper No. 378.
- [3] Konosu A. and Tanahashi M. (2005) "Development of a biofidelic Flexible Pedestrian Leg-form Impactor (FLEX-PLI 2004) and Evaluation of its biofidelity at the Component and at the Assembly Level", SAE paper No. 2005-01-1879.
- [4] UN/ECE/WP29/GRSP/INF-GR-PS/Flex-TEG (2008) "First Technology Safety Systems Design Freeze Status FLEX-PLI GTR Development Mechanical Design", TEG-054-Rev. 1, http://www.unece.org/trans/main/wp29/wp29wgs/wp29grps/pedestrian_FlexPLI.html

A SIMPLIFIED MODEL OF PEDESTRIAN UPPER LEGFORM IMPACT FOR ESTIMATE OF ENERGY-ABSORPTION SPACE UNDERNEATH BONNET LEAD

Bingbing Nie, Yong Xia, Jun Huang, Qing Zhou

State Key Laboratory of Automotive Safety and Energy

Tsinghua University

China

Paper Number 11-0014

ABSTRACT

Pedestrian upper leg impact protection is a challenging requirement in the Euro NCAP assessment. This study is aimed to develop a simplified model to provide a more reasonable estimate of the minimum energy absorption (EA) space underneath bonnet lead for upper leg impact protection. Typical shapes of upper legform impact response (the impact force vs. legform intrusion) are summarized. Then a simplified finite element model is built to represent the stiffness characteristics of vehicle front-end, especially for the local area around the bonnet leading area. Energy flow under different initial energy levels is analyzed using the simplified model. A feasible estimation on the EA space requirement for achieving specified Euro NCAP rating is established for upper legform tests.

INTRODUCTION

In the current pedestrian impact safety assessment test methods, the upper legform impactor is used to represent the human femur and pelvis in vehicle impacts. For vehicles with high front ends, e.g. SUVs, the bonnet and its leading edge are most frequent sources of injury [1]. However, compared to the pedestrian head impact protection and lower leg impact protection, there have been much fewer vehicle models that have received good scores in the Euro NCAP assessment test of the upper legform to bonnet leading edge [2]. Pedestrian upper leg impact protection is a quite challenging requirement.

The upper legform impactor consists of rigid front and rear members, with foam covered on the impact side [3]. The impactor is launched with a specified velocity and its motion is constrained by a guiding system. When contacting with the target vehicle, the upper legform moves only in the guided straight direction, representing the human femur and pelvis kinematics in real vehicle-to-pedestrian impacts [4][5].

The initial kinetic energy, velocity, and impact angle of the upper legform are specified on a look-up diagram in the test protocol based on the bonnet leading edge height (BLEH) and the bumper lead (BL) of the target vehicle. Proper spatial

arrangement and structure design of the parts underneath the bonnet lead will benefit the upper legform impact response [6]. Vehicle's styling and main styling related dimension parameters are usually determined at the very early stage in the vehicle development process, which then determine the initial kinetic energy level of the upper legform impact test. The pedestrian impact protection design is usually started in a later stage after the styling and components packaging designs are finalized or almost finalized. If the styling causes a high initial energy input for the upper legform impact, and/or the packaging does not leave sufficient EA space underneath the bonnet lead, the pedestrian protection design would be very difficult. Therefore, it is required to have a simple tool in the early vehicle development stage to estimate the required EA space for upper legform impact. The early development stage usually includes the styling and packaging designs, while most other detailed structural information may not be available.

In upper legform impacts, the sum of the impact forces and the peak bending moment measured in the main legform member are the injury indexes. The Euro NCAP test prescribes threshold values to the injury indexes for their assessment rating. In general, given the sum force below the threshold, the peak bending moment would always meet the requirement. For this reason, in this study, the impact forces are taken as the study object while the peak bending moment is only monitored. A substantial portion of the initial legform kinetic energy will be absorbed by the deformation of the vehicle body components around the impact area. The maximum displacement of the vehicle front-end structure in the impact direction is referred to as energy-absorption (EA) space.

To obtain a deep understanding to this problem, the impact response, characterized by the impact force vs. legform impactor intrusion and measured on the upper legform, should be analyzed. An ideal situation for achieving the minimum EA space underneath the bonnet lead is that the impact response is close to a square wave and the plateau force is close to the injury threshold.

Denote the initial kinetic energy of the upper legform

as E_{ini} , and the intrusion of the upper legform as D . In the Euro NCAP upper legform test rating, to get a full score, the sum of the impact forces should not be greater than 5 kN. As aforementioned, the initial kinetic energy level is determined by the geometrical parameters of vehicle front-end. Taking the highest initial energy input, 700 J, for an example, in accordance with the force requirement ($F \leq 5$ kN), the minimum EA space calculated from ideal square wave should be:

$$D_{min} = \frac{E_{ini,upper}}{F_{threshold}} = \frac{700 J}{5 kN} = 140 mm$$

(Foam compression neglected) (1).

However, both the deformations of the upper legform and the vehicle body components would contribute to the impact energy absorption. Considering that the foam compression in the early impact stage could only reach a much lower force level than the deformation of the vehicle body components in the later impact stage, in reality, it is impossible to achieve a square wave for the entire impact process. Therefore, a more reasonable approach is needed to calculate a more feasible minimum EA space requirement, and this is the objective of this study.

This paper documents the description of a simplified FE model to represent the structure stiffness characteristics of vehicle front-end and analysis of the energy flow during the impact process. Based on these analyses, it is aimed that the approach and model developed in this study can provide a more reasonable estimate of the minimum EA space underneath bonnet lead for given vehicle's front-end geometry to guide further vehicle structure design for pedestrian upper legform impact protection.

TYPICAL FORCE RESPONSE OF UPPER LEGFORM IMPACT TESTS

Figure 1 shows typical simulation results of upper legform impact on a sedan model in the middle position. In this simulation, the mass of the legform is 14.00 kg and the initial impact velocity is 9.77 m/s. The upper legform impact force response usually exhibits multi-peak characteristics. The three obvious peaks are in accordance with the first contact of the upper legform on the bonnet lead, the second and third impacts with the hard points underneath the bonnet lead. The sedan model used for generating the upper legform impact response is not designed for meeting the Euro NCAP requirement. The front-end structure is too stiff, resulting in the first force peak over the injury threshold. Besides, the space underneath the bonnet lead is not enough, resulting in the second and third force peaks over the

threshold as well. It indicates that the remaining kinetic energy of the legform is still high when it impacts with the hard points underneath the bonnet lead. To generate a more optimized impact force response, there must be sufficient EA space as well as adequate EA structure design.

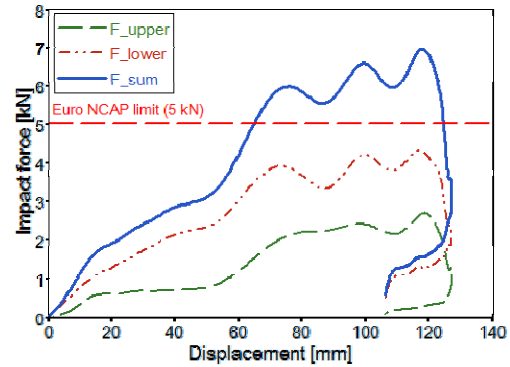


Figure 1. Typical upper legform impact response (14.00 kg, 9.77 m/s).

Although the under-bonnet structures around the upper legform impact area are very different from vehicle to vehicle, the upper legform impact responses share common characteristics. Based on test and simulation results of different vehicle models, the upper legform impact responses can be characterized by a piecewise linear approximation as shown in Figure 2. The corresponding mathematical expression is as below:

$$F(x) = \begin{cases} k_1(x - D_0) + F_0 & D_0 < x < D_1 \\ F_1 & D_1 < x < D_2 \\ k_2(x - D_2) + F_1 & D_2 < x < D_3 \\ F_2 & D_3 < x < D_4 \\ k_3(x - D_4) + F_2 & D_4 < x < D_5 \end{cases} \quad (2).$$

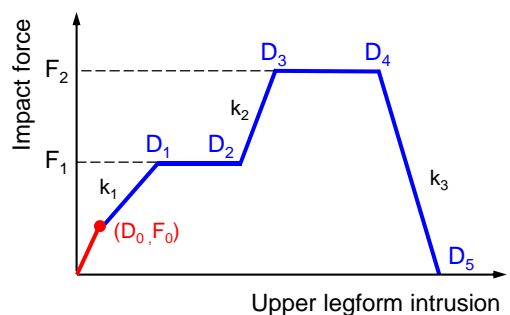


Figure 2. Piecewise linearity approximation of the upper legform impact response.

The initial soft contact stage ($0 \sim D_0$) is dominated by the foam characteristics. Since the legform foam is much softer than the vehicle bonnet lead, we assume that all the foam compression occurs before the

vehicle structure deforms. Thus the foam compression characteristics due to the upper legform impact with bonnet lead can be considered as independent of vehicle structure's characteristics. This deformation response phenomenon and the associated assumption have been confirmed by FE simulations of upper legform impact with various bonnet leads under various initial energy levels. Therefore, the value of D_0 and F_0 can be taken as constants regardless vehicle body characteristics.

The other parameters ($F_1, F_2, k_1, k_2, k_3, D_1, D_2, D_3, D_4, D_5$) are determined by vehicle front-end geometry and structural stiffness. Note that only 7 of them are independent parameters. All different combinations of the parameters can be divided into two groups: front multi-peak and front single-peak, as shown in Figure 3. Taking $F_1 > F_2$ for example, it indicates that the upper legform encounters a front peak during the impact.

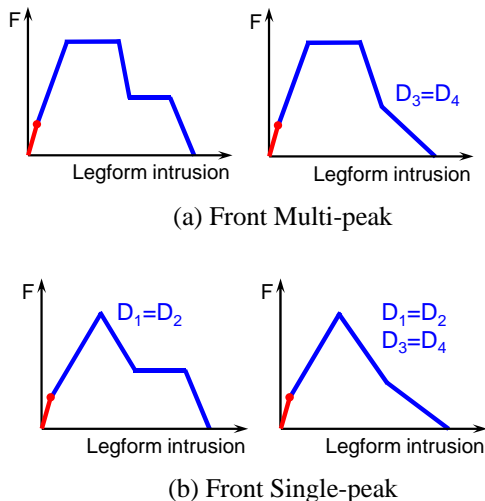


Figure 3. Possible shapes for characterizing upper legform impact responses ($F_1 > F_2$).

As aforementioned, the ideal square impact response is not realistic because of the initial soft contact. After that the force on the upper legform should reach a plateau as quickly as possible and maintain the plateau level till the legform rebounds. This is referred to as “semi-ideal” impact response, as shown by the solid line in Figure 4, and considered as the vehicle design target of upper legform impact response. In other words, the semi-ideal response represents the possible “best” structure in reality for upper legform impact. The semi-ideal response can be used to estimate a more realistic minimum EA space for achieving a good Euro NCAP rating score. Such generated EA space estimate should be taken as a lower limit for further vehicle model design.

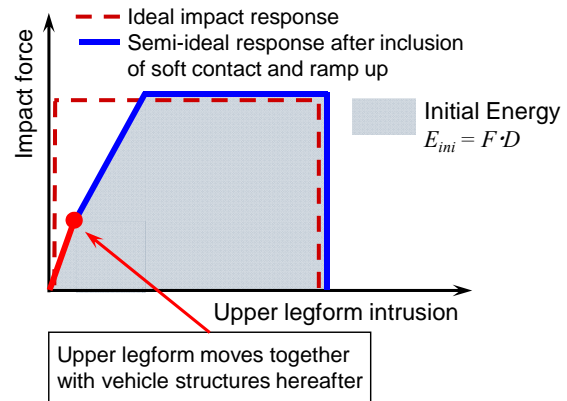


Figure 4. Vehicle design target of upper legform impact response (semi-ideal impact response).

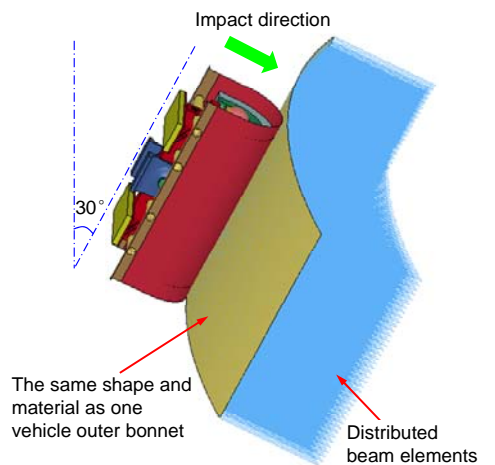
A SIMPLIFIED MODEL FOR ENERGY-ABSORPTION SPACE ESTIMATE

Setup of a simplified model

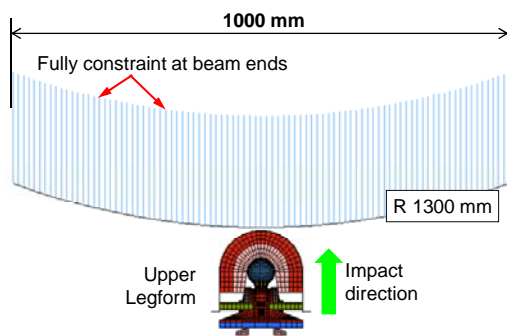
To fulfill the Euro NCAP rating requirement of the upper legform impact, only a small EA space underneath bonnet lead is needed if the vehicle front-end structure is well-designed. Although it is difficult to achieve such an ideal structure in practice, it can be considered as a design target. To estimate the minimum EA space requirement, a simplified model is built to represent equivalent structural stiffness of the vehicle front-end structure, a pretty ideal structure. The simplified model consists of beam elements and outer shell elements as a deformable panel, as shown in Figure 5. LS-DYNA finite element analysis software is used for the simplified model, the upper legform model, and the simulations. The upper legform model is developed and validated by Livermore Software Technology Corporation (LSTC) based on the pedestrian upper legform description in regulation EC No 631/2009. The outer shell elements represent the bonnet lead panel, primarily providing membrane force resistance to the upper legform impact. The beam elements represent the lump-sum, ideal and equivalent stiffness of the components underneath the bonnet lead and its deformation length represents the EA space provided by the vehicle structure.

The material and thickness properties of the shell elements in the model are adopted from the bonnet of a real vehicle model. Even though the bonnet structure properties are different from vehicle to vehicle, we feel it is appropriate to choose a typical one in the simplified model as the function of the shell elements is not as significant as that of the beam elements in terms of estimating the EA space. In the height direction, the shell panel has the same

length as the upper legform to provide a full support to the upper legform impact. The actual upper legform contact with the bonnet lead is around the middle section of the legform in tests, instead of a full contact. The full contact is a simplification and can also avoid some numerical difficulties caused by large deformation of soft solid elements in FE simulations. In the width direction, the shell panel is an arc with 1300 mm radius and 1000 mm width based on geometric characteristics of a real vehicle bonnet. The shell element size is 10 mm. The beam elements are particular to the shell elements' surface. Each of the shell element nodes is connected to a beam element. One end of the beams share nodes with the shells, and the other ends are constrained with *BOUNDARY_SPC option. The initial length of the beam elements is 200 mm, and the material model is *MAT_024 (elasto-plastic material) in LS-DYNA. The material properties (Young's modulus E and Yield stress σ_y) and geometrical parameters (beam diameter d) are design variables in further optimization to generate the most effective impact responses for EA space estimate with respect to different input energy levels.



(a) Axonometric view



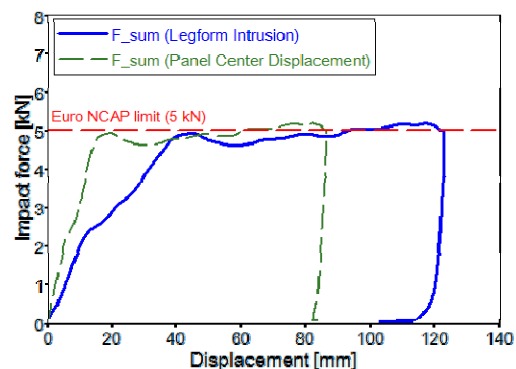
(b) Top view

Figure 5. The simplified model representing equivalent stiffness of vehicle front-end structure.

Energy-absorption space requirement

To fine tune the simplified model, the loading parameters from the upper legform are set to be 14.00 kg, 10.00 m/s, respectively, which is the upper limit of kinetic energy level (700 J) set in the Euro NCAP test protocol. The beam elements should have a quite high Young's modulus to ensure that the impact response has a quick ramp-up in the initial stage. However, if the Young's modulus is too high, it may cause force oscillations, which is not desirable. The yield stress of the beam material corresponds to the plateau force of the upper legform. In tuning the simplified model, the injury threshold for the peak impact force, 5 kN, is set as the plateau force level. A quick force ramp-up in the initial stage and a plateau force level at the injury threshold should render a minimum EA space.

By manual optimization, the values of the design variables for generating a semi-ideal impact response with 5 kN force limit can be determined. The simulation results and the corresponding parameter values are shown in Figure 6. The maximum displacement at the panel center is 86 mm (measured from the panel contact point), which is taken as the minimum EA space requirement by this semi-ideal model. This is obviously smaller than the estimated value of 140 mm based on equation (1). The upper legform intrusion is 122 mm (measured by the displacement of the rigid rear member of the legform in the impact direction). The difference between the two is mainly due to the outer legform foam compression, of which the maximum value is about 36 mm in the middle part. Therefore, 86 mm is the possible minimum EA space requirement to fulfill the Euro NCAP full score rating requirement.



Beam diameter d	0.10 mm
Young's modulus E	40.95 GPa
Yield stress σ_y	1.02 GPa
Tangent modulus $ETAN$	0.00
Possion ration ν	0.29

Figure 6. Upper legform impact response with semi-ideal simplified model.

Energy flow in upper legform impacts

During the impact process, the initial legform kinetic energy E_{ini} flows to the following sources:

- E_I : the energy absorbed by the deformation of the vehicle front-end structures
- E_2 : the energy absorbed by the deformation of the legform itself (mainly due to the compression of the outer foam)
- E_{UL} : the remaining kinetic energy of the upper legform
- E_{veh} : the kinetic energy of the vehicle

At any time during the upper legform impact process, the energy balance equation is:

$$E_{ini} = E_I + E_2 + E_{UL} + E_{veh} \quad \# (3).$$

For easy description, hereafter the analysis on energy flow is at time t_R when the upper legform starts rebound from the vehicle, and thus $E_{UL} = 0$ and $E_{ini} = E_I + E_2 + E_{veh}$. The energy flows calculated from the real sedan model simulation (Figure 1) and from the semi-ideal simplified model (Figure 5) simulation are shown in Table 1. Although the two models are not comparable in many aspects, the results in Table 1 show that the energy allocation by the simplified model is reasonable.

For the real sedan model, internal energy of the vehicle parts (E_I) due to part deformation accounts for most of the input energy of 450 J; while energy absorbed by legform foam compression (E_2) accounts for 160 J. Most of the vehicle parts get quite low velocity, which result in a low vehicle kinetic energy (E_{veh}) of about 35 J. As for the semi-ideal

simplified model, energy absorbed by the outer foam (E_2) increases to 255 J due to the regular geometric shape of the panel. This indicated that evenly compressed legform foam has a higher energy absorption capability. This is exactly why the required EA space 86 mm (Figure 6) is much smaller than the 140 mm value in equation (1) from ideal square wave estimation without foam consideration.

MINIMUM ENERGY-ABSORPTION SPACE REQUIREMENT UNDER DIFFERENT INITIAL ENERGY LEVELS

In the early stage of a vehicle development process, it is needed to estimate the minimum EA space required for upper legform impact protection. This may be done by using the simplified model developed in this study. The required EA space depends on the initial energy level of the upper legform. The parameters of the upper legform impact test, energy input, initial velocity, and impact angle, are determined by vehicle front-end geometric parameters: BLEH and BL. These styling related parameters are usually determined in the early stage as well. In the Euro NCAP look-up diagram, the BLEH and BL values are limited in the ranges of 550-1050 mm and 0-400 mm, respectively. Different combinations of the two parameters represent different front-end styling characteristics. Using 50 mm as an interval, in the ranges of BLEH and BL values, totally 99 cross combinations form the entire possible test parameter matrix. In the matrix, 70 pairs have non-zero initial energy input. These energy input levels are plotted in Figure 7 as the function of the impactor mass and initial velocity.

Table 1.
Energy flow comparison between a real sedan model and the simplified model

	Items	Sedan model	Simplified model
Simulation results	Initial energy E_{ini} [J]	668.17	700.00
	Impactor mass m [kg]	14.00	14.00
	Initial velocity v_{ini} [m/s]	9.77	10.00
	Rebound time t_R [ms]	25.0	22.5
	Legform intrusion D [mm]	144	128
Energy flow at t_R	Energy absorbed by vehicle structure E_I [J]	450	430
	Energy absorbed by legform E_2 [J]	160	255
	Kinetic energy E_{veh} [J]	35	0.4
	Hourglass energy [J]	30	10
	Energy summation E_{sum} [J]	675	695
	Difference between E_{sum} and E_{ini}	1.02%	-0.71%

The distribution shown in Figure 7 includes 13 groups. Some are scattered points and some are clustered points. These 13 groups are chosen as typical test points for upper legform impacts. In the cases of the clustered points, the center points of the clusters are chosen to represent the clusters, respectively. The simplified model is used to analyze these 13 typical cases and the results are shown in Table 2. The “Base” run refers to the parameter group for determination of the semi-ideal simplified model (Figure 6).

As aforementioned, in the Euro NCAP test protocol, the vehicle styling parameters determine initial

energy input. And the results in Table 2 clearly show the relationship between the initial energy levels and the required minimum EA space underneath the bonnet lead. In the semi-ideal simplified model (Figure 5), the legform foam is evenly compressed in the height direction, and the compression amount is definite. As verified in Table 2, the legform foam compression is equal to the legform intrusion (D) minus the EA space. For all the cases in Table 2, which are under different loadings, the legform foam compression amount is all approximately 40 mm. The relationship between the initial energy input and the EA space requirement is shown in Figure 8 (a). The solid line is the linear

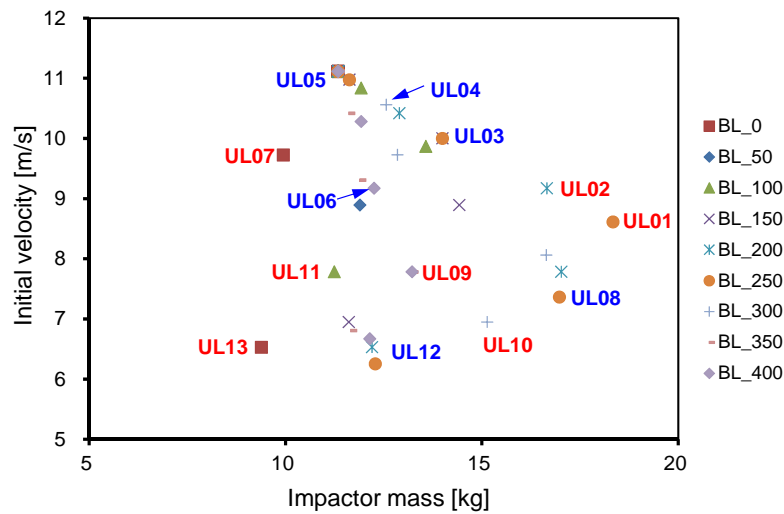
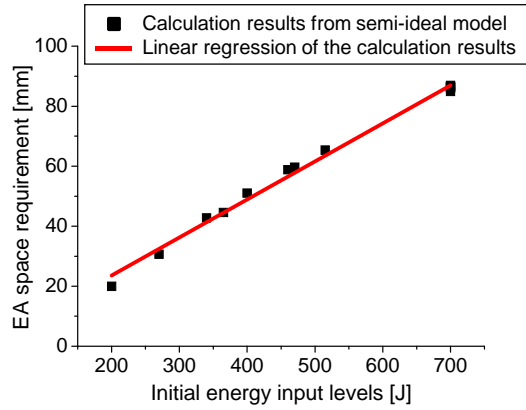


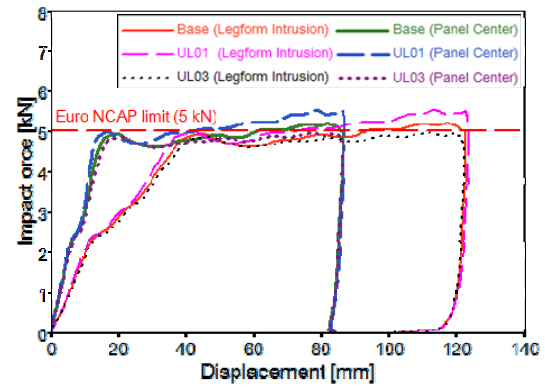
Figure 7. Distribution of all the test points for upper legform impacts.

Table 2.
Required minimum EA space for different impact energy levels

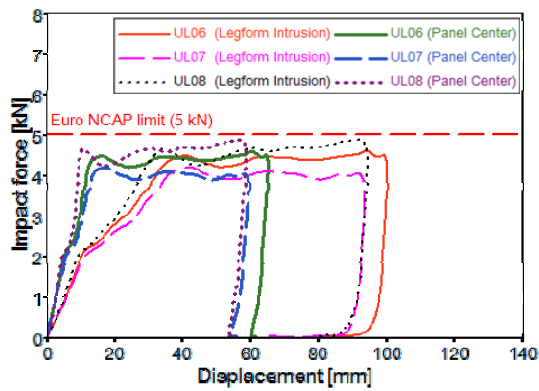
Case	E_{ini} [J]	m [kg]	v_{ini} [m/s]	D [mm]	$E_2(t_R)$ [J]	EA space [mm]
Base	700	14.00	10.00	127.8	257.9	86.5
UL01	700	16.66	9.17	128.6	258.0	86.9
UL02	700	13.82	10.06	127.7	256.0	86.5
UL03	700	12.57	10.56	127.4	255.6	86.4
UL04	700	11.34	11.11	126.8	254.1	86.1
UL05	700	18.34	8.61	126.8	254.0	84.9
UL06	515	12.26	9.17	105.5	215.5	65.4
UL07	470	9.94	9.72	98.9	202.4	59.7
UL08	460	16.98	7.36	99.6	206.0	58.9
UL09	400	13.22	7.78	90.7	189.5	51.0
UL10	365	15.14	6.94	84.0	178.0	44.6
UL11	340	11.24	7.78	81.6	173.2	42.8
UL12	270	12.15	6.67	69.4	156.3	30.7
UL13	200	9.39	6.53	57.7	135.4	20.0



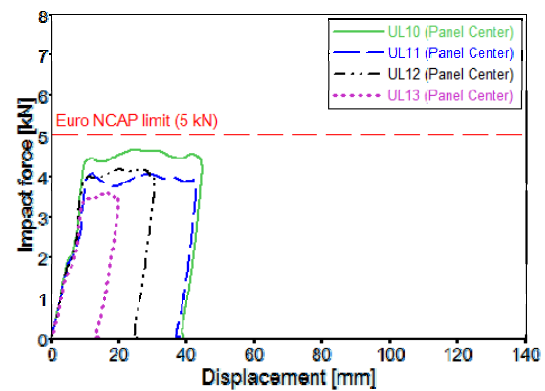
(a) Relationship between initial impact energy and EA space requirement



(b) Input energy 700 J



(c) Input energy from 460 J to 515 J



(d) Input energy lower than 400 J

Figure 8. Upper legform impact responses from the semi-ideal model.

regression of the calculation results. The minimum EA space requirement monotonically increases with the initial energy input.

Figure 8 (b) and Figure 8 (c) show the calculation results for the highest level (700 J) and the mid-level (from 460 J to 515 J) groups of initial energy, respectively. The impact responses exhibit similar shape with 5 kN peak force value as plateau. The results demonstrate that, for these two groups of the initial energy input, the semi-ideal simplified model behaves as expected for estimating the minimum EA space to fulfill the Euro NCAP full score rating requirement.

For the lowest level group of initial energy (lower than 400 J), Figure 8 (d) shows that the semi-ideal simplified model predicts the impact force from 3.6 kN to 4.6 kN, depending on the initial energy input levels. The prediction is lower than the 5 kN injury threshold, indicating that the calculated EA space may be further reduced for the 5 kN target. The reason for over-estimating the EA space is because the parameters of the semi-ideal simplified model

have been tuned for the initial energy level of 700 J (Figure 6). In the next steps, we will investigate if a simplified model applicable in a broader range can be developed.

CONCLUSIONS

Pedestrian upper leg impact protection design is related to the early stage of a vehicle product development process in at least two aspects. One is the front-end styling design since there are two styling related geometry parameters determining the initial impact energy level of the legform impactor, and a high initial energy input would require large energy absorption (EA) space underneath the bonnet lead. The other is the components packaging design underneath the bonnet where enough EA space should be reserved. In this study, a simplified model has been developed for analyzing the upper legform impact with the bonnet lead and for estimating the EA space requirement in the early stage of the vehicle development process when other structural details may not have been available. The simplified model represents equivalent vehicle

structure stiffness in the bonnet lead area where the upper legform impacts with the vehicle.

The model is referred to as the semi-ideal model. An ideal model represents a square-wave shape force-deformation response of the upper legform impact, while the semi-ideal model includes the legform foam soft contact stage and the initial ramp-up stage of vehicle structure stiffness. The impact response of the semi-ideal model consists of a quick force ramp-up in the early stage of the impact process followed by a force plateau close to the injury threshold force (Figure 6), which can be considered as the vehicle design target for obtaining the full rating score in the Euro NCAP upper legform impact test. It is possible to design an EA device placed underneath the bonnet lead such that the upper legform impact response follows that of the semi-ideal model. The response would be the lump-sum contribution from that of the legform, the vehicle bonnet lead and the EA device.

Using the simplified model, the upper legform impact force and intrusion can be calculated. For the initial energy level greater than 400 J (up to the highest limit of 700 J), the impact force is close to the 5 kN injury threshold of the Euro NCAP requirement, and the EA space underneath the bonnet lead can be estimated from the legform intrusion. For the initial energy level lower than 400 J, the EA space estimate value is greater than the needed since the simplified model is tuned for the high initial energy level.

The analysis results based on the simplified model have shown that the minimum EA space is linearly correlated with the initial energy level. This study also reveals that the compression of the upper legform foam can absorb roughly 20% - 40% of the total impact energy (Table 1), and therefore, the required EA space underneath the bonnet lead is only part of the total EA space. In the semi-ideal model, as a simplification, the legform is assumed to be in full contact with the impact target in the height direction (Figure 5). In real situation, however, the contact starts around the middle section of the legform and the contact area increases during the impact but may never reach the full contact area status, and so the foam contribution to the EA should be smaller than that calculated by the simplified model. Therefore the model only gives a lower bound of the EA space. Smaller contact area in real situation would require larger EA space underneath the bonnet lead for the 5 kN injury threshold. This also provides a guide in bonnet styling and structure design: making sure that the upper legform contact area with the bonnet lead as large as possible.

This study has provided a tool for estimating the EA space requirement underneath bonnet lead in the early stage of vehicle development. It may eliminate or reduce the iterations between styling design, packaging design and structure design for meeting the Euro NCAP upper legform impact performance requirement. In further study, more effort will be made on making the simplified model applicable in a broader range of initial energy levels and accounting for more realistic contact characteristics during the impact process. Designs of several embodied countermeasures will also be carried out to demonstrate the effectiveness of the EA space estimate based on the simplified model.

ACKNOWLEDGEMENTS

The authors would like to thank LSTC for providing us with the educational license of LS-DYNA. We also appreciate that Altair provides us with the educational license of HyperWorks.

REFERENCES

- [1] Longhitano D., Henary B., Bhalla K., Ivarsson J., Crandall J. "Influence of Vehicle Body on Pedestrian Injury Distribution". 2005 SAE World Congress, Paper Number 2005-01-1876, Detroit, Michigan, 2005.
- [2] Okamoto Y., Akiyama A., Okamoto M., Kikuchi Y. "A Study Of The Upper Leg Component Tests Compared With Pedestrian Dummy Tests". The 17th International Technical Conference on the Enhanced Safety of Vehicles (ESV), Paper Number 380, Amsterdam, The Netherlands, 2001.
- [3] Euro NCAP. Pedestrian Testing Protocol 5.1. <http://www.euroncap.com/>, 2010.
- [4] EEVC WG17 Report. "Improved Test Methods to Evaluate Pedestrian Protection Afforded by Passenger Cars". 2002.
- [5] Lawrence G., Hardy B. "Pedestrian Safety Testing Using the EEVC Pedestrian Impactors". The 16th International Technical Conference on the Enhanced Safety of Vehicles (ESV), Paper Number 98-S10-O-03, Windsor, Ontario, Canada, 1998.
- [6] Pinecki C., Zeitouni R. "Technical Solutions for Enhancing the Pedestrian Protection". The 20th International Technical Conference on the Enhanced Safety of Vehicles (ESV), Paper Number 07-0307, Lyon, France, 2007.

CAR BONNET EVALUATION AGAINST PEDESTRIAN HEAD IMPACT BASED ON A LUMPED MODELING APPROACH

Nicolas Bourdet

Caroline Deck

Rémy Willinger

IMFS, University of Strasbourg

France

Paper Number 11-0219

ABSTRACT

Nowadays, physical models of head used in pedestrian head impact standard tests are not accurate enough to represent the human head behavior and to assess the head injury risk in case of impact in a realistic way. In order to remove this technological barrier, the Strasbourg University Finite Elements Head Model (SUFEHM) is used in conjunction with a lumped model of the impact point at bonnet level in the present study. The approach consists in proposing a lumped model of the bonnet based on the experimental response of a pedestrian ISO headform impacting the bonnet surface at a velocity of 11 m/s and an impact angle of 60°. During this experimental tangential headform impact, both linear and rotational headform acceleration are recorded, and these data allow to characterize the stiffness, plasticity, energy dissipation as well as apparent mass of the bonnet lumped model. The model of the impact point at bonnet level consists of a rigid plate representing the bonnet impacted surface and connected to a fixed point by a general non linear spring. The non linear stiffnesses were implemented to the bonnet model in normal and tangential direction in terms of force-displacement. For this approach, the force was obtained by multiplying the acceleration by the headform mass and the displacement was derived from double integration of the headform acceleration. As a demonstrator the approach was conducted numerically on a car bonnet FEM which was impacted by an ISO headform FEM. The validation of the method consists in simulating the impact of the finite element model of the headform-bonnet lumped model and comparing its response to the headform FEM impact against the complete bonnet FEM simulation in terms of resultant linear and rotational acceleration. In a last step the SUFEHM is used for the simulation of the impact against the above defined bonnet lumped model in order to assess the injury risk for the impact point under study.

INTRODUCTION

In current standards and regulation, most head injury criteria such as HIC are based and developed from physical models that are now widely used [1,2,3]. Indeed, for the pedestrian protection

regulation, the European Enhanced Vehicle Safety Committee (EEVC WG10 and WG17) has developed test procedures to assess the level of pedestrian protection for vehicle fronts. The European directive (2003/102/EC) [1] consists of head impact, upper leg impact and lower leg impact.

The directive as well as the EuroNCAP pedestrian testing protocol [2] consider very simplified impactors, especially for the head. The headform used is a hemispherical object covered with an elastomeric skin. The injury criteria is the HIC (Head Injury Criterion) [4] is computed with the head linear acceleration components and the resultant value has to be below 1000 for an adult head for instance. Ueno and Melvin [5] as well as DiMasi *et al.* [6] found that the use of either translation or rotation alone may underestimate the severity of an injury. Zhang *et al.* [7] concluded that both linear and angular accelerations are significant causes of mild traumatic injuries. More recently, Deck *et al.* [8] conducted an in depth analysis on the contribution of rotational and linear acceleration under pedestrian accident conditions. It can be concluded that the rotational acceleration had a huge influence on both intracerebral loading and brain-skull relative motion, supposed to lead, respectively, to neurological injuries and subdural haematoma. As a conclusion, these authors unanimously suggested that any future head protection standard should integrate the rotational component in addition to the linear one in order to enable a realistic evaluation of the brain loading conditions and consequently of the head-injury risk prediction. A number of attempts towards improved head injury criteria have been reported in the literature both based on global parameters [9] and Finite Element (FE) modeling [10]. In the framework of EU project APROSYS SP5 'Biomechanics' in 2007 [11], improved head injury criteria based on a state of the art of head FE model have been developed in terms of skull strain energy, CerebroSpinal Fluid (CSF) pressure and brain VonMises stress respectively as injury parameters for skull fracture, subdural hematoma and neurological injuries.

The use of finite element models of the human head to test the pedestrian injury risk, will require characterization and modeling of the car bonnet. If this procedure is considered appropriate for use in standards and regulation, it reveals a major inconvenience about cost due to modeling and validation of the complete car bonnet. The aim of this study is to propose a lumped model of the impact point on the bonnet based on the experimental tests using a pedestrian headform. The final goal however is to include the numerical simulation using the finite element model of the head impacting the above defined lumped model for a more realistic head injury assessment.

MATERIAL AND METHOD

Insofar as the prediction of head injury is more accurate with injury criteria based on finite element modeling of the head, it is essential to have a model of the mechanical behavior of the impact point at bonnet. This mechanical characterization of the "bonnet point" will be a dynamic test using the ISO headform at an impact velocity close to the pedestrian standard tests, i.e. 11 m/s and an angle to define relatively to the impact surface. The ISO headform has to be equipped with a rotational velocity sensor in addition to the existing linear accelerometers. The idea in the present study is no longer having a biofidelic headform, but a reasonable mass, an inertia and a geometry with an initial velocity in order to characterize the impact point under shock conditions. A lumped model of the impact point is then developed from the headform experimental responses, in terms of inertia, elasticity, plasticity and absorbed energy along the normal direction and in term of friction along the tangential direction. In a final step, this lumped "bonnet point" model is coupled with the finite element model of the human head to assess the injury risk of the determined impact point.

Characterization of "bonnet point"

To demonstrate the feasibility of this study, a validated finite element model of a car bonnet has been used and illustrated in figure 2. The model

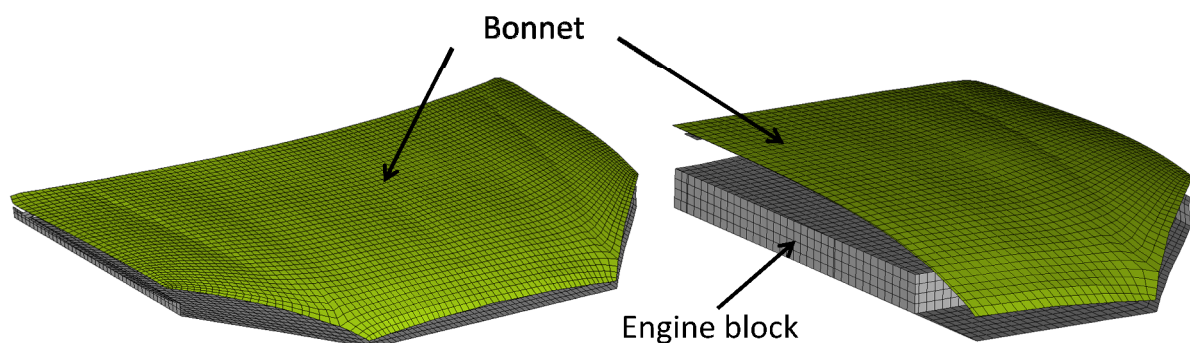


Figure 2. General view of the bonnet and the engine block.

was used in Tinard *et al.* [12] study and is consisted of an upper panel modeled by shell elements and an engine block considered as a rigid body. The material law of the upper panel used for the model is an elastoplastic material whose mechanical characteristics are reported in table 2.

Table 1. Mechanical properties of the bonnet FFE model.

ρ [kg.m ⁻³]	E [MPa]	ν	σ_e [MPa]	b [MPa]	n	σ_m [MPa]
2700	50000	0.3	60	567	0.6 2	65

The standard ISO headform model is represented in figure 1. It consists of an aluminum sphere, an aluminum plate and a rubber skin. Each part is modeled with an elastic law with values reported in table 2 in accordance with Lawrence [13]. The head model is made of 3020 solid elements.

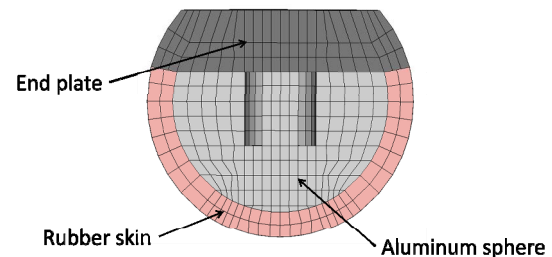


Figure 1. Standard ISO pedestrian headform model.

Table 2. Mechanical properties of the different parts of the pedestrian headform FE model.

	P [kg m ⁻³]	E [MPa]	ν
Rubber skin	1 950	7	0.4
Aluminum sphere	2 800	200 000	0.29
End plate	2 800	200 000	0.29

To illustrate the methodology allowing to develop the lumped parameter model of a "bonnet point", all data have been extracted from simulation based on finite element method. The numerical test consists in simulating the pedestrian standard test with an ISO headform as illustrated in figure 3.

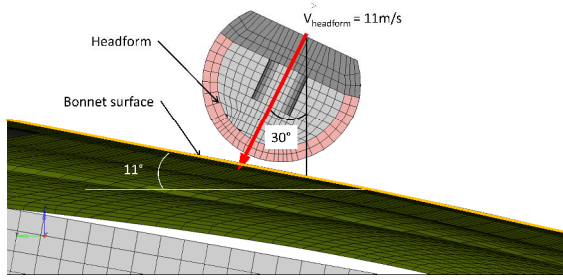


Figure 3. Illustration of the pedestrian standard test reproduce numerically.

As stated in the regulations, the headform impacts the bonnet surface with a 60° incline with horizontal. Considering the bonnet point as illustrated in figure 3, the tangent plane is 11° to the horizontal axis..

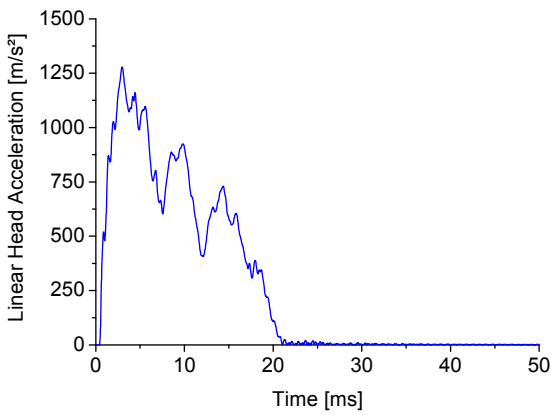


Figure 4. Representation of linear acceleration of the headform.

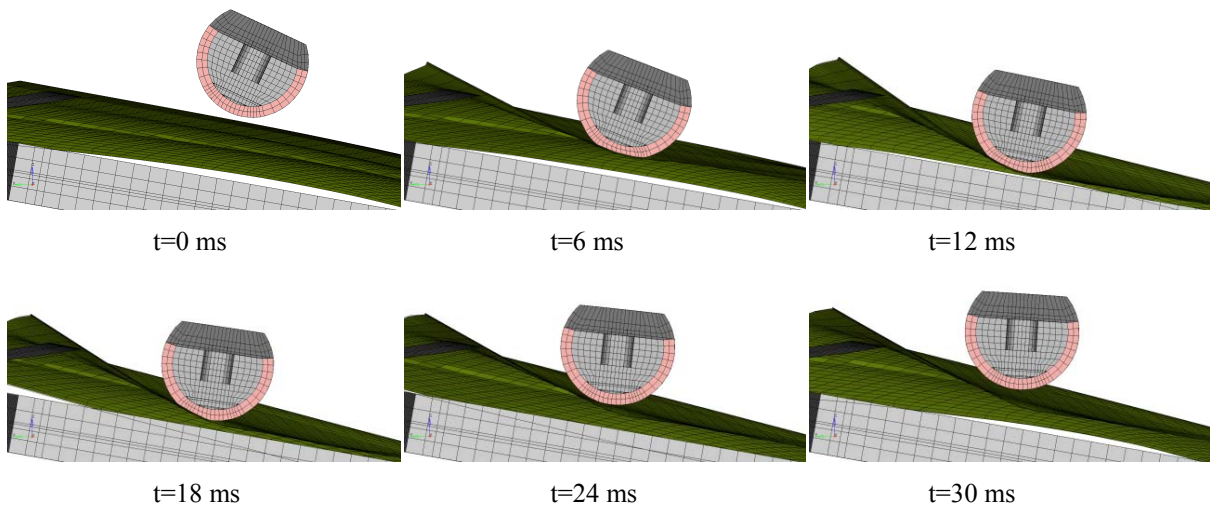


Figure 6. Simulation of the standard test using a pedestrian ISO headform on a bonnet.

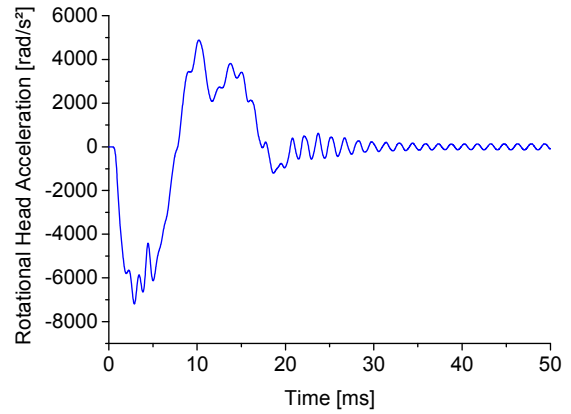


Figure 5. Representation of rotational acceleration of the headform.

The output data are extracted from the simulation in terms of linear and rotational accelerations at the headform center of gravity as plotted in figure 4 and figure 5. It should be recalled that in the final methodology this step will obviously be conducted experimentally only.

Subsequently, these output data are the components that constitute the input to the characterization and modeling step of the lumped "impact point" model.

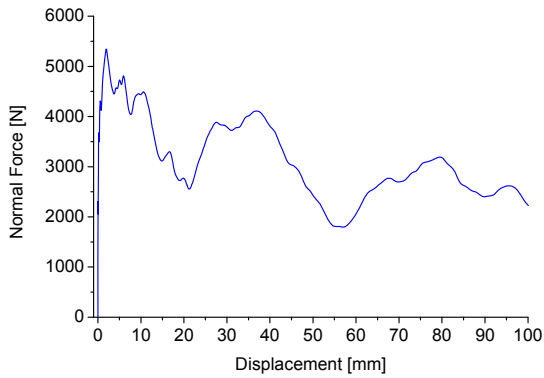


Figure 7. Representation of the normal force-displacement behavior of bonnet impacted by a headform of 4.5 kg at 11 m/s inclined of 19° with normal of the impacted surface.

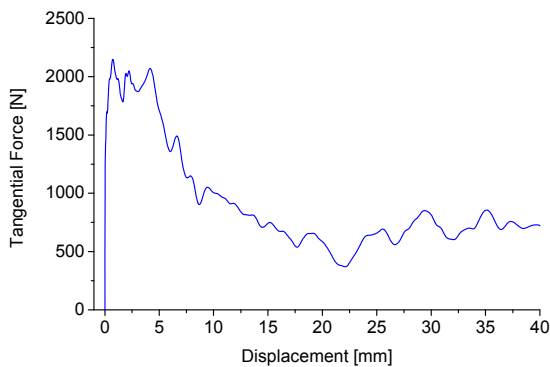


Figure 8. Representation of the tangential force-displacement behavior of bonnet impacted by a headform of 4.5 kg at 11 m/s inclined of 19° with normal of the impacted surface.

For the lumped model parameters identification, first the normal behavior of the impact was obtained by projecting the headform acceleration to the normal axis of the bonnet surface and multiplying it by the head mass of 4.5 kg. The normal acceleration was double integrated to get the bonnet deflection. The force-displacement curve can then be plotted as shown in figure 7 and represents therefore the normal behavior of the bonnet. In a similar way, the tangential behavior is extracted from the linear acceleration projected on the tangential axis and plotted in figure 8.

Lumped model of “bonnet point”

The modeling of the "bonnet point" by a lumped parameter model consists of a rigid plate with a mass located at its center of gravity linked to the reference space by a generalized nonlinear spring, as illustrated in figure 9. The rigid panel is constrained in rotation in three axes and in translation along the transversal axis. At the spring element, only normal and tangential linear stiffness are implemented in the model. Those stiffnesses are extracted from the force-displacement behavior of the bonnet point after the headform impact

experiment (or simulation in this study). Concerning the rigid panel, it is modeled in shell elements with a thickness of 0.1 mm and a concentrated mass at the node linked to the spring element of 1e-7 kg. The choice of a low mass was done to avoid an initial force caused the inertia effect of the panel at contact moment of the head on the plate. Nevertheless, it is needed to adapt the force-displacement curves for the spring element to apply due to non-zero mass at the rigid panel recommended for the finite element computation. The simplified force-displacement curves modeling the “bonnet point” are represented in figure 10 and figure 11.

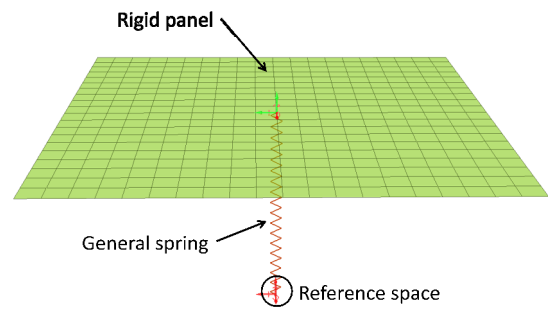


Figure 9. Illustration of the « bonnet point » lumped model.

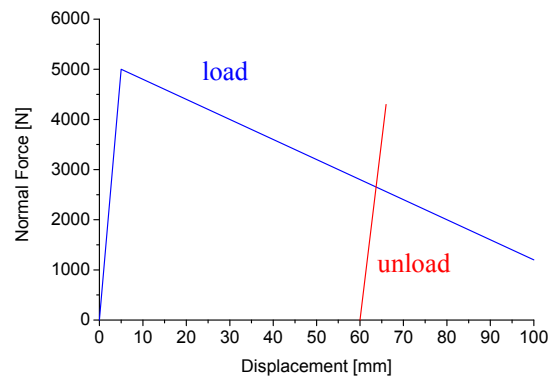


Figure 10. Representation of the normal force-displacement curve implemented in the spring element.

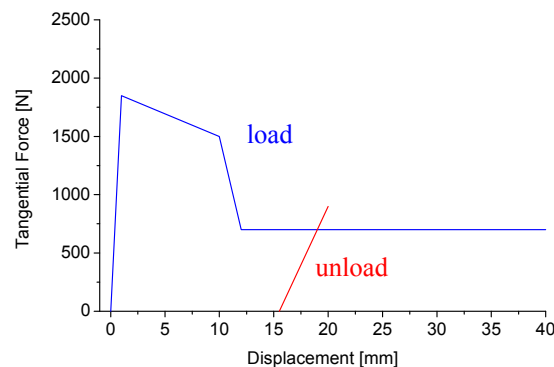


Figure 11. Representation of the tangential force-displacement curve implemented in the spring element.

The validation of the lumped parameter model of the "bonnet point" was carried out by impacting the headform inclined of 60° with the horizontal axis on the rigid panel with a velocity of 11 m/s as illustrated in figure 12. The computed responses are the linear and rotational accelerations of the headform as well as the plate deflection and the headform velocity.

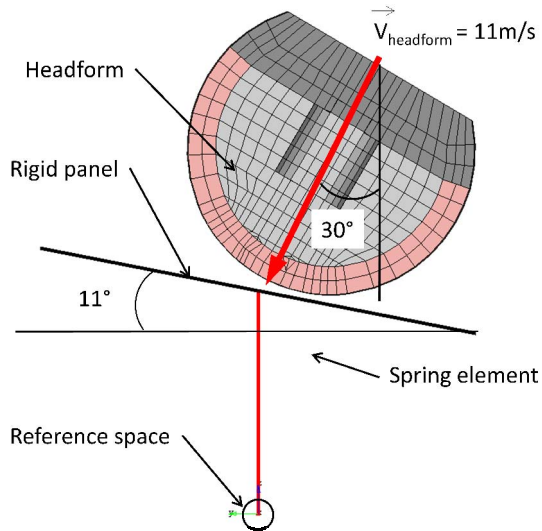


Figure 12. Representation of initial conditions of the headform to validate the "bonnet point" lumped model.

RESULTS

Figure 15 shows the simulation animation of the impact. The linear and rotational accelerations of the headform are superimposed on those extracted from the numerical simulation of the standard test with the finite element model of the complete bonnet and are plotted in figure 13 and figure 14. A good accordance of the headform accelerations can be observed, demonstrating a realistic lumped model of the "bonnet point". The linear acceleration pulse is a little bit shorter for the lumped model compared to the finite element model one. The

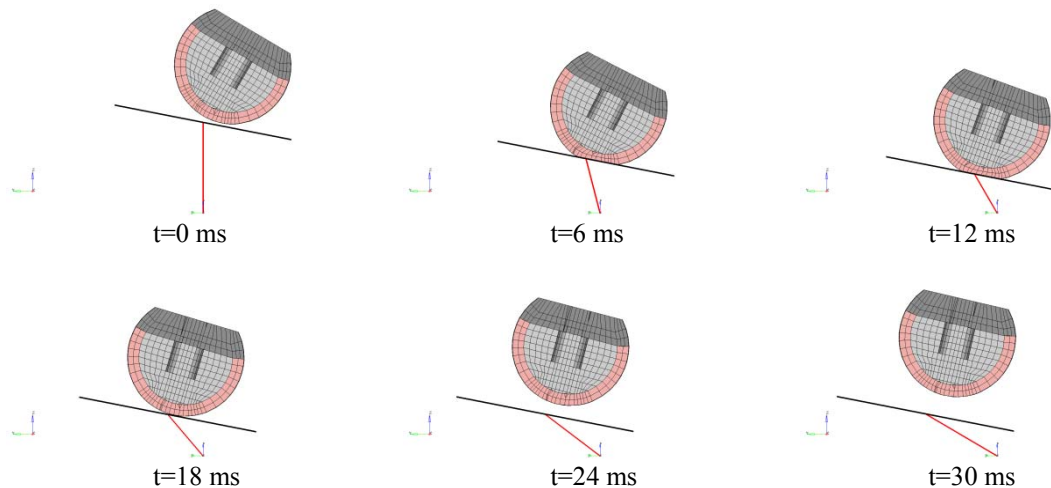


Figure 15. Simulation of the headform impact with the lumped "bonnet point" model.

maximum linear acceleration is 134 g for the lumped model compared 130 g for the finite element model, i.e. a 3 % deviation. Both calculated HIC are also very close with a HIC of 938 for the lumped model against a HIC of 927 for the finite element model, i.e. a 1.2 % deviation.

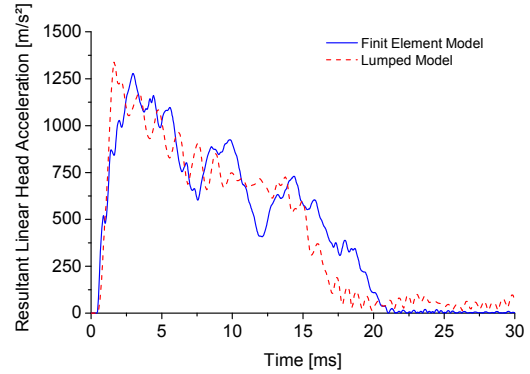


Figure 13. Superimposition of the linear headform accelerations computed with the FE and lumped bonnet model.

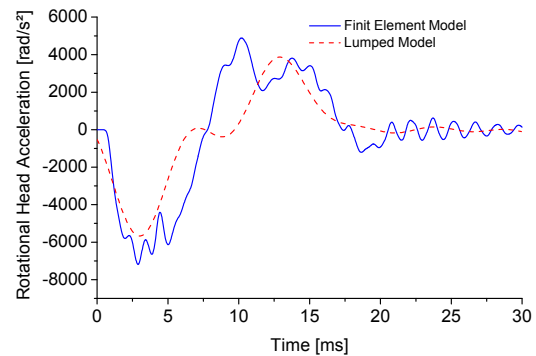


Figure 14. Superimposition of the rotational headform accelerations computed with the lumped and FE bonnet model.

Concerning the rotational acceleration, the deviation is slightly higher (about 10%) as illustrated in figure 14. This difference can be observed in figure 16 in terms of rotational velocity. However the shape of the curve is in accordance with the result from the full finite element simulation. The final rotational velocity is about 5 rad/s for the lumped model compared to 6 rad/s for the finite element model. The deflection of the rigid panel reached 65 mm which is in accordance with the result from the complete bonnet, as illustrated in figure 17.

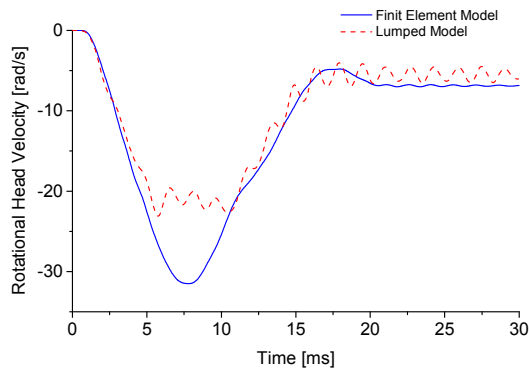


Figure 16. Superimposition of the headform rotational velocity computed with the FE and lumped bonnet model..

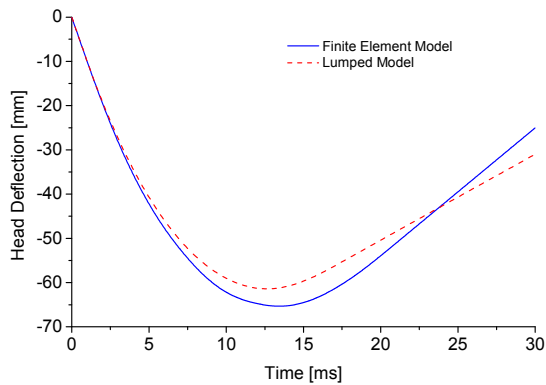


Figure 17. Superimposition of the headform displacement computed with the FE and lumped bonnet model.

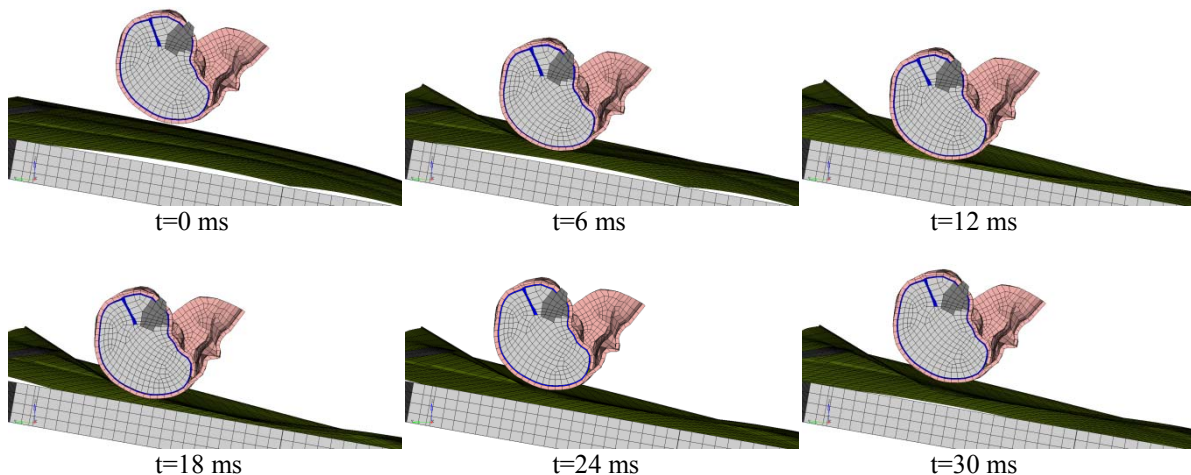


Figure 20. Simulation of the SUFEHM impact against the bonnet FE model

The final step of the novel methodology presented in this study is to use the head finite element model of Strasbourg University (SUFEHM) to compare the lumped model of "bonnet point" with the complete finite element model of bonnet in terms of intracerebral injury risk. This step aims at validating fully the lumped model as the bonnet FE model is only a research step which will not be conducted in the test method under development. The SUFEHM model developed by Kang *et al.* [14] and validated by Willinger *et al.* [15] was propelled frontally against the finite element model of the full bonnet at the same impact point as previously with ISO headform as illustrated in figure 18.

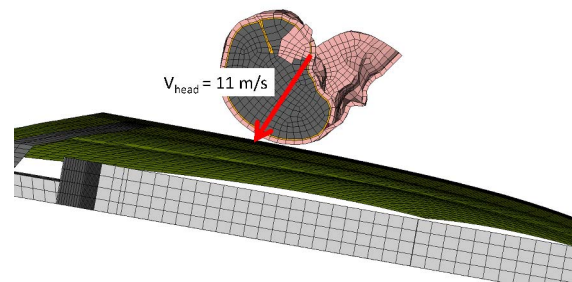


Figure 18. Initial condition for the impact of the SUFEHM on the finite element model of the bonnet.

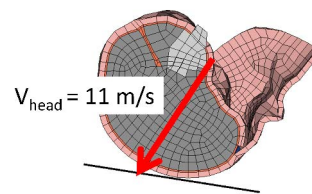


Figure 19. Representation of the initial condition for the impact of the SUFEHM on the lumped model of the bonnet.

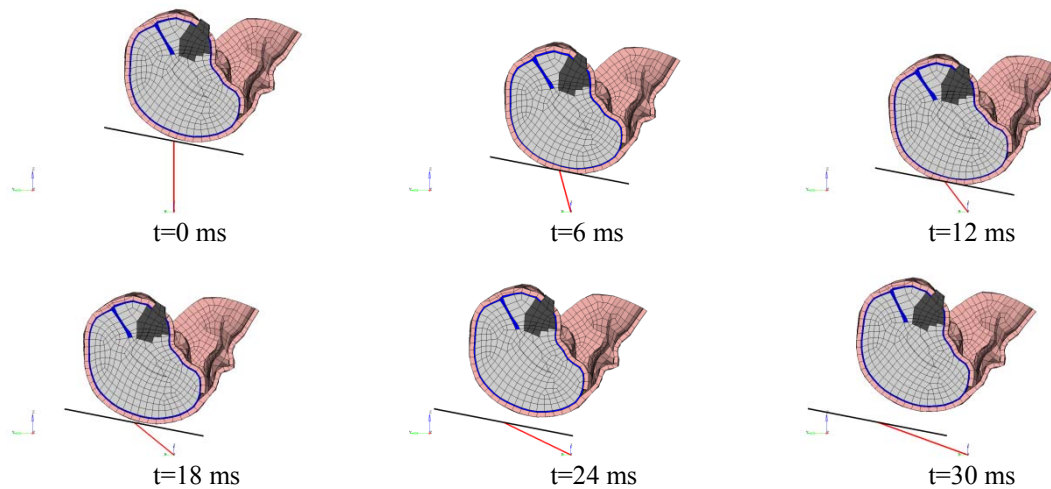


Figure 21. Simulation of the SUFEHM impact against the lumped bonnet model

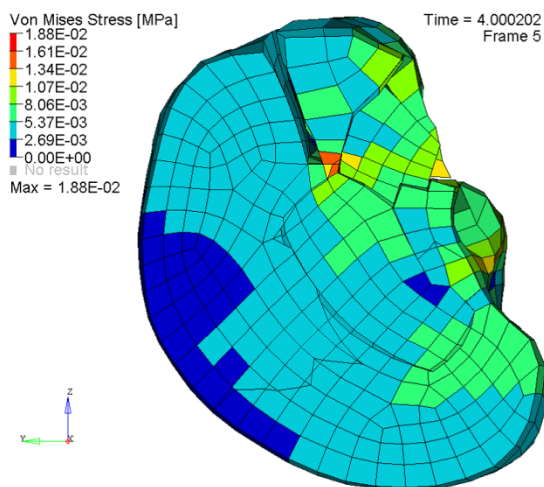


Figure 22. Representation of intracerebral Von Mises Stress in case of impact of the SUFEHM with FE bonnet model.

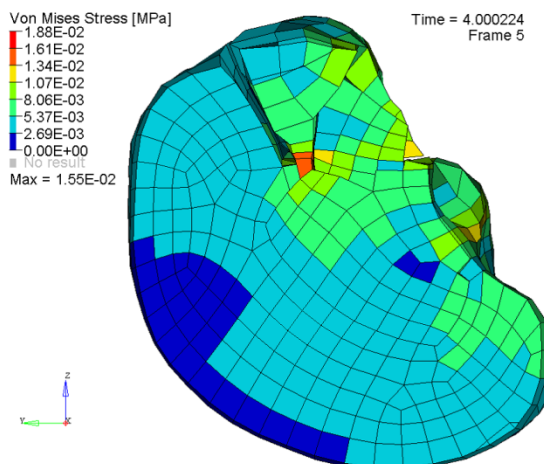


Figure 23. Representation of intracerebral Von Mises Stress in case of impact of SUFEHM with lumped model.

Figure 20 and figure 21 show the simulations of the impact between respectively SUFEHM vs bonnet finite element model and SUFEHM vs lumped bonnet model. Both simulations are in very good

accordance. It can be observed that the Von Mises Stress distributions are very similar. The maximum stress appears at same location and at same moment, as illustrated in figure 22 and figure 23. The stress is slightly lower for the lumped model of the “bonnet point” than for the full FE bonnet model as reported in table 3. Consequently, the risk of neurological injury is slightly underestimated 0.9% for bonnet point against 3.4% for FE bonnet.

On the contrary, the intracranial pressure for cerebrospinal fluid is higher leading to a risk of hematoma injury of 22.1% for the lumped bonnet model compared to 19.6% for FE bonnet model, as reported in table 4.

Table 3. Comparison of neurological injury risk computed with FE and lumped bonnet models.

	Brain Von Mises Stress [kPa]	Neurological Injury Risk [%]	
		Moderate	Severe
FE Bonnet	18.8	3.4	1.5
Bonnet Point	15.5	0.9	0.5

Table 4. Comparison of hematoma injury risk computed with FE and lumped bonnet models.

	CSF Pressure [kPa]	Hematoma Injury Risk [%]
	FE Bonnet	-115.5
Bonnet Point	-117.6	22.1

DISCUSSION

Limitation of the existing head pedestrian standard test is often discussed as it is carried out with a very simple headform and a calculated injury criterion (HIC) which doesn't take account rotational effect. An intensive use of the head finite elements modelling allowed to propose more accurate injury criteria of the head. This model can be coupled to the impact point models in order to simulate the direct impact for a more realistic head injury

assessment. This novel approach needs to characterize and model the impacted structure.

In the present study it is proposed to model the bonnet impact point by a lumped model. This modeling is based on the experimental standard test including a rotation velocity sensor fitted to the headform. In order to check the feasibility of such a procedure, this experimental step has been simulated numerically only in the present study. In a further step a complete experimental versus numerical approach of the method should be conducted.

The main limitation of the study is the surface contact which does not represent the real contact caused due to the fact that the normal direction is unchanged. It results to a tangential effect which is not perfectly reproduced and has to be improved. Nevertheless, the linear components from the lumped model simulation are in accordance with the complete bonnet one with a 3% deviation only.

The fact that this feasibility is only carried out with finite elements modeling constitutes another limitation of this study. To complete this work, the use of experimental data from tests carried out on real bonnets has to be done.

CONCLUSION

The approach which consists in modeling the impacted "bonnet point" by a lumped parameter model whose properties are identified from the standard experimental headform tests will contribute to evaluate more realistically the bonnet protective performance through the coupling of the method with the human head associated with more accurate injury criteria.

The first results are very encouraging since the impact simulation of a head finite element model on both, the full FE and lumped models of the bonnet lead to a very similar head injury risk assessment. The next step will be to conduct a full experimental versus numerical evaluation of a given bonnet, before going further towards a new test method proposal.

Acknowledgement

This work has been developed with the French project Amélioration Sécurité Piéton (ASP).

REFERENCES

1 Directive 2003/102/EC of the European Parliament and of the Council, November 2003.

2 EuroNCAP Pedestrian Testing Protocol, EuroNCAP, 2004.

3] ECE 22 05, Uniform provision concerning the approval of protective helmets and their visors for driver and passengers of motor cycles and mopeds, 2002.

4 J. Hutchinson, M.J. Kaiser, H.M. Lankarani, The head injury criterion (HIC) functional, *Applied Mathematics and Computation*, 96 (1998) 1-16.

5 K. Ueno and J.W. Melvin, Finite element model study of head impact based on Hybrid III head acceleration: the effects of rotational and translational acceleration, *J. Biomech. Eng.* 113 (1995), pp. 319–328.

6 F. DiMasi, R.H. Eppinger, and F.A. Bandak, Computational analysis of head impact response under car crash loadings, *Proc. of the 39th STAPP Car Crash Conference*, 1995, pp. 425–438.

7 L. Zhang, K.H. Yang, and A.I. King, A proposed injury threshold for mild traumatic brain injury, *J. Biomech. Eng.* 126 (2004), pp. 226–236.

8 C. Deck, D. Baumgartner, and R. Willinger, Influence of rotational acceleration on intracranial mechanical parameters under accidental circumstances, *Proc. of the IRCOBI Conference*, Maastricht, The Netherlands, 2007, pp. 185–197.

9 J.A. Newman, N. Shewchenko, and E. Welbourne, A proposed new biomechanical head injury assessment function—The maximum power index, *Proc. of the 44th STAPP Car Crash Conf. SAE 2000-01-SC16*, 2000.

10 L. Zhang, K.H. Yang, R. Dwarampudi, K. Omori, T. Li, K. Chang, W. Hardy, T.B. Khalil, and A.I. King, Recent advances in brain injury research: a new human head model development and validation, *Proc. of the 45th STAPP Car Crash Conference*. 45 (2001), pp. 369–393.

11 C. Deck, M. Neale, and R. Willinger, APROSYS SP5.1.1.b report, Improved model based head injury criteria, 2007.

12 V. Tinar*, C. Deck, F. Meyer, N. Bourdet and R. Willinger, Influence of pedestrian head surrogate and boundary conditions on head injury risk prediction, *International Journal of Crashworthiness* Vol. 14, No. 3, June 2009, 259–268

13 G.J.L. Lawrence, Assessment of the FTSS 4.5 kg aluminium headform as a possible alternative for EEVC WG17, Report S222C/VF—Pedestrian Protection Procedures, 2005.

14 H.S. Kang, R. Willinger, B. Diaw, and B. Chinn, Validation of a 3D anatomic human head model and replication of head impact in motorcycle

accident by finite element modelling, Proc. of the 41st STAPP Car Crash Conference, 1997, pp. 329–338.

15 R. Willinger, H.S. Kang, and B. Diaw, Three-dimensional human head finite element model validation against two experimental impacts, Ann. Biomed. Eng. 27 (1999), pp. 403–410.

DYNAMIC PROPERTIES OF HUMAN CANCELLOUS BONES

Sudipto, Mukherjee
Anoop, Chawla
Kartik, Marwah
Lucky, Grover
Joel, Keishing

Mechanical Engineering, Indian Institute of Technology Delhi
India
Paper Number 11-0429

ABSTRACT

A micro drop system consisting of an impactor supported by twin parallelogram linkages was designed to enable guided drop height as low as 10mm. The system has been used to measure dynamic compressive response of human cancellous bone for strain rates of 135/s, 150/s and 175/s. The percentage variation of Young's modulus from its mean value of 0.083GPa obtained at these strain rates is 54.5%, which is significant, suggesting that bones become stiffer during severe impacts.

INTRODUCTION

With the rapid economic and social development in 21st century, the incidence of road accidents has increased tremendously. The Global Burden of Disease Report, published by the World Health Organization, predicts that road traffic accidents are projected to rise from the ninth leading cause of death globally in 2004 to the fifth in 2030 (WHO, 2004). In developing countries like India, 80,000 people are killed annually on roads, amongst whom 70-80% are vulnerable road users (Mukherjee, 2003). With continuous advancement in computer technology and numerical methods, computer simulations have become an important tool in analyzing biomechanical response and understanding injury mechanisms. Finite element analysis became a standard tool for the evaluation of bone mechanical properties. FE models, with realistic geometry and accurate material properties can predict the human body response for different loading and boundary conditions. These models can be used to improve the design of vehicle structure by predicting the level of injury during vehicle-pedestrian collision. The process of determining the geometry of human body models using CT and MRI is fairly well established, but rate dependent material properties are scarce. This paper describes a methodology to ascertain the mechanical properties of cancellous bones under compressive loading at strain rate up to $\sim 175/s$ for which a micro-drop system was designed.

RESEARCH OBJECTIVE

The objective of this study was to characterize the dynamic compressive response of human cancellous bone at strain rates representative of loading during car impacts. For this a compliant drop mechanism was designed to record the stress and strain variations at the desired strain rates and estimate the modulus of elasticity of cancellous bone specimens.

DESIGN OF COMPLIANT MECHANISM

The requirement of the drop mechanism is that the impactor moves vertically in a straight line. A double parallelogram linkage generates a straight line motion without change of orientation. The impactor is guided by two such linkages arranged symmetrically on either side (See Figure 1).

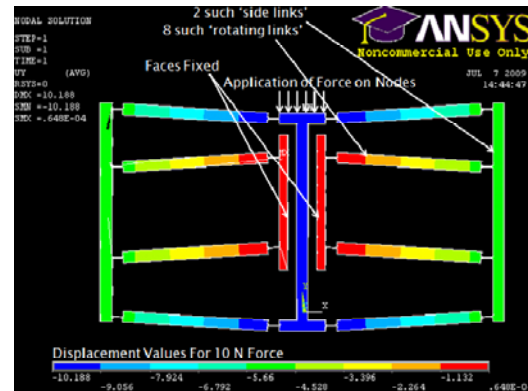


Figure 1. Compliant mechanism showing parallelogram linkages and application of force.

A key requirement is to minimize dissipation of energy in traverse as the specimen is of thickness of the order of 1mm. Use of compliant joints eliminates wear and frictional losses and ensures that the dynamics of the joint are negligible during impact. Use of revolute joints would dissipate energy due to friction and secondary impacts within the revolute joints. Hence compliant joints are used (See Figure 2).

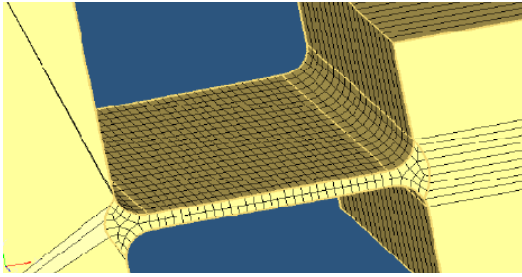


Figure 2. Meshing at the compliant joint.

Specimen Parameters and Design Calculations

The specimen to be tested is a human cancellous bone. Cylindrical specimen with properties and dimensions as given in Table 1 was to be used. These values were used initially as estimates to design the mechanism.

Table 1. Parameter values related to testing

Property	Value	Symbol
Strain rate	200	$\dot{\epsilon}$
Strain	3 % = 0.03	ϵ
Height of specimen	2 mm	l_o
Diameter of specimen	10 mm	d_o
Young's modulus	0.2 GPa	$E_{specimen}$
Cross-sectional area	$7.85 \times 10^{-5} m^2$	A_o
Volume of specimen	$1.57 \times 10^{-7} m^3$	V_o
Amount of deformation	60 μm	

The energy absorbed by the specimen is calculated from the estimate of the Young's modulus of the bone along with the bone dimensions and strain in the bone. The velocity of impact is calculated from strain rate and is assumed to be constant during the impact. By fixing the impact velocity, the drop height of the impacting mass is ascertained. For this the energy absorbed by the specimen is set to be 5% of the energy carried by the dropping mass/impactor. Drop mass is estimated from the energy requirement.

EXPERIMENTAL SETUP

The test set-up consists of an eye bolt and a turnbuckle attached to the top platen of the outer frame (See Figure 3) to raise the drop mass. A load cell transducer (ISOTRON Force Sensor, Model

2311-10) capable of measuring dynamic forces up to 2200N, with an output sensitivity of 10mV/lbf and a frequency response of 75kHz is mounted below the bottom platen and is used to measure the force-time history during the test (See Figure 4).

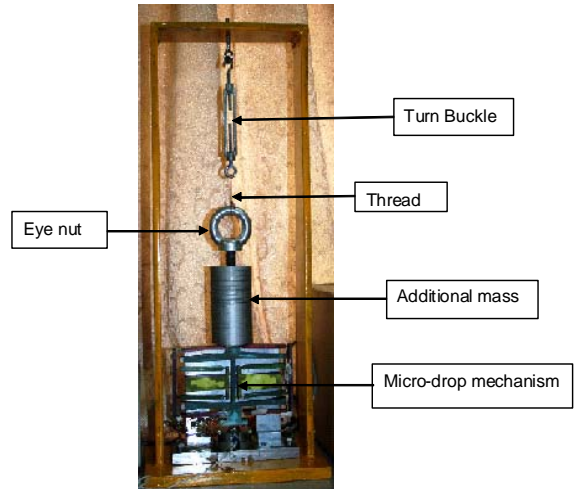


Figure 3. Micro-drop set up.

The additional mass is glued to the upper part of the micro-drop mechanism (See Figure 3). An arrangement is made with an eye nut and additional mass for lifting up the impactor with the help of turn buckle and thread. The webs of the compliant joint are strain gauged and bridged. Bone specimen is mounted on the top of the load cell (See Figure 5) using accelerometer wax for impact testing.



Figure 4. Load cell inside the specimen subassembly.

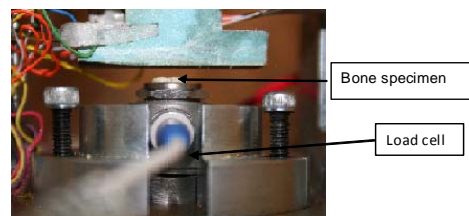


Figure 5. Bone specimen on the load cell.

PREPARATION OF BONE SPECIMEN

Specimen preparation, by grinding the specimen flat, is needed to have a good contact between impactor and specimen. Also, the specimen thickness is to be machined to desired values (See Figure 6).

Tests are performed in an unconfined condition, that is, the specimens are allowed to expand freely in the lateral direction. Unconfined tests are preferred so as to reduce the number of contact surfaces and the friction coefficient between the specimen and the constraining surfaces as it may lead to increase the uncertainties in the experiment.



Figure 6. Bone specimen after machining.



Figure 7. Experimental Setup.

The displacement measurement system using the strain gauges is calibrated by raising the impactor to a specified height. To start the test, the thread is burnt to free the impactor. The displacement and load data is recorded on two channels of a oscilloscope. The entire experimental setup is shown in Figure 7.

RESULTS

The test is conducted on the dry humerus bone specimens with dimensions shown in Table 2 and **Error! Reference source not found.** The experiment is done at strain rates of 135/s, 150/s and 175/s. The forces on the specimen (recorded via the load cell beneath it) and displacement of compliant mechanism (recorded via strain gauges put on the compliant joints' webs) were recorded synchronously. Time $t = 0$ corresponds to start of bone.

Table 2. Experimental parameters 1

Thickness (mm)	Diameter (mm)	Strain Rate (/s)	Velocity (mm/s)	Drop Height (mm)	Mass (kg)
1.7	5	135	229.5	2.7	3.21
1.7	5	150	255	3.3	2.60
1.7	5	175	297.5	4.5	1.91

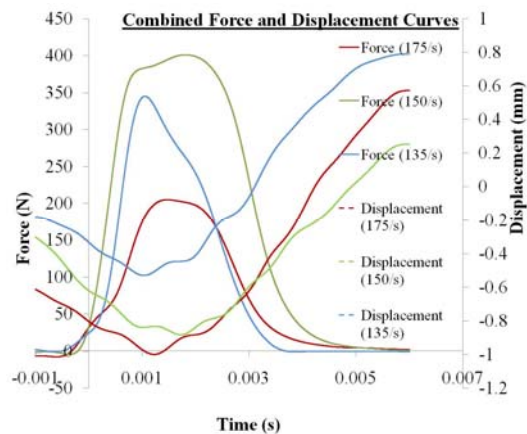


Figure 8. Combined force and displacement plot for strain rate of 135/s, 150/s and 175/s (Specimen information in Table 2).

The displacement v/s time curve shown in Figure 8 and **Error! Reference source not found.** represents bridge output from the strain gauges mounted on the webs of the compliant joints. As the impactor moves downwards the displacement reading reduces. The displacement value at the neutral position is 0 mm and negative below this position. The force v/s time curves represent the readings from the dynamic load cell kept under the bone specimen. The impact on the bone is below the neutral position and the force values start to increase. The force reaches a maxima corresponding to a minima in the displacement. Subsequent to this the impactor hits the catching plates (meant to limit the compression in the bone specimen) and bounces off. This results in the force dropping down and the displacement increasing again.

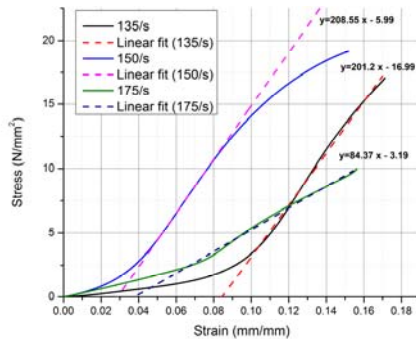


Figure 9. Combined stress-strain plot for strain rate of 135/s,150/s and 175/s (Specimen information in Table 2).

The time history curves were filtered and stress-strain curves for different loading conditions (i.e. varying strain rate) and different specimens were obtained from the geometric parameters. The stress-strain curves were observed to have a toe region followed by a linear region. Between the loading rates of 135/s and 150/s, the change in stiffness after the toe region is not significant, but the toe region decreases. The stiffness for the highest strain rate, 175/s is estimated to be about 85 MPa, which is lower than the value of about 200 MPa estimated at 135/s and 150/s.

CONCLUSION

A compliant mechanism was designed to carry out impact tests on cancellous bones at strain rates up to 175/s. The mechanism was fabricated along with suitable attachments to facilitate testing. The testing was done at strain rates which are typical in vehicle and pedestrian collision (50-200/s). The variation of stress with strain was ascertained at these strain rates. A distinct toe region is visible in stress-strain plots. The Young's modulus of dry cancellous bones is found to lie between 0.08 GPa and 0.2GPa (See Figure 9). The cancellous bones exhibit

The proposed setup is seen effective in determining response of isolated bone specimen in direct drop tests. There is need to conduct more tests, from different regions as well as from similar structure to infer the characteristics fully including study of the variation due to apparent density of the bone.

REFERENCES

[1] Mukherjee, S., A. Chawla, D. Mohan, and M. Metri. 2003. "Modelling of Body Parts Consisting of Bones as well as Soft Tissue: An Experimental and FE Study." In Proceedings - International

IMPACTOR DEVELOPMENT FOR THE ASSESSMENT OF ACTIVE PEDESTRIAN PROTECTION SYSTEMS

Edmund Marx
Werner Bieck
Thierry Mousel

IEE S.A.
Luxembourg
Paper Number 11-0177

ABSTRACT

Although pedestrian protection regulation does not yet cover the complete testing of active protection systems, Euro NCAP introduced in 2011 a pop-up hood test protocol [1]. Part of this assessment is a physical impact of a leg impactor against the vehicle front-end at the system's lower deployment threshold speed to test the sensing systems' response.

As the leg impactors used for injury assessment are not suitable for sensor testing, some first generation "sensor assessment impactors" were developed. Three of them can be selected within the Euro NCAP testing: IEE lower limit impactor, PDI, TRL SensorLeg. But as each of these impactors has certain limitations, further research was needed to develop an impactor reproducing a representative human impact.

This paper describes the development of an enhanced impactor with the highest possible level of abstraction, representing an appropriate effective mass not depending on the vehicle front-end geometry, showing human-like material properties and suitable for testing the "lower limit" case. The "lower limit" is defined as the lowest possible impact imprint that a sensing system must detect in a pedestrian-vehicle collision.

A first step in the development is based on LS-DYNA MADYMO coupled simulations where collisions between various MADYMO model statures (six-year-old child, 5% female, slim tall male, 50% male) and a variable test rig are evaluated. The test rig consists of variable load paths representing hood leading edge, lower bumper stiffener and the crossbeam area. In a second step, calculations are performed with an IEE in-house finite element human pedestrian model that is based on a driver knee-thigh-hip model which was further developed to a pedestrian model. This model was also scaled to represent the same adult pedestrian statures as mentioned above.

Both simulation results were cross-checked and resulting differences were elaborated in a sensitivity analysis regarding knee-joint bending, knee-joint shear stiffness and contact stiffness of the MADYMO models.

The resulting impactor with a mass of approximately 6.6 kg at maximum abstraction level represents the lower limit against a wide range of different vehicle front-end designs. Omitting the knee joint allows the representation of the lower limit stature, which can be the 5th percentile female, the slim tall male or the six-year-old child, depending on the front end geometry. The impactor has a flexible robust core and the tissue is made of PU material replicating human tissue characteristics. The impactor can be shot with a propulsion system or used in driving tests.

The applicability of the impactor may be restricted for low bumper vehicles with a sensor mounting height below 400 mm above road level.

As the development of active protection systems including A-pillar airbags is ongoing, there is a pressing need for defining procedures testing the sensors triggering these systems. A "lower limit" impactor properly reproducing pedestrian-bumper interaction in a realistic way is a crucial element within such tests.

INTRODUCTION

The first pedestrian protection regulations that became effective in 2005 in the European Union and in Japan initiated a novel kind of vehicle safety technology: pop-up hoods.

These deployable hoods were an answer to the legislative needs on head protection, helping to realize compliance without having to compromise on aesthetic design. Especially for sports cars or sporty limousines it would have violated the design philosophy if the necessary clearance between hood and rigid engine bay components would have been created by simply raising the hood line. Pop-up hoods allow for a sporty design, and the energy absorbing clearance is provided only if a vehicle-to-pedestrian collision occurs. A sensing system in

the vehicle front-end analyses the impact characteristics and decides whether hood lifting actuators need to be triggered or not.

While the initial pedestrian protection regulation as well as the upcoming Global Technical Regulation (GTR Nr. 9) [2] precisely define the tests and the criteria for the injury risk assessment of the human leg and head, little attention has so far been given to the specificities of pop-up hood systems. Regulation has not yet defined performance criteria for the sensors that trigger the hood lifting actuators. Current head protection assessment of pop-up hood vehicles is done with the hood by default in a deployed position, assuming that the sensing and triggering system works as intended in a real-life situation.

Early 2011, Euro NCAP started addressing this loophole by introducing a test procedure for deployable hood systems. As a first step, the protocol requires to simulate collisions between the vehicle and pedestrians of various statures in order to define the "hardest-to-detect" pedestrian also called the "lower limit" case. The impact speed corresponds to the lower deployment threshold speed, i.e. the minimum driving speed at which the systems are activated, typically around 20-25 km/h. Four parameters have to be simulated: effective mass, energy, force and intrusion. Whether the six-year-old child, or the 5% female or the 50% male corresponds to the "hardest-to-detect" pedestrian depends, to a certain extent, on bumper height and the height of the pedestrian's centre of gravity. In a second step, physical tests are made with an "appropriate" impactor, representing the "hardest-to-detect" pedestrian. The impact speed again corresponds to the lower deployment threshold speed. The head injury assessment impacts will only be made on the deployed hood if the hood is actuated during these tests. If the hood is not actuated, it will remain in the undeployed position for the head impactor tests.

The leg impactor currently used for the leg and knee injury assessment (EEVC WG17 lower legform impactor) as well as the future impactor (FlexGTR) are not suitable for testing the sensitivity of sensors of deployable hood systems. These impactors represent an "upper limit" with regards to the above mentioned impact parameters, which makes them suitable for injury risk assessment, but they are not able to represent a "lower limit" pedestrian. In addition, the material properties of their outer skins differ from the characteristics of human tissue and muscles. Therefore, their interaction with the bumper in the crucial early impact phase (~20 ms) is unlikely to be pedestrian-like.

In order to reliably reproduce a human impact, various stakeholders developed a new impactor type, "sensor assessment impactors". Due to different approaches, the resulting impactors show some significant differences. Three of these impactors can be selected within the Euro NCAP testing: the IEE lower limit impactor (6 kg), the Pedestrian Detection Impactor (PDI) (9.9 kg) and the TRL SensorLeg (13.4 kg). As each of these first generation impactors has certain limitations, IEE decided to conduct extensive simulations and research, in order to further improve the existing "lower limit impactor" concept in view of developing an impactor that reliably reproduces a "real-life" lower limit human impact.

MOTIVATION FOR IMPACTOR DEVELOPMENT

When IEE started to develop the pedestrian detection sensor system Protecto, the self-evident question that came up was how the sensor could be properly tested. One would require an impactor able to reproduce the interaction of muscles and tissue of a real human leg with the vehicle front bumper in the early phase of the impact. At the same time, the impactor should be able to reproduce a "worst-case" scenario in which the energy transfer into the bumper would be at the lower end of what could be expected in real pedestrian-to-vehicle collisions. IEE analyzed the leg impactors which were available or under development for the leg and knee injury risk assessment tests, but found them not suitable. The weight of these impactors was too high (representing the leg of a 50% male) and the characteristics of their outer materials differed from the ones of human muscle and tissue. Therefore IEE decided to develop its own impactor, the "IEE lower limit impactor".

The IEE lower limit impactor – 1st generation

Simulations of a large range of pedestrian-vehicle collisions and extensive research for an appropriate "tissue" material led to an impactor with following characteristics:

- weight 6 kg
- steel core surrounded by PU resin
- diameter 76 mm
- length 334 mm
- PU thickness 18 mm

This lower limit impactor as shown in figure 1 can be used in driving or propulsion tests. A second variant was designed to be used in pendulum tests (impactor weight reduced to 4.19 kg to compensate for pendulum mass). A Finite-Element model (LS-DYNA) of the leg impactor was also created. In

impact tests, the vertical alignment of the impactor relative to the bumper shall be such that the centre of gravity of the impactor hits the bumper leading edge. The impactor can be used in a speed range from 20 km/h up to 55 km/h.

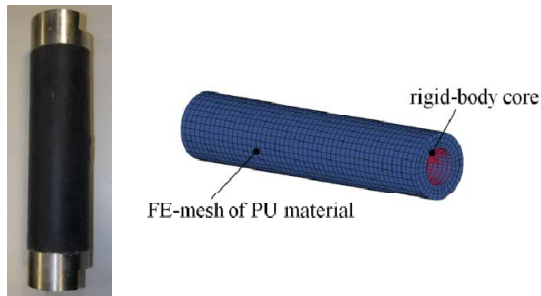


Figure 1. The lower limit impactor and its FE-model.

During testing, the impactor has proven to be very robust, and reproducibility of impacts and sensor signals was very good.

The weaknesses of the impactor

In the course of time, more enhanced simulations have shown that the impactor weight is still slightly too high to represent a worst case "lower limit" impact case, a weight of 5 kg would be more appropriate for such an impactor concept.

The initially chosen concept of aligning the centre of gravity of the impactor to the bumper leading edge aimed at reproducing the "lower limit" case independently from the vehicle bumper height. A disadvantage of this concept is that the impactor does not interact with the front-end's so-called lower bumper stiffener due to its limited length. This can be of concern for vehicles where the lower bumper stiffener's x-position is similar to the one of the main bumper. For such front end geometries, interaction with the lower bumper stiffener can initiate additional rotation into the collision object and thus reduce the energy transfer into the bumper. As a consequence, the signal then measured by a pedestrian impact detection sensor can be lower than the one that would be measured without lower stiffener interaction with the collision object. Another disadvantage is using a rigid core tube for bone/ligament representation, which leads to overestimation of human impact energy when applying the impactor at velocities higher than 20 km/h.

The new impactor concept aims at rectifying these weaknesses in order to be a suitable "lower limit" impactor for a broad range of vehicle front end geometries and designs.

HUMAN MODELING

Appropriate pedestrian models are crucial in order to realistically simulate and reproduce a pedestrian-to-vehicle collision. Special attention has to be given to the capability of the model to simulate the early phase of the leg-bumper interaction.

Currently, a wide range of human models is proposed for analyzing vehicle pedestrian collisions. The selection includes Rigid Multi Body Models as well as Finite Element Models (see Appendix I of [1]). The RMB- and FE-model types have a few advantages and disadvantages either related to their characteristics or to their computing needs.

Table 1. Comparison of Rigid Multi Body and Finite Element pedestrian models

Model	Advantages	Disadvantages
Rigid Multi Body	- handling/complexity - calculation time	- low local resolution - poor representation of bone geometry - poor contact reproduction (no tissue)
Finite Elements	- high local resolution - good representation of bone geometry - good contact reproduction (tissue model included)	- handling/complexity - calculation time

Existing human models

One of the best known RMB models is the MADYMO model [3], which is available in various pedestrian statures. The MADYMO pedestrian model was developed to reproduce the kinematics of a pedestrian during the impact with a vehicle as well as during the "throw-off" phase. While the model is very well validated for this area of application, its suitability for reproducing pedestrian-vehicle bumper interaction in the very early phase of the collision is quite limited.



Figure 2. The MADYMO family [3].

Pedestrian-bumper interaction can be reproduced much more precisely with FE-models. Figure 3 shows a selection of existing pedestrian FE-models.

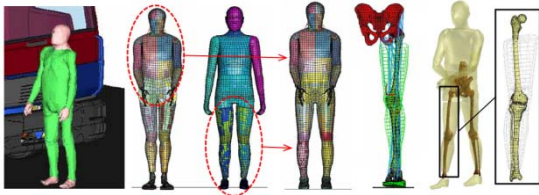


Figure 3. Human FE models from left to right: HUMOS [4], THUMS [5], H-Model [6], JAMA/JARI [6], A-LEMS [7], HONDA [8][9].

These are full FE models, except the Honda model, which is a hybrid model with a rigid upper body. While THUMS may have some shortcomings in leg geometry (legs too close together), the JAMA/JARI model appears to be the most advanced model, as it combines the upper body of THUMS with the lower body of the H-model, and has an adequate leg distance.

A Hybrid model, like the one developed by Honda, is likely to offer the best compromise: lower limbs with detailed FE bones, tissue and ligaments to guarantee an appropriate leg-bumper interaction, and a simplified upper body to reduce computational needs.

The IEE-WPI FE-Model

IEE developed a hybrid pedestrian model, based on the work of C. Silvestri and M. H. Ray [10, 11] which resulted out of a NHTSA research project. The original WPI injury model represents a driver sitting in a vehicle. IEE modified the model in the following areas:

- Repositioning: standing upright
- Discrete knee ligament modeling was replaced by shell element modeling using correct material definitions [12]
- Integration of additional shell elements representing tissue and knee capsule, ensuring necessary overall knee joint stabilization
- The solid femur model approach was replaced by shell elements
- Human skin and tissue was modeled using shell and solid elements, using correct material definitions [13]
- Some additional muscles were implemented
- The upper body is represented by rigid multi body elements

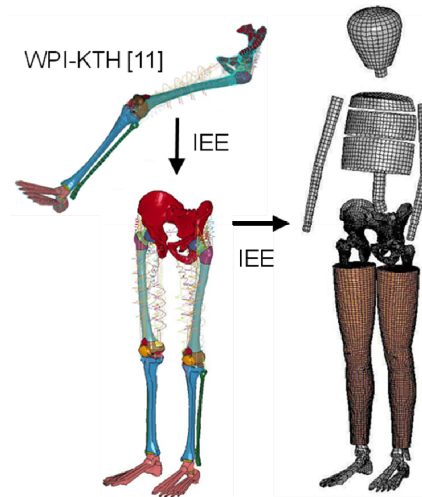


Figure 4. Development steps from the WPI model to the IEE-WPI hybrid pedestrian model.

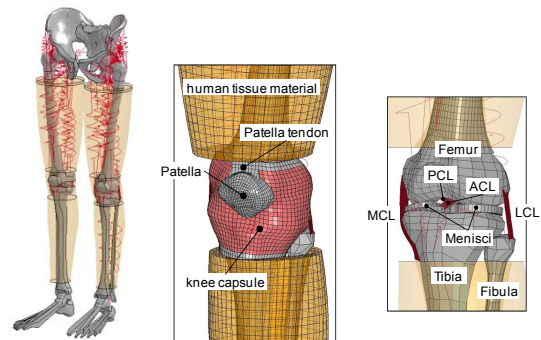


Figure 5. Detailed FE-model for leg, hip and knee area showing muscle, tissue and ligament definitions.

The IEE-WPI models' overall kinematic was validated comparing the impact response with the MADYMO pedestrian model, while the response for several best known load cases regarding lateral impact on lower limbs was validated using literature. For details on the validation methods, see the references:

- Kinematics [14]
- Knee Ligaments [12]
- Femur/Tibia [15]
- Knee [15] [16] [17] [18]
- Tissue [13]
- Muscles [19]

Figure 6 shows the first 250 ms of a simulated vehicle collision against a 50% male MADYMO model as well as against the IEE-WPI model. The good overlap of the movements over time of both models shows that the IEE-WPI can appropriately reproduce pedestrian kinematics.

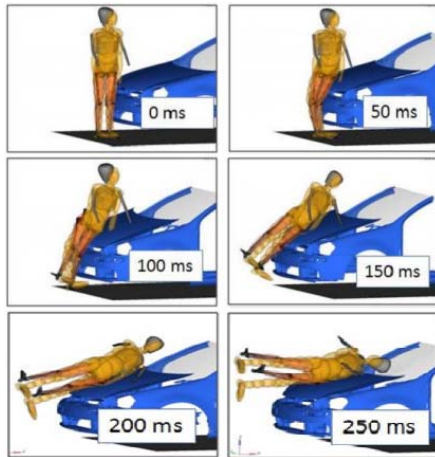


Figure 6. Lateral vehicle impact against the 50% male MADYMO and IEE-WPI model.

VEHICLE TO PEDESTRIAN COLLISION

Besides the pedestrian model, it is important to use a vehicle model which is representative of a vehicle that complies with the legislative passive safety requirements regarding leg and knee injuries.

Vehicle front-end model

The vehicle is represented by a variable test rig made up of the elements which interact with the pedestrian in the early impact phase. It consists of an upper, middle and lower load path corresponding to the bonnet leading edge, the bumper/crossbeam area and the lower bumper stiffener of a vehicle front-end. All three elements can be varied in x- and z-direction in order to represent various front-end geometries as well as vehicle types. A crossbeam foam with a density of 30 grams/liter is chosen as this corresponds with the foams used in modern vehicles with "pedestrian-friendly" bumpers (older vehicles typically used harder foams). The forces versus time values are measured at crossbeam level, where the contact sensors are usually located. The whole setup is assumed to be rigid behind the foam parts and is moving at constant velocity into the object.

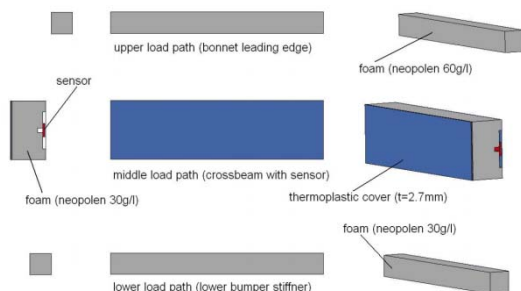


Figure 7. Variable test rig: side-, frontal- and isometric view.

Test rig vs. real vehicle front-end structures

Impact simulations of the IEE lower limit impactor with the test rig model are compared with simulations on existing vehicles. All of these vehicles have a "pedestrian friendly" bumper.

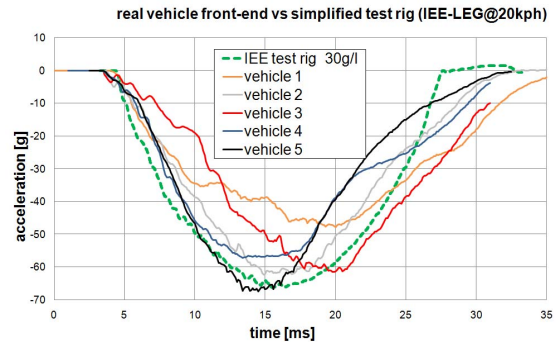


Figure 8. Impactor acceleration data comparison for test rig and vehicle impacts.

The curves show that the chosen test rig appropriately reproduces the front end of modern vehicles

Usage of a reverse engineered PDI model

As the Pedestrian Detection Impactor (PDI) is widely used in the development and testing of pedestrian sensing systems, it has been included in a few comparative simulations.

IEE made use of a reverse engineered PDI-model, validated according to [20], where an ECE R21 pendulum test is performed hitting the impactor at a height of 470 mm above ground level.

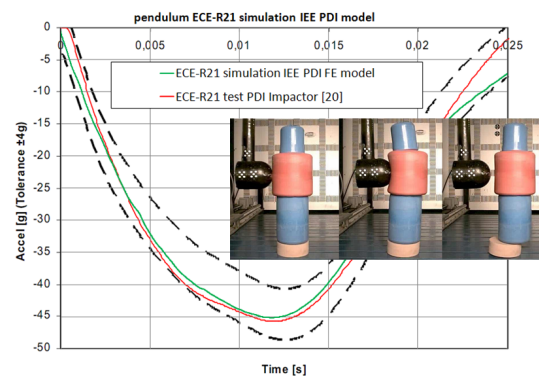


Figure 9. Validation of the reverse engineered PDI-model [20].

The pedestrian-to-vehicle interaction

In view of reproducing a "worst case scenario" from the impact sensing point of view, it is important to make sure that there is only a single

leg interacting with the front-end in the early stage of the collision. Whether a standing pedestrian model with parallel legs is reproducing a single leg interaction in the first 20-25 ms of the lateral impact (at 20 km/h) depends on the implemented representation of leg geometry, especially on the defined knee distance.

For some pedestrian models there is very early interaction between the impacted leg and the 2nd leg, which then immediately leads to a double leg impact, while for other models interaction with the second leg only takes place after more than 20 ms after first contact with the bumper.

For simulation models where early interaction of the 2nd leg is an issue, it is recommended to position the model in a distinct walking stature.

The impact of pedestrian model type and walking posture

When comparing a 50% male IEE-WPI model with a 50% male MADYMO model, both in a standing posture with the legs in parallel, significant geometrical differences between both models can be observed (figure 10).

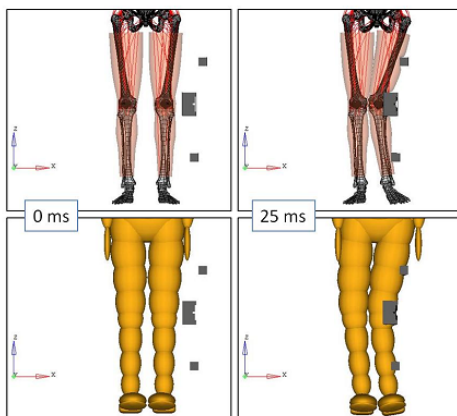


Figure 10. 50% male IEE-WPI (top) vs. MADYMO (bottom), 20 km/h, 0-25 ms.

The simplified leg geometry of the MADYMO defines a significantly smaller knee distance, and the rigid elements of the upper legs are almost in contact. Therefore both legs of the MADYMO interact very early in the collision (within the first 5 ms), which leads to a rather severe impact scenario representative of a "two leg collision" but not of a less severe single leg collision. For the IEE-WPI model, interaction with the 2nd leg is only observed after about 22 ms due to a better representation of the hip-leg anthropometry. At this point in time, the sensing system should already have taken a fire/no-fire decision.

Figure 11 shows force over time simulation curves for a selection of collision partners. For the IEE-WPI model the influence of leg muscle activation is also shown. Activation of the muscles leads to a higher force peak. For the MADYMO models it can be observed that a standing posture creates a much higher impact severity than a walking posture. The difference is especially significant for the 50% male (red curves), but also for the 6-year-old a notable difference can be observed (blue curves). The curves are compared to the 1st generation IEE "lower limit" impactor and also to the PDI impactor (the development of which was based on a standing 6 year MADYMO model).

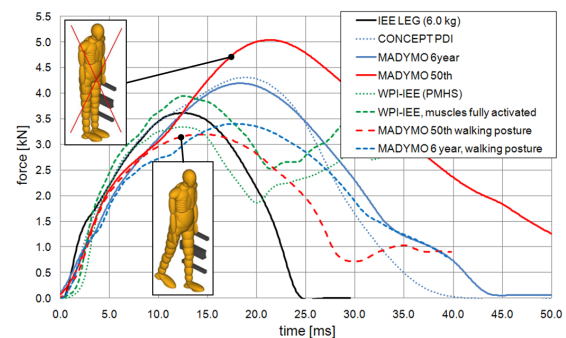


Figure 11. F(t) comparison of various collision partners, 20 km/h.

Some research has already been made to improve the biofidelity of the MADYMO leg model by implementing a more human-like knee. The figures below compare the initial MADYMO knee characteristics to the modifications applied by the University of Virginia (UVa) [21].

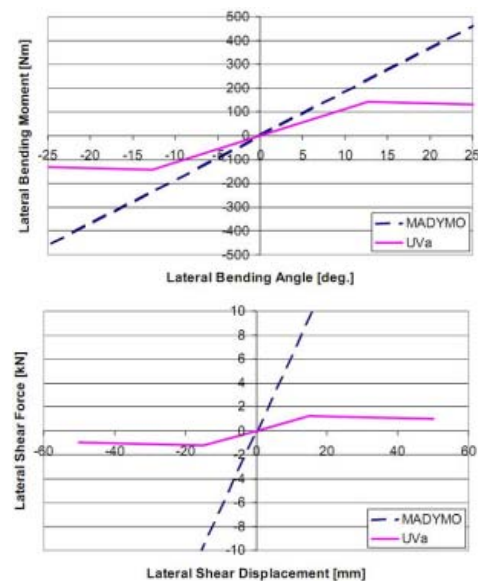


Figure 12. Modified knee bending and shear stiffness according to [21].

The orange spotted curve in figure 13 shows the effect of these modifications, and the additional effect of an adapted contact stiffness is illustrated by the solid orange line. This most biofidelic variant shows higher peak force, while the contact duration is reduced compared to the original MADYMO model. The obtained MADYMO force transient $F(t)$ versus collision time is close to the one of the IEE-lower limit impactor.

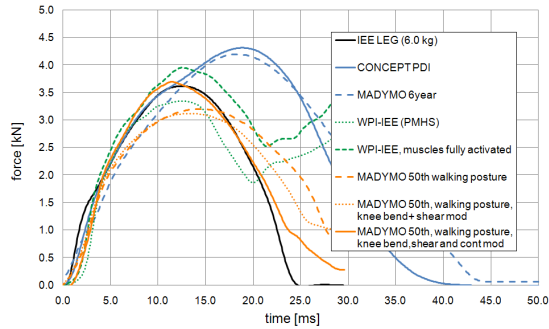


Figure 13. Influence of knee shear, knee bending and contact modification on MADYMO's $F(t)$ curves, 20 km/h.

Momentum transfer and effective impact mass

In order to identify the "hardest to detect" pedestrian, the effective impact mass is considered as a representative parameter. Its calculation is based on the conservation of momentum, neglecting inelastic processes during the constitution phase of the impact. In general, this assumption is only valid for low speed impacts which have to be considered anyway in order to determine the "lower limit" pedestrian. Other parameters like energy transfer or intrusion can be helpful to increase the precision of the evaluation, but they require a more careful evaluation of the overall impact scenario.

A more simplified analytical approach is schematically described in figure 14. When the vehicle front-end gets into contact with a walking pedestrian, the leg-bumper interaction mechanism can be seen as a (non-linear) dual-spring system. The overall compression α of two colliding objects with relative speed v_0 in the centre-of-mass system CM can be described by following differential equation [22]:

$$\mu \cdot \ddot{\alpha} = -k(v_0, Y, T) \cdot \alpha^n \quad (1)$$

with non-linear total spring constants k , an exponent n to be quantified experimentally and the so called reduced mass $\mu = m \cdot M / (m + M)$. k depends on impact location Y , impact speed v_0 and ambient temperature T .

Integrating equation (1) provides a simple relationship between maximum compression α_{\max} and the corresponding collision time τ_{\max} :

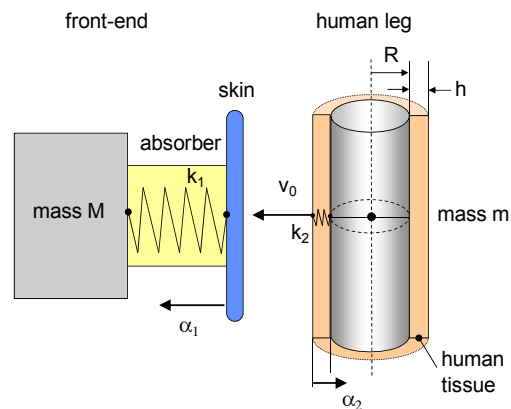
$$\frac{\alpha_{\max}}{\tau_{\max}} = \frac{v_0}{\sqrt{\pi \cdot c(n)}} \quad (2)$$

with integration constant $c(n)$.

In the same way the effective impact mass $m \ll M$ of the colliding object can be determined according to equation (1) taking the force peak as the integration end point, an approach also proposed in the EURO NCAP protocol.

$$m \cdot v_0 = \int_0^{\tau_{\max}} F(t) \cdot dt \quad (3a)$$

The value depends on front-end stiffness and geometry as the leg cannot be treated as simple rigid body due to inelastic processes (injury effects) and energy absorption limits of the front-end at higher impact speed.



- $\mu \equiv m$ - impact mass ($M \gg m$)
- M - car mass
- v_0 - impact speed
- T - ambient temperature
- Y - lateral impact position
- α - total compression..... $\alpha = \alpha_1 + \alpha_2$
- k - total spring constant..... $k = k_1 \cdot k_2 / (k_1 + k_2)$

Figure 14. Schematics describing the collision between a car front-end and an impacting object in the centre-of-mass system.

An alternative approach not based on the absolute peak force defines the corresponding effective impact mass as follows:

$$m' \cdot v_0 = \int_0^{\tau_{\text{trigger}}} F(t) \cdot dt \quad (3b)$$

This approach is more aligned with the way pedestrian contact sensors operate. The sensors have a certain trigger level followed by a certain sensing time before the algorithm has to take the decision to fire or not to fire the hood actuators. The available sensing time depends on the total system response time TRT (TRT = sensing time + actuator triggering + plus hood lifting time), and TRT must be smaller than the most critical head-to-impact time HIT for the 6-year-old child. The minimum TRT required by pop-up hood systems typically allows for a sensing time of 20 ms before an actuator trigger decision has to be taken.

In the following all force versus time plots have been evaluated on the basis of a 1 kN sensor trigger level as a starting point and then integrating $F(t)$ for a duration of $\tau_{\text{trigger}} = 20$ ms as maximum sensing time at 20 km/h impact speed.

It has to be pointed out that a typical single-leg bumper collision at 20 km/h lasts about 15-20 ms for common absorbers fulfilling passive safety requirements. Thus, depending on the applied leg model, almost twice the momentum \mathbf{p} will be transferred within 20 ms sensing time (e.g. IEE leg with τ_{max} at 12 ms) while other impactors representing more severe impacts will introduce only \mathbf{p} or even less than that (c.f. figure 15). A physically correct evaluation of the impact strength (independent from any sensing system) requires a comparison of specific impact related parameters like τ_{max} or \mathbf{p} as defined by equation (3a).

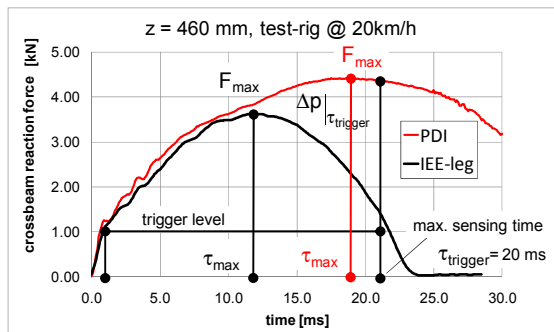


Figure 15. Typical $F(t)$ transient curves for two different types of impactor models (taken from Fig.31) exemplifying the effective mass concept described in the text.

This kind of evaluation can be done straightforward in case of impactors but it might be more difficult for complex pedestrian models at high impact speed due to double-leg collisions. Table 2 compiles the momentum transfer in case of no time limits and shows the related effective impact mass which can be detected. For comparison, the data for 20 ms sensing time is also included.

Table 2.
Effective mass and momentum transfer comparison

Evaluation Method	IEE-LEG 20 km/h	PDI 20 km/h
Peak force (eq. 3a) $\Delta p @ F_{\text{max}}$ [Ns]	32.9	54.3
effective impact mass [kg] resulting from (3a)	5.9	9.8
TRT dependent $\Delta p @ 20\text{ms}$ [Ns] (eq. 3b)	55.4	69.7

TEST RIG TO PEDESTRIAN COLLISION SIMULATION

The subsequent graphs and charts show simulation based relative comparisons of various impactor and human-model collisions against a variable test rig. The analysis is performed at 20 km/h, the lowest threshold speed at which sensors should detect a car-to-pedestrian collision

Test results for standard human models

The following graphs show the crossbeam reaction force versus time for the following pedestrian models:

- 50% male and 5% female using IEE-WPI
- 6 year MADYMO with changed contact stiffness, walking posture

The crossbeam height is varied in steps of 20 mm, from 400 mm to 500 mm above the ground.

The smaller the pedestrian, the more the curves diverge for varying crossbeam levels. The data for the 6-year-old child is most sensitive to changing crossbeam heights followed by the 5% female, while the data for the 50% male is quite robust against crossbeam height variations.

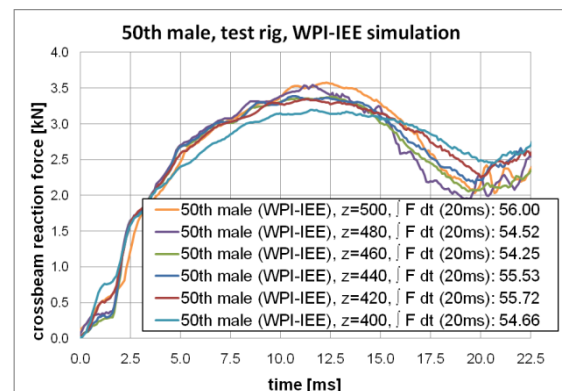


Figure 16. $F(t)$ and $\int F dt$ (Ns@20 ms) variation for 50% male as a function of crossbeam height z (mm).

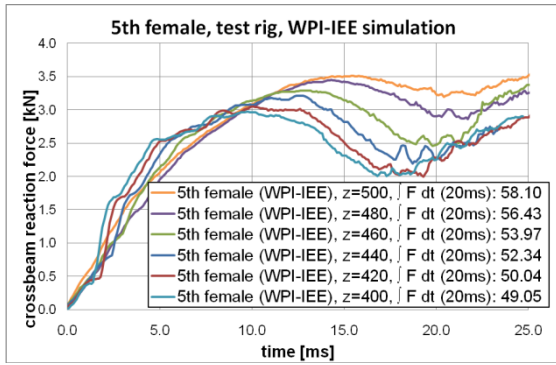


Figure 17. $F(t)$ and $\int F dt$ (Ns@20 ms) variation for 5% female as a function of crossbeam height z (mm).

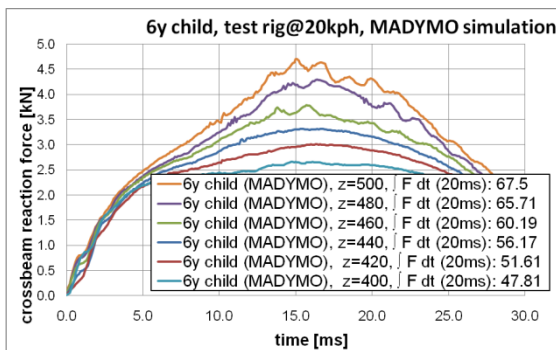


Figure 18. $F(t)$ and $\int F dt$ (Ns@20 ms) variation for 6-year-old child (walking posture) as a function of crossbeam height z (mm).

This effect can be explained by the change of the impact point relative to the pedestrians centre of gravity and hip joint, respectively. For the small pedestrian the relative change between the varying impact point height and the centre of gravity height is more important than for a tall pedestrian where the same crossbeam height variation leads to a less substantial relative change.

In the next step, the calculated momentum transfer is used to identify the "hardest to detect" pedestrian for various crossbeam heights. In addition, the data generated for the 1st generation IEE leg impactor is compared to the other pedestrian models.

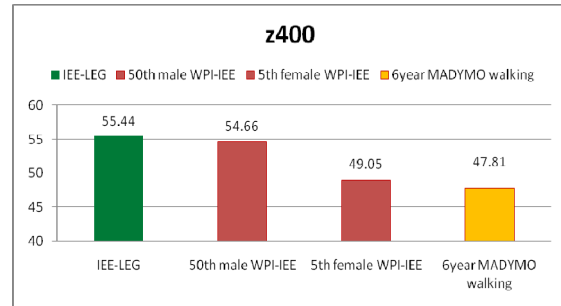


Figure 19. Momentum transfer comparison for crossbeam height of 400 mm, Δp in [Ns@20ms]

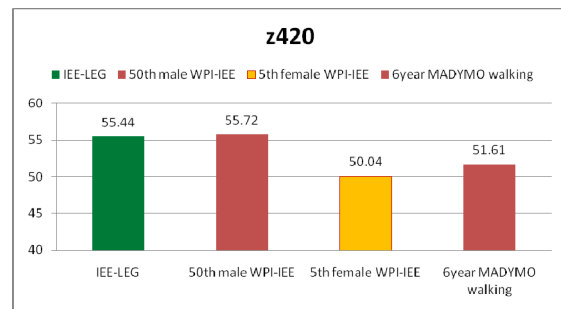


Figure 20. Momentum transfer comparison for crossbeam height of 420 mm, Δp in [Ns@20ms]

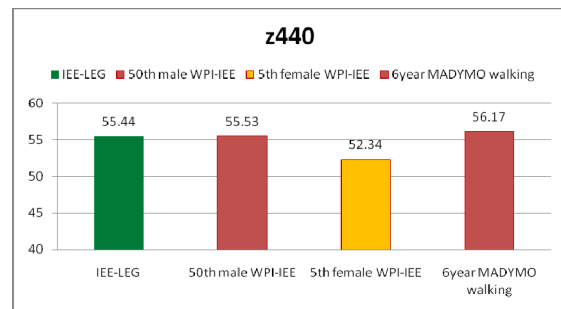


Figure 21. Momentum transfer comparison for crossbeam height of 440 mm, Δp in [Ns@20ms]

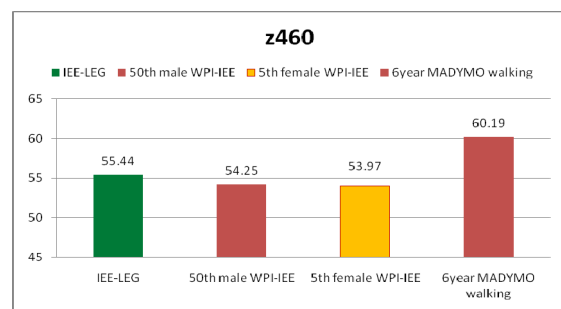


Figure 22. Momentum transfer comparison for crossbeam height of 460 mm, Δp in [Ns@20ms]

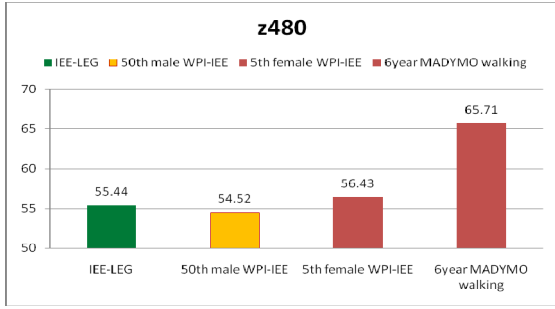


Figure 23. Momentum transfer comparison for crossbeam height of 480 mm, Δp in [Ns@20ms]

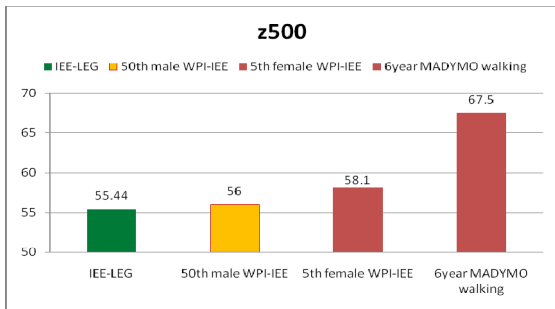


Figure 24. Momentum transfer comparison for crossbeam height of 500 mm, Δp in [Ns@20ms]

For a crossbeam height of 400 mm, the 6-year-old child is the "worst case" pedestrian. For the bumper height range from 420 mm to 460 mm the 5% female is the hardest to detect pedestrian, and for a crossbeam height of 480 mm and 500 mm the situation changes again with the 50% male being the "lower limit" case.

Table 3. Overview on the "hardest to detect" pedestrian relative to the crossbeam height

Height z	Minimum momentum transfer [Ns @ 20ms]	Hardest to detect pedestrian
400 mm	47.81	6-year-old child
420 mm	50.04	5% female
440 mm	52.34	5% female
460 mm	53.97	5% female
480 mm	54.52	50% male
500 mm	56.00	50% male

The 1st generation IEE lower limit impactor is appropriately applicable for bumper heights from 460 mm to 500 mm, while for lower bumper heights it creates an impact severity above the "hardest to detect" pedestrian.

The VC-COMPAT research project [23] analysed the crossbeam heights of 55 vehicles. The mean crossbeam height was 469 mm. Almost all vehicles (except 4WD and Light Commercial Vehicles) had a significant part of their crossbeam surface in the height range between 400 mm and 500 mm. As the crossbeam is a typical location for a pedestrian

detection sensor, the above impact simulations are representative of a major part of the "real-life" vehicles.

Test result for non-standard human model

In addition to the standard human model sizes, a further set of simulations was realised by using an IEE-WPI "slim tall male". The size of the model corresponded to a 50% male, while the weight was reduced to the one of a 5% male.

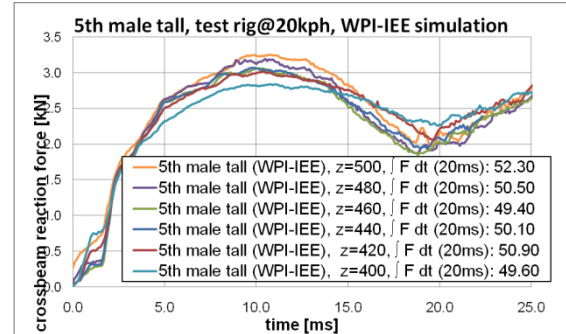


Figure 25. $F(t)$ and $\int F dt$ (Ns@20 ms) variation for 5% tall male (weight =5th size=50th) as a function of crossbeam height z (mm).

When comparing the momentum transfer values to the ones of table 2, it appears that this slim tall male would represent a "hardest to detect" pedestrian for bumper heights from 440 mm to 500 mm.

This result is consistent with the above discussed findings as the slim tall male has a comparatively high centre of gravity (similar to the 50% male), but with a significantly lower mass. Due to these proportions it even beats the 5% female with regards to a "lower limit" case for a bumper height of 440 mm.

These results indicate that also non standard pedestrian sizes have to be considered when searching for a "worst case pedestrian". Further investigations with other models may be necessary to confirm these findings.

Therefore the subsequent impactor development and the related analysis are mostly based on findings realized with standard pedestrian statures.

THE IEE LEG IMPACTOR GENERATION 2

As discussed and shown above, the 1st generation IEE "lower limit" leg impactor has some small, but in certain cases non-negligible weaknesses:

- As it is not positioned on the ground but rather used as a "center-of-gravity to

bumper" impactor, there is no interaction with the vehicle's lower bumper stiffener which might be relevant for certain sensor systems.

- The impactor has a very rigid core defining much too strong impacts at high speed.
- It is not a realistic "lower limit" for bumper heights below 440 mm

These issues are successfully addressed by the new impactor design.

Concept of the IEE G2 impactor

The illustration below shows a schematic representation of the IEE leg impactor Generation 2 (G2), in the following called the IEE G2 impactor.

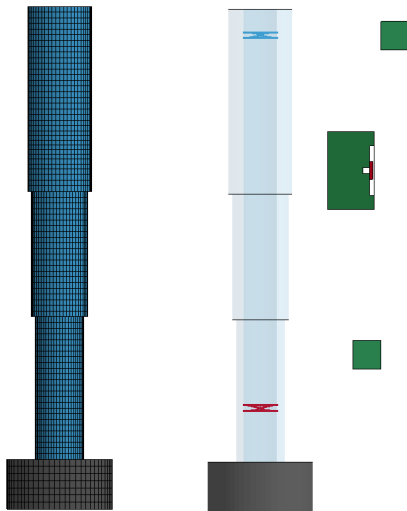


Figure 26. The IEE G2 impactor model positioned in front of the test rig.

The core of the IEE G2 impactor consists of a carbon fiber reinforced tube with two concentrated masses, one towards the top of the impactor (blue) and one towards the lower end (red) (see figure 26). The core is surrounded by a Wevo PU material for human muscle and tissue representation. This material guarantees a humanlike interaction with the bumper in the early contact phase. The diameter of the core is 45 mm, and the total impactor diameter varies from 70 mm at the lower end to 90 mm at the upper end, with a center segment of 80 mm. The impactor weighs 6.6 kg and can be positioned on a 70 mm high base to ensure reproducible friction in driving tests. Including the base, the impactor has a total standing height of 700 mm.

Table 4. Comparison of the IEE impactors

	IEE lower limit	IEE G2 impactor
Year	2006	2011
Weight	6 kg	6.6 kg
Length	334 mm	630 mm
Diameter	76 mm	70-90 mm
Core	massive steel	carbon fiber tube
Conc. masses	no	Yes

The impactor itself has a height of 630 mm. When used with a propulsion system, the ground clearance has to correspond to the height of the base plate.

The geometry of the G2 impactor has changed significantly compared to the 1st generation lower limit impactor. The length has doubled and the diameter increases from bottom to top, while the weight has only slightly increased. The flexible core and the two concentrated masses are meant to allow for a certain impactor bending and a more realistic rotation, depending on the point of impact.

IEE G2 impactor test results

A simulation series was performed with the IEE G2 impactor, in line with the previous simulations using the same test rig configuration.

The following graph shows the crossbeam reaction force versus time and momentum transfer values for the IEE G2 impactor for crossbeam height variations from 400 mm to 500 mm.

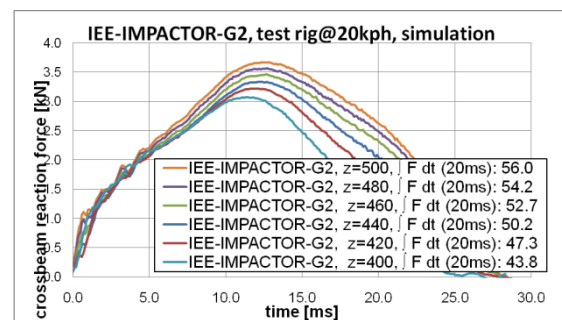


Figure 27. $F(t)$ and $\int F dt$ (Ns@20 ms) variation for the IEE G2 impactor as a function of crossbeam height z (mm).

Peak pulse and pulse duration vary with the impact location height and the momentum transfer $\int F dt$ (20 ms) increases with impact height. This is a first solid indication that the impactor is able to address a shift in impact location relative to its centre of mass and the response is as intended.

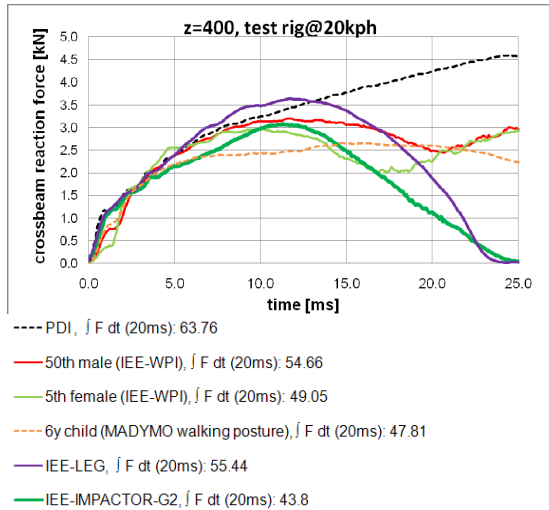


Figure 28. $F(t)$ and $\int F dt$ (Ns@20 ms) comparison for impact height of 400 mm.

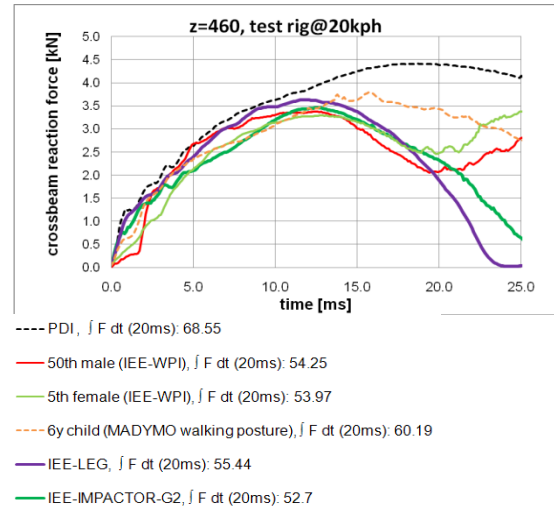


Figure 31. $F(t)$ and $\int F dt$ (Ns@20 ms) comparison for impact height of 460 mm.

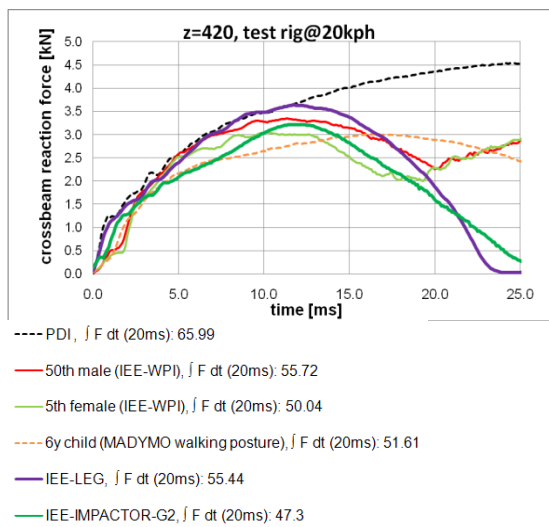


Figure 29. $F(t)$ and $\int F dt$ (Ns@20 ms) comparison for impact height of 420 mm.

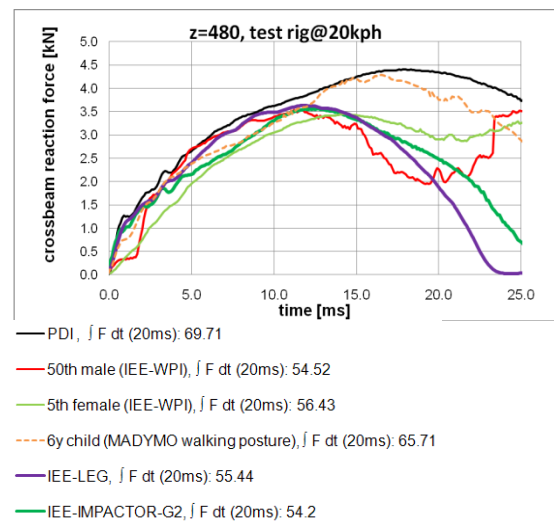


Figure 32. $F(t)$ and $\int F dt$ (Ns@20 ms) comparison for impact height of 480 mm.

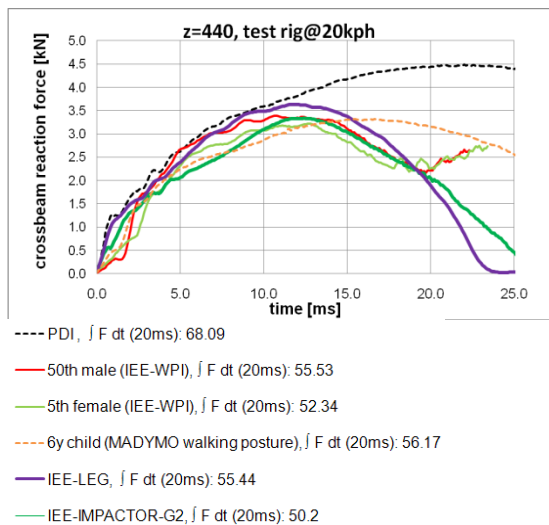


Figure 30. $F(t)$ and $\int F dt$ (Ns@20 ms) comparison for impact height of 440 mm.

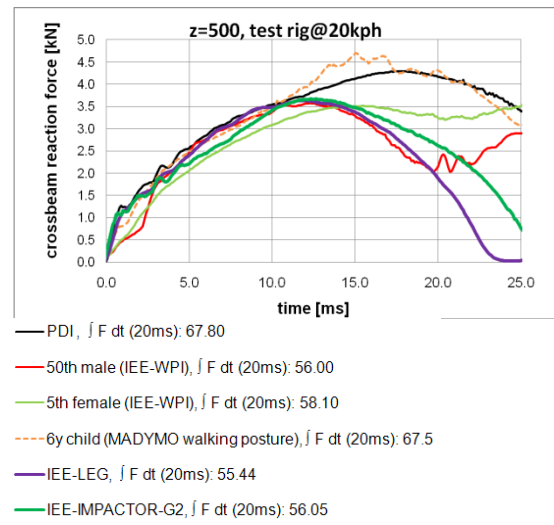


Figure 33. $F(t)$ and $\int F dt$ (Ns@20 ms) comparison for impact height of 500 mm.

In a next step the $F(t)$ curves of the IEE G2 impactor are compared to the ones of the various previously simulated pedestrian models (6-year-old child, 5% female, 50% male) and impactors (IEE lower limit leg, PDI). This is again repeated for an impact height range from 400 mm to 500 mm.

The simulation results confirm that the IEE G2 impactor is suitable to address pedestrian collisions with vehicles having different crossbeam heights, while at the same time the impactor is a suitable representation of the "hardest to detect" pedestrian.

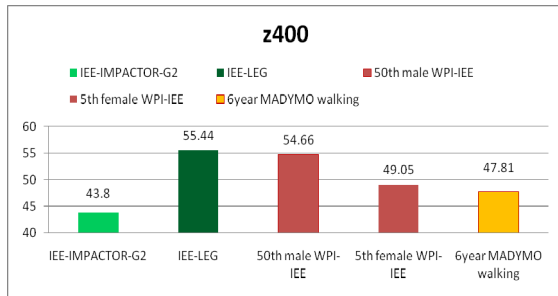


Figure 34. Momentum transfer comparison for crossbeam height of 400 mm, Δp in [Ns@20ms].

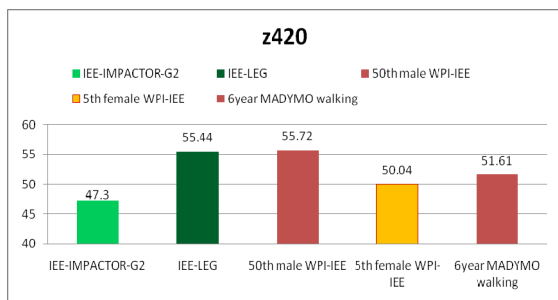


Figure 35. Momentum transfer comparison for crossbeam height of 420 mm, Δp in [Ns@20ms].

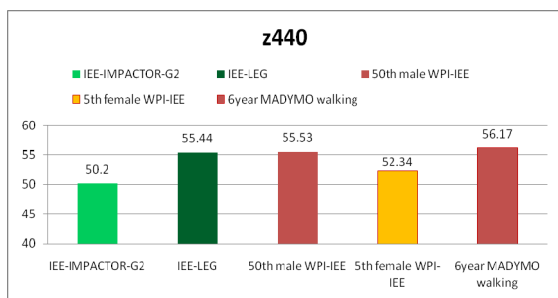


Figure 36. Momentum transfer comparison for crossbeam height of 440 mm, Δp in [Ns@20ms].

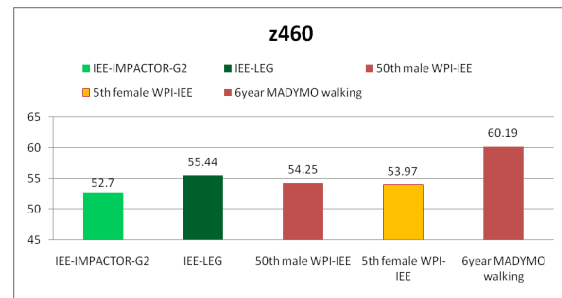


Figure 37. Momentum transfer comparison for crossbeam height of 460 mm, Δp in [Ns@20ms].

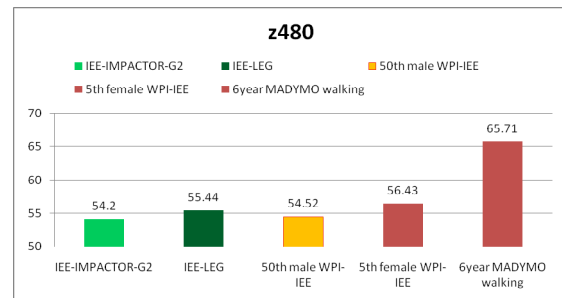


Figure 38. Momentum transfer comparison for crossbeam height of 480 mm, Δp in [Ns@20ms].

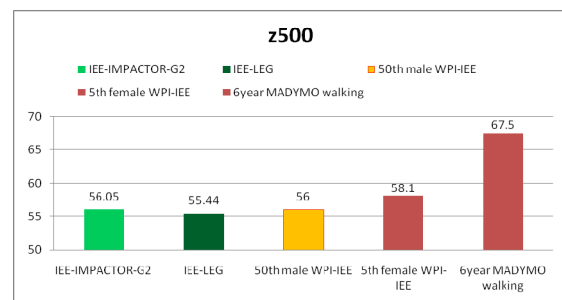


Figure 39. Momentum transfer comparison for crossbeam height of 500 mm, Δp in [Ns@20ms].

The figures 34 to 39 draw a direct comparison of the momentum transfer in order to better illustrate the "lower limit" capability of the IEE G2 impactor.

For any impact location height, the IEE G2 impactor represents a "lower limit" relative to the specific "worst case" standard pedestrian model, no matter if it is the 6-year-old child (for $z = 400$ mm), the 5% female (for $z = 420 - 460$ mm) or the 50% male (for $z = 480 - 500$ mm). The new impactor concept successfully meets all the challenges that had to be tackled.

Limitations of the applicability

While the IEE G2 impactor can be successfully applied as a "lower limit" for collisions between "standard pedestrian statures" and vehicles with bumper heights between 400 and 500 mm, there

might nevertheless be some limitations in its applicability.

These limitations can be related to more extreme front end designs, with higher or lower bumpers than the investigated ones.

On the other side, non-standard pedestrian models can also lead to impact scenarios where the human model can generate momentum transfers that are even below the ones of the IEE G2 impactor. Table 5 gives an overview on how well the IEE G2 impactor can represent the lower limit case. When including the investigated non-standard pedestrian model (slim tall male), the IEE G2 covers very well the "hardest to detect" pedestrian model for bumper heights from 400 mm up to 440 mm.

Table 5.
Comparison of momentum transfers

Height z	IEE G2 impactor [Ns@20ms]	Hardest to detect, excl. non-standard model [Ns@20ms]	Hardest to detect, incl. non-standard model [Ns@20ms]
400 mm	43.80	47.81	47.81
420 mm	47.30	50.04	50.04
440 mm	50.20	52.34	50.10
460 mm	52.70	53.97	49.40
480 mm	54.20	54.52	50.50
500 mm	56.05	56.00	52.30

For the evaluated bumper heights in the range of 460 mm to 500 mm, the slim tall male generates a momentum transfer which is about 6.5% below the one of the IEE G2 impactor. This appears to be an acceptable underestimation, especially when taking into consideration the major improvements that have been achieved compared to the 1st generation impactor.

OUTLOOK

During the generation and evaluation of the findings presented in this paper, a few subjects were identified which would deserve to be covered by subsequent research.

IEE plans to extend the IEE-WPI pedestrian model family to the 6-year-old child. This would allow us to cover the full range of "hardest to detect" pedestrians and to run all future evaluations based on a hybrid FE-model.

The test rig simulations were conducted with a test rig geometry setup that was representative of "normal" vehicle front end geometries. As the test rig allows to shift the three elements in x-and z-direction, more extreme configurations can be realized and analyzed in future investigations.

Actually, a real IEE G2 impactor is in construction in order to be able to run physical tests as done with the original IEE 1st generation impactor. It reflects correct pedestrian impact physics and is meant to be a test tool at varying velocities.

CONCLUSIONS

The paper has given an overview on the various steps that were taken in order to realize an improved impactor which aims at representing the "hardest to detect" pedestrian for a broad range of vehicle front-end configurations. The impactor can be used as a test tool to evaluate the detection performance of pedestrian detection sensors used to trigger pop-up hood systems or, in the future, windscreen or A-pillar airbags.

The simulation results have shown that a significant improvement could be achieved with the new IEE G2 impactor compared to the 1st generation lower limit impactor. The concept of the impactor has been optimized in order to guarantee interaction with all vehicle front end elements that can also interact with a real pedestrian.

The IEE G2 impactor is a very suitable "lower limit" impactor for all evaluated bumper heights. The deviations the impactor shows when including the slim tall male to the analysis are within an acceptable range.

The impactor also appears to be a very good compromise regarding the level of abstraction compared to a real leg, and the expected robustness of a real physical impactor model.

REFERENCES

- [1] Euro NCAP pedestrian testing protocol, Version 5.2.1 (www.euroncap.com)
- [2] Global Technical Regulation No. 9 Pedestrian Safety (<http://www.unece.org/trans/main/wp29/wp29wgs/wp29gen/wp29registry/gtr9.html>)
- [3] TNO: MADYMO, Human Models Manual; Release 7.1, June 2009
- [4] INRETS FRANCE <http://humos2.inrets.fr/>
- [5] TOYOTA Motor Corp.: THUMS, Total Human Model for Safety; TMC press release, May 2010

- [6] T.Sugimoto, K.Yamazaki:
First Results of the JAMA Human Body Model Project; JAMA/JARI; Paper 05-0291, 19th ESV 2005
- [7] A.Soni, A.Chawla, S.Murkherjee:
Effect of Muscle Contraction on Knee Loading for a Standing Pedestrian in lateral Impacts;
Paper 07-0458, 20th ESV 2007
- [8] Y. Takahashi, Y. Kikuchi, F. Mori, A. Konosu:
Advanced FE Lower Limb Model for Pedestrians;
Paper 03-0218, 18th ESV 2003
- [9] Y. Takahashi, Y. Kikuchi, F. Mori:
Full-Scale Validation of a Human FE Model for the Pelvis and Lower Limb of a Pedestrian; SAE International 2008-01-1243, 2008
- [10] M.H.Ray, private communication
- [11] C.Silvestri, M.H.Ray: Development of a Finite Element Model of the Knee-Thigh-Hip of a 50th Perc Male including Ligaments and Muscles; International Journal of Crashworthiness, Vol.14, No.2, pp:215-229, 2009
- [12] J.A.W. van Dommelen, B.J. Ivarsson, M.M. Jolandan, S.A. Millington, M. Raut, J.R. Kerrigan, J.R. Crandall, D.R. Diduch: Characterization of the Rate-Dependent Mechanical Properties and Failure of Human Knee Ligaments; SAE International 2005-01-0293, 2005
- [13] C. Untaroiu, K. Darvish, J. Crandall, B. Deng, J.-T. Wang: Characterization of the Lower Limb Soft Tissue in Pedestrian Finite Element Models; Paper 05-0250, 19th ESV 2005
- [14] J. van Hoof, R. de Lange, J. S. H.M. Wismans:
Improving Pedestrian Safety Using Numerical Human
TNO, Stapp Car Crash Journal Vol.47, 2003-22-0018
- [15] J. Kerrigan, K. Bhalla, N. Madeley, J. Funk, D. Bose, J. Crandall: Experiments for Establishing Pedestrian-Impact Lower Limb Injury Criteria; SAE International 2003-01-0895, 2003
- [16] D. Bose, K. Bhalla, L. Rooij, S. Millington, A. Studley, J. Crandall: Response of the Knee Joint to the Pedestrian Impact Loading Environment; SAE International 2004-01-1608, 2004
- [17] J. Kajzer, Y. Matsui, H. Ishikawa, G. Schroeder, U. Bosch: Shearing and Bending Effects at the Knee Joint at High Speed Lateral Loading; SAE International 973326, 1999
- [18] J. Kajzer, Y. Matsui, H. Ishikawa, G. Schroeder, U. Bosch: Shearing and Bending Effects at the Knee Joint at Low Speed Lateral Loading; SAE International 1999-01-0712, 1999
- [19] A. Soni, A. Chawla, S. Mukherjee, R. Malhotral: Sensitivity Analysis of Muscle Parameters and Identification in Low Speed Lateral; Impact at just below the Knee; SAE International 2009-01-1608, 2009
- [20] CONCEPT TECH:
CONCEPT-6yo PDI, User Manual-Specification-Certification;
Concept Technology, Graz
- [21] L. van Rooij, M. Meissner, K. Bhalla, J. Crandall, D. Longhitano, Y. Takahashi, Y. Dokku, Y. Kikuchi: The evaluation of the kinematics of the MADYMO human pedestrian model against experimental tests and the influence of a more biofidelic knee joint; University of Virginia, 2003
- [22] W. Goldsmith: Impact – The Theory and Physical Behaviour of Colliding Solids, Dover Publications, 1960, 2001
- [23] T. Martin (UTAC)
Improvement of Vehicle Crash Compatibility through the Development of Crash Test procedures (VC-COMPAT) (2005)

SAFETY REQUIREMENTS FOR SMALL MOTORISED ALTERNATIVE VEHICLES

Michael Paine

Vehicle Design and Research Pty Limited, Australia

Paper Number 11-0108

ABSTRACT

In recent times there has been an increase in the development, availability and use of small, motorised vehicles that may be alternatives to more conventional modes of personal transport such as bicycles or cars. Much of the interest in these 'alternative vehicles' (AV) is in their perceived benefits for pollution and congestion reduction.

To date there has been no uniform global approach to rules and standards governing the use of AVs. Regional requirements have mostly been applied on an ad hoc basis, differing significantly between jurisdictions. This has led to a highly prescriptive approach. This has tended to constrain innovative design, often because the vehicle concerned does not meet a regulatory definition.

In many jurisdictions there appears to be confusion amongst retailers, suppliers, consumers and enforcement agencies as to what types of AV may be legal and what rules govern their use. The differences between jurisdictions also mean that manufacturers and suppliers cannot easily design a single vehicle to market in a number of regions.

We review the types of AV that are available, or are under development, the limitations of the infrastructure on which they might be used and the safety issues arising from a mix of conventional road/path users and AVs.

INTRODUCTION

Alternative Vehicles (AVs) are small motorised wheeled vehicles that are used for personal transport but differ in construction from conventional vehicles such as cars, motorcycles and bicycles and do not comply with applicable vehicle regulation for cars or motorcycles. In Australia most types of AV cannot be registered and cannot be used on public infrastructure. Exceptions include electric wheelchairs, mobility scooters and power-assisted pedal cycles.

There are an increasing number of new types of AV that attract public attention. There is also lobbying to allow these vehicles to be used on public paths, cycleways or roads. The argument is often put forward that these vehicles will be used instead of cars and so will result in reduced pollution and less

traffic congestion. Countering this are concerns about the safety of pedestrians and cyclists, if these vehicles are used on footpaths or bicycle paths, and concerns about the riders of these vehicles, if they mix with conventional cars.

A review of international practices suggests that jurisdictions are having difficulty catering for alternative vehicles. There are no international vehicle standards that can be applied in their entirety to cover all concerns about the safety and operation of alternative vehicles.

ROAD VEHICLES

In Europe there is a class of vehicles known as quadricycles that are car-like but are not required to comply with modern crashworthiness requirements. Similarly, in the USA there are regulations to allow Low Speed Vehicles on some roads.

Transport Canada and the Insurance Institute for Highway Safety have each conducted crash tests of quadricycles and have expressed strong concerns about the lack of crashworthiness and the risk to occupants in relatively low speed collisions with cars.



Figure 1. Transport Canada crash test of a car-like quadricycle vehicle (40km/h full frontal)

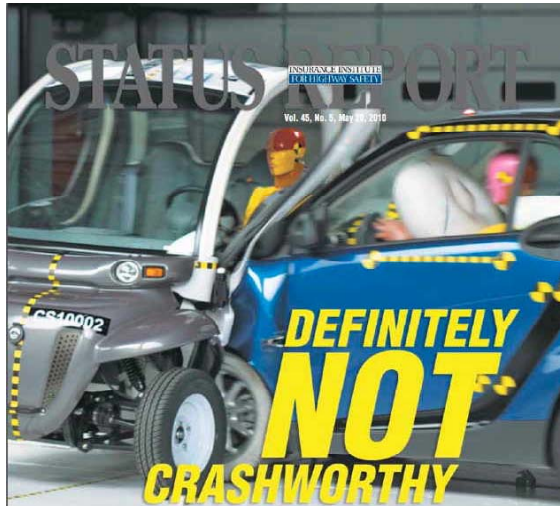


Figure 2. Cover of IIHS Status Report

In contrast there are now several models of fully electric car that have similar environmental benefits to electric quadricycles but are designed to meet car crashworthiness standards. For example the Mitsubishi i-MiEV recently achieved a 4 star rating from the Australasian New Car Assessment Program.

In the author's view any car-like vehicle should be required to meet crashworthiness regulations that apply to conventional cars. They are not considered to be alternative vehicles.

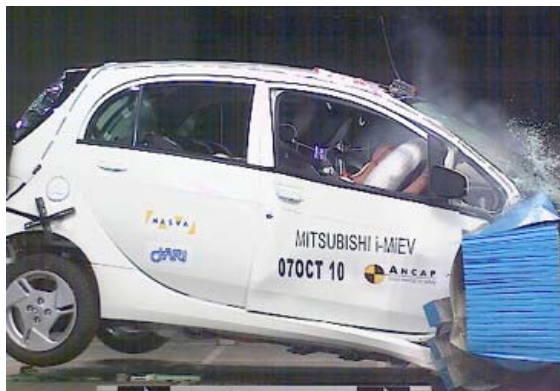


Figure 3. ANCAP crash test of Mitsubishi i-MiEV (64km/h frontal offset)

Power-assisted bicycles (PAB) are a form of AV that regularly shares the roads with cars. Like cyclists and motorcyclists, the riders of these vehicles are highly vulnerable to injury in a collision, compared with car occupants. A key difference, compared with quadricycles, is that the riders of bicycle-like vehicles feel vulnerable and usually ride accordingly.

In Australia power-assisted bicycles are limited to a motor power of no more than 200W. They must also have human (pedal) power as the primary means of propulsion. There are proposals to change from power-limiting to electronic speed-limiting for electrically powered PABs. The concept is that the electrical propulsion cuts out at speeds above 25km/h (the same as light mopeds in some European countries) but the rider can still use pedal power (or other human power) to travel at higher speeds, like a conventional bicycle.

Based on an analysis of speed and injury risk (see later), it is proposed that no AV be capable of powered travel in excess of 25km/h and that only those AVs capable of human propulsion above this speed be permitted to use roads with traffic travelling at commuting speeds (e.g posted speed limit greater than 50km/h). This is the current situation with power-assisted and unpowered bicycles in Australia.

In Australia bicycle lanes beside roads and dedicated bicycle paths are designed for a bicycle no more than 800mm in width. This width limit should apply to all AVs.

FOOTPATH VEHICLES

Vehicles that are intended to mix with pedestrians on footpaths are associated with special safety concerns. With frail (aged or very young) pedestrians any type of collision could lead to serious injury and even the need for a pedestrian to dodge out of the way of a vehicle can be hazardous. Therefore a vehicle used on footpaths must be capable of travelling and manoeuvring at very low speeds (one or two km/h) so their riders can avoid collisions with pedestrians.

It is noted that bicycles are not capable of travelling at the very low speeds needed for safely mixing with pedestrians because they need to travel at a minimum speed in order to be stable. This is one reason that most jurisdictions do not let bicycles ride in pedestrian areas - except where there are shared facilities designed for this purpose.

Footpath vehicles should also be top speed limited (4km/h for busy areas and 10km/h for other areas - see later). Limits on vehicle width are also appropriate. In Australia there are national guidelines for the design of footpaths and these are based on a standard unpowered wheelchair that is 740mm wide. This maximum width would be appropriate for any AV that uses a footpath.

AVs are being promoted as a "green" alternative to cars and as a means of commuting to work or to a bus/train station. Any relaxation of current requirements to permit AVs on footpaths should be based on stringent safety and environmental

conditions. Zero tailpipe emissions and minimal engine noise are appropriate (i.e. electric powered AVs). Portability is also a consideration. A kerb mass limit of 60kg would allow the rider to manually negotiate steps and other common obstacles and for two people to lift the vehicle, where necessary. An exception is mobility scooters designed for mobility-impaired riders, where extra features are needed and a kerb mass limit of 150kg is recommended.

BICYCLE PATHS

Most major cities in Australia have strategies to encourage bicycle use, including the provision of infrastructure designed for bicycles, such as dedicated bike paths (separate from roads) and shared paths where pedestrians and bicycles travel in an orderly manner. Bike paths are usually designed for vehicles no more than 800mm in width travelling at up to 25km/h, where conditions permit. These limits should apply to AVs using bike paths.

It is important that any AVs that use bike paths do not hinder the flow of bicycle traffic. Therefore it is recommended that any powered AV be capable of maintaining a speed of 8km/h on a 5% gradient.

SAFE SPEEDS

The risk of fatal injury in the event of a collision is strongly linked to the collision speed that, in turn, is linked to vehicle travelling speeds. The fatality risk for pedestrians and cyclists reaches 5% at collision speeds of 25km/h and 10% at 30km/h (Wrangborg 2005). The corresponding values for modern cars are 65km/h and 70km/h respectively. Car occupants have much less risk due to advanced restraint systems (seat belts and airbags), a strong passenger compartment and energy absorbing structures at the front.

This analysis indicates that, for vulnerable road users, collisions in excess of 25km/h should be avoided. This is the proposed maximum powered speed for any AV. Under many circumstances lower speeds are appropriate.

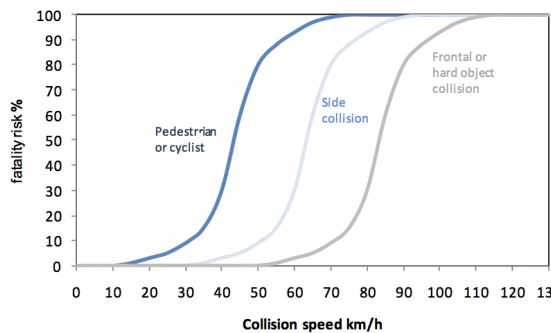


Figure 4. Risk of fatal injury (Wrangborg 2005)

A design aim for pedestrian infrastructure should be to minimise the risk of any collision with a vehicle. A primary factor in collision avoidance in these cases is vehicle speed.

In a study of the pedestrian danger from reversing motor vehicles, Paine (2003) evaluated the probability of collision avoidance for a range of detection distances and car speeds. The results apply to any vehicle moving slowly in either the forward or the reverse direction. Based on 95% collision avoidance, a rule of thumb is that the vehicle speed in km/h should be no more than twice the detection distance in metres. Therefore, for a vehicle travelling at 10km/h, the detection distance (at which the driver is alerted to an object in the path of the vehicle) should be no less than five metres.

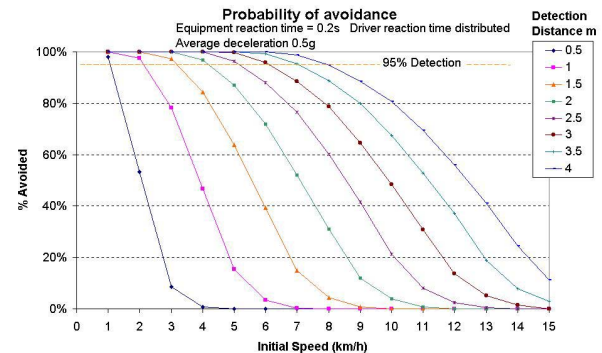


Figure 5. Low speed collision avoidance (Paine 2003)

The results of this analysis place severe limitations on the safe speeds at which alternative vehicles can share infrastructure with pedestrians. On un-crowded footpaths (typical of residential streets and shared paths) a 5m hazard detection distance is considered typical. In these circumstances a 10km/h speed limit is appropriate. On busy footpaths and footpaths with visual obstructions, such as blind corners, a hazard detection distance of 2m is considered typical and so a 4km/h limit would be appropriate.

Mobility scooters have a collision-avoidance disadvantage because the front of the vehicle is some one metre forward of the rider's eyes ("forward projection" = 1m). This reduces the distance available to stop once a hazard is detected. It is therefore important that conservative decisions are made about appropriate speeds for AVs on footpaths.

With the proposed electronic speed limiting of AVs there is scope to have speed ranges to suit the particular infrastructure. In this case a speed range indicator, clearly visible to other infrastructure users, would be appropriate.

OTHER CONSTRUCTION REQUIREMENTS

Other vehicle construction to be considered include:

- Maximum acceleration
- Braking performance
- Rider controls (throttle, braking, steering)
- Height with rider
- Tipping stability
- Manoeuvrability
- Lighting & conspicuity
- Minimum and maximum noise
- Vehicle identification

CONCLUSIONS

Since infrastructure on which AVs would be expected to operate tends to be bicycle or pedestrian-based there is good scope for achieving a global or national standard that will be compatible with existing infrastructure and will ensure that AVs can operate safely amongst other infrastructure users. It is recommended that an international working group be formed to develop a draft standard for construction and performance of AVs, taking into consideration the factors raised in this paper. It is important that infrastructure designers contribute to this standard.

The development of technical standards is only one part of an overall policy framework to deal with AVs. More daunting are the tasks of determining if and how vehicle registration and rider licencing should apply to AVs and which types of AV should be allowed to use public infrastructure. There are also issues of accident insurance and regulation amendments to consider.

Vehicles complying with a global technical standard should not automatically be granted access to public infrastructure. If, after a range of policy issues have been considered, it is decided that particular types of AV will be allowed to use public infrastructure in a certain region then global technical standards will assist in the implementation of this policy.

REFERENCES

Austroroads (2009), Guide to Road Design – Part 6A: Pedestrian and Cyclist Paths, ISBN 978-1-921551-81-9

Griffiths, M. et al., (2010), Review of Motorised Mobility Devices, report prepared for Vicroads (publication pending).

Lewis G, (1973), The Manoeuvrability and Braking Performance of Small Wheeled Bicycles when Ridden by Children., Transport and Road Research Laboratory Report LR 500, Crowthorne, Berkshire UK.

Neilson, ID and Armour, JS (1985), Safety aspects of the Sinclair C5 electrically assisted pedal tricycle, research report 55, Transport and Road Research Laboratory (TRRL), Crowthorne, UK.

NSW Roads and Traffic Authority, (2008), Better regulation of motor-assisted pedal cycles: issues and solutions

Paine M, (2001), Analysis of the Relative Safety Performance of Bicycles and Scooters, research report prepared for Vicroads, Melbourne, 2001.

Paine M, (2003), The Danger to Young Pedestrians from Reversing Motor Vehicles, Proceedings of 18th Conference on the Enhanced Safety of Vehicles

Schoon C. (2004), "Traffic legislation and safety in Europe concerning the moped and the A1 category motorcycle", Swedish National Road Administration, Report R-2004-10.

Turner S, Roozenburg A & Binder S, (2009), Cycle safety: reducing the crash risk. NZ Transport Agency research report 389

Turner S, Roozenburg A, & Francis T, (2006), Predicting accident rates for cyclists and pedestrians. Land Transport New Zealand Research Report 289

UK Dept for Transport, (2010), Proposed amendments to the Electrically Assisted Pedal Cycles Regulations 1983

UK Dept for Transport, (2010), Whether the law should be changed to permit small one-person Electric Personal Vehicles (EPVs) to use public roads and cycle tracks.

UK Dept for Transport, (2010), Consultation on proposed changes to the laws governing powered mobility scooters & powered wheelchairs

Wrangborg P, (2005) A New Approach to a Safe and Sustainable Road Structure and Street Design for Urban Areas, Road Safety on Four Continents Conference, Warsaw.

DISCLAIMER

This paper represents the author's views and does not represent the views or policy of any organisation. It is intended as a discussion paper and is based on research conducted for several projects over the past decade. I thank my colleagues in those projects.